

MODEL-BASED ESTIMATION OF ADIABATIC  
FLAME TEMPERATURE DURING  
COAL GASIFICATION

by

Ihsan Mert Sarigul

A thesis submitted to the faculty of  
The University of Utah  
in partial fulfillment of the requirements for the degree of

Master of Science

Department of Chemical Engineering

The University of Utah

December 2012

Copyright © Ihsan Mert Sarigul 2012

All Rights Reserved

# The University of Utah Graduate School

## STATEMENT OF THESIS APPROVAL

The thesis of **Ihsan Mert Sarigul**

has been approved by the following supervisory committee members:

<u><b>Mikhail Skliar</b></u>	, Chair	<u><b>10/25/2012</b></u> Date Approved
<u><b>Kevin Whitty</b></u>	, Member	<u><b>09/10/2012</b></u> Date Approved
<u><b>Anthony Butterfield</b></u>	, Member	<u><b>09/10/2012</b></u> Date Approved

and by **JoAnn Lighty**, Chair of  
the Department of **Chemical Engineering**

and by Charles A. Wight, Dean of The Graduate School.

## **ABSTRACT**

Coal gasification temperature distribution in the gasifier is one of the important issues. High temperature may increase the risk of corrosion of the gasifier wall or it may cause an increase in the amount of volatile compounds. At the same time, gasification temperature is a dominant factor for high conversion of products and completing the reactions during coal gasification in a short time. In the light of this information it can be said that temperature is one of key parameters of coal gasification to enhance the production of high heating value syngas and maximize refractory longevity.

This study aims to predict the adiabatic flame temperatures of Australian bituminous coal and Indonesian roto coal in an entrained flow gasifier using different operating conditions with the ChemCAD simulation and design program. To achieve these objectives, two types of gasification parameters were carried out using simulation of a vertical entrained flow reactor: (1) oxygen-to-coal feed ratio by kg/kg and pressure and (2) steam-to-coal feed ratio by kg/kg and pressure.

In the first part of study the adiabatic flame temperatures, coal gasification products and other coal characteristics of two types of coals were determined using ChemCAD software. During all simulations, coal feed rate, coal particle size, initial temperature of coal, water and oxygen were kept constant. The relationships between flame temperature, coal gasification products and operating parameters were fundamentally investigated.

The second part of this study addresses the modeling of the flame temperature relation to methane production and other input parameters used previous chapter. The scope of this work was to establish a reasonable model in order to estimate flame temperature without any theoretical calculation. Finally, sensitivity analysis was performed after getting some basic correlations between temperature and input variables. According to the results, oxygen-to-coal feed ratio has the most influential effect on adiabatic flame temperature.

## TABLE OF CONTENTS

ABSTRACT .....	iii
ACKNOWLEDGEMENTS .....	vii
CHAPTER	
1. INTRODUCTION .....	1
1.1 Gasification Terms .....	3
1.2 Basic Reactions of Coal Gasification .....	4
1.3 Choice of Gasifier .....	6
1.3.1 Entrained Flow Gasifier .....	7
1.3.2 Shell Gasification Process .....	8
1.4 Challenges of Measuring Temperature .....	9
2. LITERATURE REVIEW .....	13
2.1 Effect of Temperature on Reactor Performance .....	14
2.2 Effect of Operating Conditions on Reactor Performance .....	16
2.3 Gasifier Outlet Temperature as a Function of Methane .....	17
2.4 Tunable Diode Laser Technology .....	20
2.5 Modeling of Temperature in Entrained Flow Gasifier .....	21
2.5.1 Polynomial Model .....	21
2.5.2 Power Law .....	24
2.5.3 Estimation of Sensitivity Coefficients of Nonlinear Model .....	25
3. SIMULATION SETUP AND PROCEDURE .....	29
3.1 Shell Gasification Diagram Setup .....	29
3.2 The Gibbs Free Reactor .....	30
3.3 Methods and General Assumptions .....	31
3.3.1 Method and Approach .....	31
3.3.2 Overall Assumptions .....	36
3.4 Simulation Procedure .....	37

4. RESULTS: SIMULATION OF COAL GASIFICATION .....	64
4.1 Influence of Steam-to-Coal Ratio and Pressure on Gasification.....	64
4.2 Influence of Oxygen-to-Coal Ratio and Pressure on Gasification.....	68
4.3 Influence of Oxygen-to-Coal and Steam-to-Coal Ratios on Gasification.....	72
5. MODELING OF ADIABATIC FLAME TEMPERATURE .....	97
5.1 Modeling of Adiabatic Flame Temperature Corresponding to Different System Parameters in Entrained Flow Gasifier.....	97
5.2 The Correlation between Methane Concentration and Gasification Temperature.....	98
5.3 Effect of Oxygen-to-Coal Ratio on Adiabatic Flame Temperature and Composition of Methane at Different Steam-to-Coal Feed Ratios.....	99
5.4 Effect of Steam-to-Coal Ratio on Adiabatic Flame Temperature and Composition of Methane at Different Oxygen-to-Coal Feed Ratios.....	100
5.5 Modeling of ChemCAD Results.....	101
5.5.1 Linear Model.....	103
5.5.2 Second Order Polynomial Model.....	104
5.5.3 Power Law.....	105
5.5.4 Response Surface Methodology (RSM).....	106
5.5.5 Multivariate Power Model.....	108
5.6 Sensitivity Analysis.....	110
6. CONCLUSIONS AND RECOMMENDATIONS FOR FUTURE WORK.....	116
6.1 Summary of Results.....	116
6.2 Recommendations for Future Work.....	120
APPENDICES	
A. ADIABATIC FLAME TEMPERATURE RESULTS.....	122
B. DESIGN PARAMETERS.....	125
REFERENCES.....	126

## **ACKNOWLEDGEMENTS**

I wish to thank Petroleum Pipeline Corporation for generously sponsoring this study. I would also like to take this opportunity to express my gratitude to the faculty and staff of the Department of Chemical Engineering at the University of Utah, especially to my committee members, Dr. Kevin Whitty and Dr. Anthony Butterfield. With special thanks to Dr. Mikhail Skliar, my advisor during graduate education, for all guidance and support he has so graciously offered. Finally, I would like to thank my family for all their patience and encouragement.



## **CHAPTER 1**

### **INTRODUCTION**

As the energy demands increase in the world, scientists have had to focus on new energy resources. Still, the need for energy, more than past years, has increased the importance of coal. The products that are produced by coal gasification can be used in different processes. The most common processes, that are being used today, can be described as energy and fuel production and electricity generation. Relatively, the heat and energy that are generated from coal combustion and gasification are more than the energy generated from the other primary energy sources such as biomass and wind energy. Because of this situation, the demand of coal and coal products are constantly increasing in the world. While the energetic potential of coal mines are evaluated, it can be seen that far Asia, North America and Eastern Europe are the leaders in terms of coal reserves. Almost 75% of coal is being provided from these three important areas (1).

Coal gasification is an important energy production technology and a key syngas source in the industrial world. Most of the chemical processes which require a huge energy demand are basically getting the power and energy using coal gasification and combustion. They also use the gasification products for different purposes. Hydrogen and carbon monoxide can be used in reactant for other chemical processes or producing electricity. These gasification products are being used to generate the substitute natural gas and other fuels as well.

Coal types are always tested by operators who work in gasification and combustion plants to get high quality coal products. The adiabatic flame temperature is one of the important parameters for coal type. If the gasifier temperature exceeds the adiabatic flame temperature of coal combustion or gasification, dissociation probably will occur and the amount of gasification products will begin to decrease slightly. The first aim of this research was the prediction of adiabatic flame temperature based on operating conditions. A computational software model was utilized to determine the flame temperature by applying different input parameters such as oxygen-to-coal feed ratio, steam-to-coal feed ratio or system pressure. Temperature in the gasifier is one of the important elements that deserves emphasis. High temperatures may increase the risk of corrosion of the gasifier wall or it may cause the amount of volatile compounds to ascend. Simultaneously, gasification temperatures are a dominant factor for high conversion of products and completing the reactions during coal gasification in a short time.

Recently, the effect of oxygen and steam on gasification temperatures, that are necessary factors for coal gasification, have been seriously studied by scientists (2, 3). New research areas have already emerged to ascertain an ideal temperature at optimum oxygen-to-coal and steam-to-coal feed ratios (4), then at this temperature point to raise the gasification products to the maximum level. In this study, gasification temperatures and products of Australian bituminous coal and Indonesian roto coal are determined using the ChemCAD software program. In addition, the modeling of gasification temperatures was completed with the help of different data.

### 1.1. Gasification Terms

Coal gasification is a coal conversion process by which combustible gas from coal known as syngas, is produced. Gas obtained by coal gasification can be used in many ways: for electricity production, in chemical industry for petroleum, methanol, and ammonia synthesis, for ore reduction, as an industrial fuel, for residential heating, etc.

The cold gas efficiency is the ratio between the chemical energy content in the product gas compared to the chemical energy in the fuel (based on the lower heating value). The cold gas efficiency is calculated in the following way (5):

Cold gas efficiency =

$$\frac{\text{Product gas ( mass fraction*Lower Heating Value)}}{\text{Fuel ( mass fraction*Lower Heating Value)}} * 100 \quad (1.1)$$

In this study, cold gas efficiency (CGE) was calculated by:

$$\text{CGE} = [m_{\text{H}_2} * \text{LHV}_{\text{H}_2} + m_{\text{CO}} * \text{LHV}_{\text{CO}} + m_{\text{CH}_4} * \text{LHV}_{\text{CH}_4}] / [m_{\text{coal}} * \text{LHV}_{\text{COAL}}] * 100 \quad (1.2)$$

Another important consideration in gasification is carbon conversion. Carbon conversion is defined as the amount of carbon in the product gas divided by the amount of carbon in the fuel (5). Carbon conversion is influenced by fuel particle size, fuel type, temperature, and residence time in the gasifier. The particle size can not be varied in a range that is intended for commercial application, because the size of the feeding system and the reactor is relatively small in the lab-scale set-up. The oxygen-to-coal feed ratio has a great effect on carbon conversion. The maximum carbon conversion is reached at a high oxygen-to-coal ratio. The carbon conversion generally increases with increasing

temperature. In the process of self-regulating, if the temperature in the reactor lowers, the amount of char produced rises and the amount of heat produced in the combustor increases as well. This results in a surge in an increase in gasification temperature. In this study carbon conversion was calculated by the following formulas:

$X_c = [\text{Carbon in the product gas} / \text{Carbon feed rate in coal}] * 100$  or,

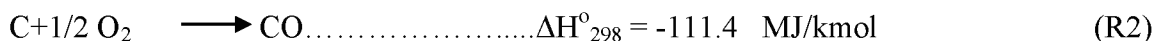
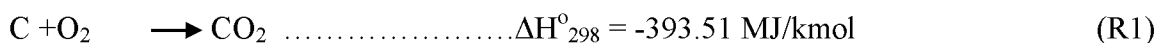
$$X_c = [(W_{CO} + W_{CO_2} + W_{CH_4}) / W_C] \quad (1.3)$$

Any solid carbon in the product is the unconverted product. So another way to calculate conversion is:

$$X_c = [1 - (\text{carbon remaining as solid product} / \text{carbon with entering coal})] * 100 \quad (1.4)$$

## 1.2 Basic Reactions of Coal Gasification

Coal gasification is essentially comprised of two major processes: Pyrolysis (between 573 K and 773K) and char gasification (4, 5). During the coal gasification process, a carbon considered as feedstock at elevated pressure and high temperature range is converted in a gasifier in the presence of steam and oxygen to the mixture of carbon monoxide and hydrogen commonly known as synthesis gas. The chemical reactions, which take place in the gasifiers, are the fundamental part of the coal gasification. Some of the more important of which are :



Reactions (R1) and (R2), which produce most of the heat required by the endothermic gasification reactions (R3) and (R4), are highly exothermic oxidation reactions. The oxidation reactions that completely consume all of the oxygen present in the entrained flow gasifier go on very fast. Therefore, most of the gasifier operates under reducing conditions. Char-vapor reaction (R3) is endothermic, and with increased temperature, the rate of reaction become fast. Finally, it leads the amount of H<sub>2</sub> and CO in the product gas to increase. Another reaction which takes an important place during the coal gasification is the water-gas shift reaction (R5). The main characteristic of this reaction can be stated the forming of H<sub>2</sub> and CO<sub>2</sub> with the basis of H<sub>2</sub>O and carbon monoxide reactants (5). Moreover, H<sub>2</sub>/CO ratio in the final mixture is considerable changed by the water-gas shift reaction with increased temperature. The reason of this change is explained as H<sub>2</sub> and CO<sub>2</sub> contents in the product gas decrease. However, it does not greatly impact the heating value of the synthesis gas, because the heat of combustion of H<sub>2</sub> and CO on a molar basis are almost identical if the water is not condensed. Methane formation, reaction (R6), is generally obtained at high pressures and low

temperatures and thus, is mainly important in lower temperature gasification systems. Methane formation which does not consume oxygen is also an exothermic reaction and, therefore, this type of reaction eventually increases the efficiency of gasification and the final heating value of the synthesis gas (4).

### **1.3 Choice of Gasifier**

Although there are several types of flow reactors such as fluidized bed reactor and fixed bed flow reactor used in the industry, the entrained flow gasifier was selected for the coal gasification in this study. There are several reasons to choose this type of gasifier (6). These reasons are explained below.

The entrained flow gasifiers, which are designed for high operating conditions, can be adapted for most of the coal types. In an entrained flow slagging gasifier, coal particles generally undergo two conversion stages that take place almost simultaneously because of the high heating rate. A higher throughput can be achieved due to a high temperature scale where the coal particles are substantially dissociated in the gasifier. The contents of unexpected products such as methane and tar do not yield at a significant level due to the high temperature ranges. The unexpected products easily leave the reactor after coal gasification. However, the air need for oxidation reactions which occur in the burner zone is higher than for the other types of gasifiers. In addition, the entrained flow gasifiers have the ability of the removal the major part of ash particles above the the flame temperatures. The entrained flow gasifiers with refractory or water-cooled steel walls depend on a slag layer to conserve the gasifier walls and reduce the heat loss through the wall. Finally,  $\text{NO}_x$  formation can be neglected for these types of gasifiers and corrosive slags do not have a great influence on operating conditions (7).

### 1.3.1. Entrained Flow Gasifiers

In entrained-flow gasifiers, air, coal and steam go through the top of the gasifier (see Figure 1.1). The gasification products are collected at the bottom of the gasifier. The quench water is used to cool down the ash particles and slurry mixture. Then, the ash content is removed after finishing the gasifications. The coal gasification is operated at high temperature and elevated pressure in order to fuse coal into inert slag. The small coal particle size and high temperatures also allow the gasification reactions to take place at short residence time and a very high rate. Hydrogen, carbon monoxide and a small amount of hydrocarbon gases are produced by oil, tar and other liquids composed from devolatilization of coal inside the gasifier. The entrained flow gasifiers have the ability to use any coal type and result in the clean syngas (8).

Matyas et al. (8) demonstrated the coal which fed into the entrained flow gasifier in either a slurry or a dry form. Although a lock hopper system is used for dry form, the high-pressure slurry pumps are generally preferred for slurry form of coal feed. They also indicated that the slurry feed, which is a basic operation, initiates water into the gasifier reactor. The consequence of this extra water which needs to be evaporated is a product synthesis (high  $H_2/CO$  ratio) gas. However, it unfortunately contains a lower thermal efficiency.

Entrained flow gasifiers typically display the following characteristic: Temperature does not deviate significantly within the reactor. However, it depends on the gasifier zone. The gasifier temperature is higher in burner zone than that in the reductor section because of oxidation reactions. Even though residence time is quite short compared to other types of gasifiers, the huge amount of oxygen is required to complete

the reactions. A variety of solid feedstocks are usually utilized for design and operation of the entrained flow gasifiers where slag formation frequently occur. Finally, these types of gasifier contain low cold gas efficiency even though carbon conversion are high enough for industrial application (9).

### **1.3.2 Shell Gasification Process**

In this study, coal gasification was performed using Shell gasification process. (The background of Shell gasification technology is discussed in this chapter). A Shell coal gasification scheme, which exhibits a dry feed system is illustrated in Figure 1.2.

According to this technology, a coal, which is dried and powdered, is supplied to opposite parts of the gasifier while oxygen follows to the gasifier below the coal feeding zones. Furthermore,  $N_2$  is considered as inert gas which carries out the coal particles into the reactor and it helps to pressurize the feed hoppers to the reactor operating pressure around 4.2 MPa. Slag/solid gas mixture, which flows up through the gasifier at about  $1800^\circ\text{C}$ , is removed at the bottom of the reactor. A cold recycle synthesis gas stream—the estimation temperature is around  $300^\circ\text{C}$ —is fed into the gasifier in order to decrease the temperature of gasification products. Similarly, the quench gas reduces the syngas mixture to around  $850^\circ\text{C}$ . The most important drawback of the cooling step is that if the temperature of unquenched syngas is detected at about  $1700^\circ\text{C}$ , the steam boiler tubes located in the syngas cooler do not resist this high level temperature. Nonetheless, quenching gas reduces the gasifier temperature to an allowable rank, a very important step during the gasification process. Finally, the fly ash includes unconverted carbon due to the lack of oxidant. This is recycled to the coal feed system (8, 9).



### 1.4 Challenges of Measuring Temperature

To measure the temperature inside the gasifier is fundamental to the coal gasification process. The efficiency of coal products, slag formation in the gasifier and ideal operating conditions can be controlled by measuring of temperature. However, there are some challenges that need to be solved for measuring the temperature, in other words, one of the biggest difficulties facing gasifiers is the challenge in procuring a certain temperature inside the gasifier. Gasification process normally takes place around 1800°F and pressures of 100-800 psi (10). In a power plant, slagging coal gasifiers should operate and be set to work above the fusion point of ash. The aim of this attempt is the melting of ash inside the gasifier. Then, the ash is mixed with the corrosive slag. Hence, the ash falls from the walls of the gasifier.

The other challenges of measuring temperature that occur during coal gasification are large and/or rapid changes in temperature, erosion by particulates, attack by molten slag of variable compositions and hot corrosive gases, including alkali vapor (10).

Current gasifiers use thermocouples, thermistors and indirect measurement techniques in order to control and measure the temperatures. Unfortunately, these methods have limited life and accuracy. Thermocouples do not withstand to the high temperatures inside the gasifier. Indeed, they are broken down dramatically or display inaccurate measurement due to deviation from the actual temperature. Thermocouples also have other drawbacks such as stability and repeatability. Thermistors, which are not as rugged as thermocouples, also have package size and low sensitivity problems in a wide range of temperatures (11).

A rugged, reliable diagnostic system must be taken into account for all types of gasifiers in order to achieve not only a better life but also improved fuel economy and reliability. A reliable diagnostic system would also provide valuable information for other systems down the road, particularly heat values for the combustion turbines that could improve their efficiency, and thus maximize gasification's great potential.

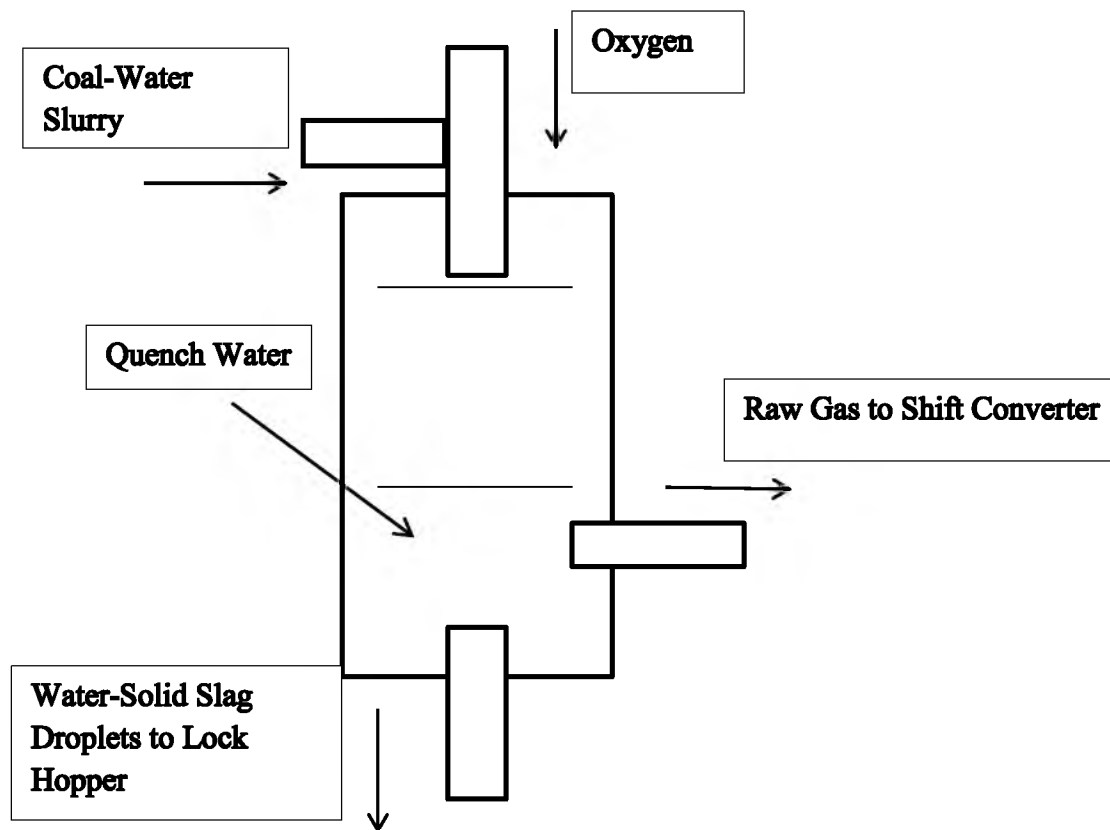
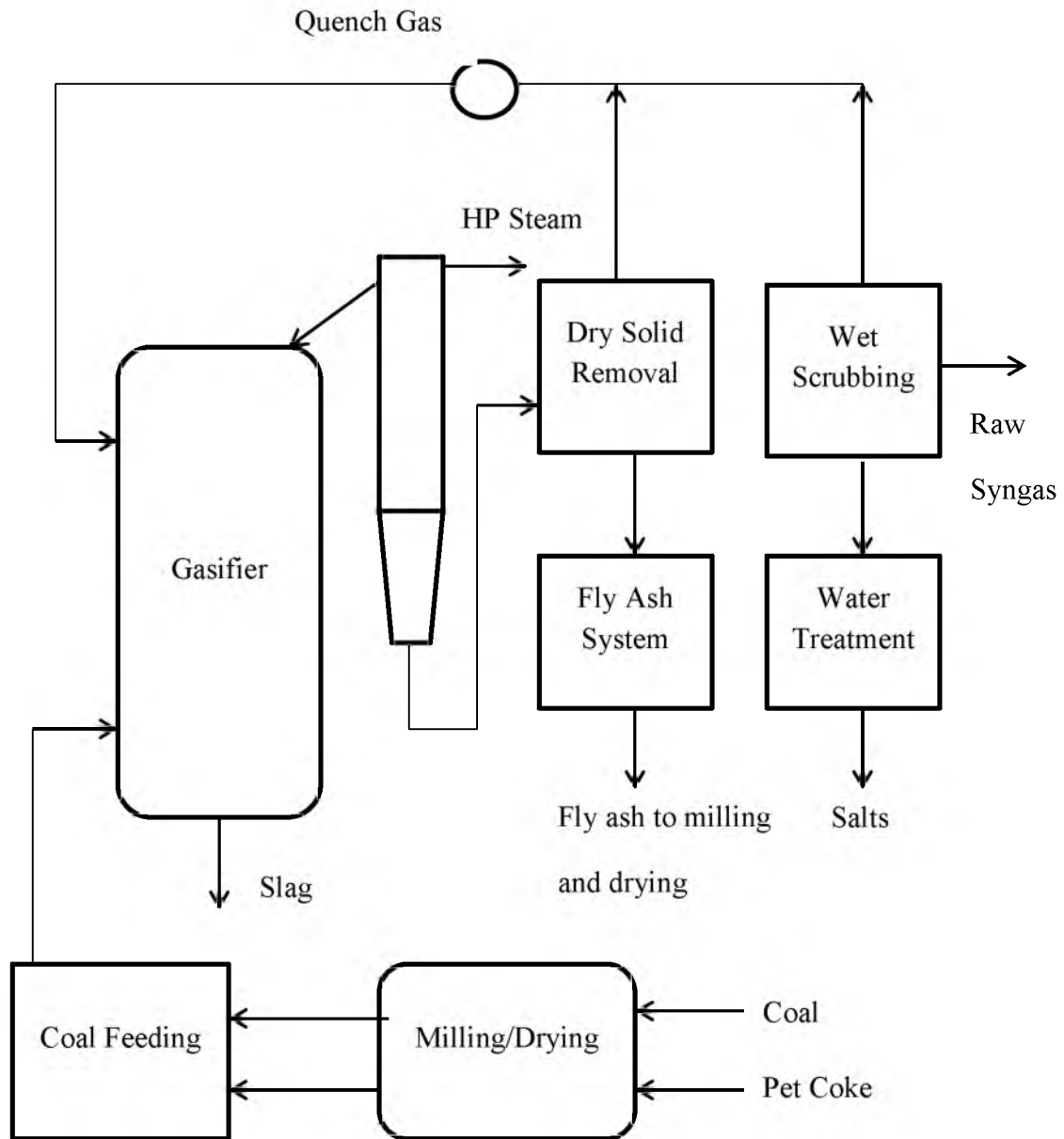


Figure 1.1 Schematic of entrained flow gasifier with water quench



**Figure 1.2 :** Shell coal gasification process

## **CHAPTER 2**

### **LITERATURE REVIEW**

Coal is the most prominent energy source for the generation of electric power in the USA and Europe. The energy information administration (EIA) report states that coal used for electric power generation will rise in the next quarter century. Improved gasification is the indispensable step toward the development of commercial Integrated-gasification Combined Cycle (IGCC), and sensors for continuous monitoring of gasifier temperature and syngas energy content required to enhance the production of the high heating-value syngas while maximizing refractory longevity and other maintenance issues (12).

Gasification which produces energy from fuels for heating, electricity and industrial applications is a new and advance technology. Gasification is more efficient technology than combustion because it contains a multistage combustion steps which provide high conversion efficiency and low emissions. Coal gasification is defined as a coal conversion process by which combustible gas from coal is produced.

The ash properties of coal often specify the temperature in the gasifier. If the ash melting point of any coal type is very high to operate, the flux is generally added to the coal feed stream to reduce the ash melting point. The oxygen is significantly consumed at high temperature ranges during coal gasification process and this either causes to decrease the overall system efficiency or requires more oxygen need. Thus, system

temperature should be arranged with known oxygen-to-fuel and steam-to-fuel ratios in order to optimize the process control. Since most modern gasification processes operate at 30 bar or higher, temperatures of above 1300°C are required in order to produce a synthesis gas with a low methane content (13).

### **2.1 Effect of Temperature on Reactor Performance**

The effect of gasifier temperature on gasification products and reactor performance is one of the most important subjects in studying coal gasification. It has been recognized that the adiabatic flame temperature and its evolution have a major influence on the conversion of coal, syngas production and composition of gasification products.

Lee et al. (14) studied the coal pyrolysis in a fluidized bed reactor. In their study, a model of the two-phase theory on coal gasification in a thermobalance reactor and coal pyrolysis in a fluidized bed was proposed to predict the gas compositions. The char particles for the thermobalance reactor were prepared by devolatilization of Australian bituminous coal, which was heated from room temperature to 900°C at a rate of 10°C min<sup>-1</sup> and then maintained for 30 min at 900°C. The coal-particle diameters for the pyrolysis and gasification reactions were 0.25 to 1.0 mm. To eliminate the influence of diffusion on reaction rate, experiments were performed with varying sample sizes and masses. They gasified 0.3–0.6 g of char in the size range 0.3–1.0 mm in a thermobalance reactor.

Furthermore, Lee et al. (14) carried out pyrolysis and gasification in a fluidized-bed reactor made of 316 stainless steel. The solid particles were supported on a bubble-cap distributor which contained seven bubble caps (4×2.0 mm i.d.) that served as

air and steam distributors. Eight pressure taps were installed on the wall at 0.1 m height distances to measure temperature and pressure, and six K-type thermocouples were similarly adjusted along the bed height. To conclude their study, the effect of temperature on gasification gas compositions was determined. Their research also indicates the effect of reaction temperature on gas compositions from coal gasification based on model predictions. The product gases are 30–40% H<sub>2</sub>, 23–28% CO, 27–35% CO<sub>2</sub>, and 6–9% CH<sub>4</sub>. As the reaction temperature is increased, the yields of H<sub>2</sub> and CO increase due to a rise in steam gasification and pyrolysis. At the same time, the CO<sub>2</sub> yield decreases when combustion reactions decrease. The yields of CO and CO<sub>2</sub> are increased in the product gas since the combustion reaction is faster than the steam-gasification char reaction. The amount of CH<sub>4</sub> decreases with increasing reaction temperature since it is mainly produced by pyrolysis. Their model clearly predicts the experimental data well and much better than previously published models. Therefore, Lee et al. (14) concluded that pyrolysis plays an important role in coal gasification, especially for coals with higher volatile contents.

The effect of temperature on cold gas efficiency, carbon conversion and gas heating values have been investigated by Taba and Irfan (15). According to their findings, temperature is one of the most significant operating parameters because it affects both gaseous composition and carbon conversion through oxidation and gasification reactions. Furthermore, gas yield, heating value, cold gas efficiency and finally char and tar yields in coal gasification processes are affected by gasifier temperature. This effect depends on thermodynamic behaviour of the reactions and the balance between endothermic and

exothermic reactions. Taba and Irfan (15) also indicate that there is a limitation to how high the temperature can rise due to its effect on the ash fusion and volatile matter.

Taba and Irfan (15) concluded that carbon conversion and cold gas efficiency (CGE) increase with the rise of temperature while hydrocarbons and tar contents are decreased. This observation is mainly due to the higher temperature at which endothermic reactions involved in the gasification become more dominant. This result for cold gas efficiency is only because their reactor was electrically heated and the energy for that heating is not accounted for. Otherwise cold gas efficiency decreases with increasing oxygen-to-steam feed ratio. Theoretically, the yield of coal gasification depends upon various parameters such as temperature, pressure, particle size of coal, types of fuel used and the fuel/gasifying agent ratio; these parameters are equally important and interact with each other during gasification, but temperature is by far the most significant factor (3).

## **2.2 Effect of Operating Conditions on Reactor Performance**

The oxygen-to-coal ratio, steam-to-coal ratio, pressure and ash content of coal substantially influence the gasification temperature and coal products. Nguyen et al. (16) developed a two stage equilibrium model to investigate the role of oxygen-to-coal and steam-to-coal ratios on reactor performance and on carbon conversion and composition of the product gas in an entrained-flow coal gasifier. Nguyen's model—which has been validated with experimental data taken from previous studies—is composed of two separate stages including char-gasification and gas-phase reaction; in the first, carbon conversion is estimated with solid-gas reactions; in the second, the product gas composition is calculated. Water consumption involved in the equilibrium reaction of the



first stage is expressed as an exponential function of temperature. This study confirms that carbon conversion and product gas composition are influenced decisively by the oxygen-to-coal ratio. The optimum range of the steam-to-coal ratio and the total yield of CO and H<sub>2</sub> depend on the type of coal and particle size.

Nguyen et al. (16) also explained the product gas composition of each component and the gasification temperature at various oxygen-to-coal ratios. According to their research, as the oxygen-to-coal feed ratio increases, the CO composition increases considerably while H<sub>2</sub>O, H<sub>2</sub> and CO<sub>2</sub> decrease slightly. Furthermore, the research also exhibits the gasifier temperature rises as the oxygen-to-coal ratio increases due to exothermic combustion (16, 17). Finally, when the steam-to-coal ratio increases, the H<sub>2</sub>O and CO<sub>2</sub> compositions increase proportionally; while CO decreases, H<sub>2</sub> and CH<sub>4</sub> change little with steam-to-coal ratios.

Higman and Burgt (13) indicate that the advanced gasification systems are mostly operated between 10 bar and 100 bar to conserve energy and keep down the equipment size. With the calculations all performed at 1000°C, Higman (18) examined gas composition changes with pressure. In addition, the CO concentration decreases dramatically while the other gas components do not change significantly. He also figures out that at this temperature, 1000°C, the actual changes of gas composition with pressure is almost negligible.

### **2.3 Gasifier Outlet Temperature as a Function of Methane**

Higman and Burgt (13) report that under conditions where methane is the only hydrocarbon that is present, it is a reasonable approach for entrained flow gasifiers since the coal footprint assumes to reach chemical equilibrium between gas phases. They

further conclude that, in general, the temperature of a dry-slurry feed gasifier can be monitored by the concentration of methane product gas. In fact, the methane content should be determined for process control in entrained flow gasifiers. Otherwise, it does not considerably affect on energy and mass balance in the reactor (13).

As the gasification reactions and the coal feed stock have an important effect on methane content, the amount of methane frequently has to be determined by the calculations in the dry-coal feed entrained flow gasifiers where heat loss occurs due to the membrane wall. However, the gasifier temperature can not easily be monitored by the analyzer since the measuring of product gas which leaves the reactor is really difficult. Here, Higman (18) suggests a method called 'post-mortem' to overcome that issue.

The post-mortem method says that the gas sample which leaves the reactor can directly be measured in a cooled and thin tube after cooling down. The analysis is performed after finishing this operation (13, 18). Currently, researchers are debating why trace amounts of methane appear in the product gas when the gasification reactions take place in the entrained flow slagging gasifier, given that the methane hardly plays a role in the calculations. Moreover, with a view to process control, ignoring the methane exceedingly facilitates the calculations. Higman (18) mentioned that if the isomethane lines agree with the isotherms, the gasifier temperature approaches pretty much to the actual one. In fact, he claims that this is only partly acceptable. Higman and his research group provide a valuable indication of the outlet temperature, but on calculating the actual temperature on the basis of gas analysis, values differ from reasonable expectations. However, introducing correction factors with the calculated temperatures

based on the other gas components, the  $\text{CH}_4$  content becomes an extremely worthwhile determinant of the reactor and gasifier temperature.

To accommodate liquid and slurry-type combustible wastes, Yun and Ju (19) developed a gasification/melting facility that can operate up to 10 bar and  $1550^\circ\text{C}$  with a maximum of 1 ton/day capacity. In developing the system, Yun and Ju's main focuses were keeping the reaction with the minimum amount of expensive fuel and utilizing cheap waste oil instead for energy input efficiency. In their study, methane concentration dropped rapidly with increasing temperature. Inevitably, at temperatures as high as  $1400^\circ\text{C}$ , structural damage to thermocouples occurred on the inner diameter surface of the gasifier during long runs. The directly contacting thermocouples cause an increased risk of corrosion and thermal melting during the measurement of variables. Therefore, finding an indirect way of measuring the gasifier temperature is very important. When the thermocouple suffered damaged in Yun and Ju's study, the methane concentration was used as an indirect indicator of gasifier temperatures, which were measured by a direct contacting thermocouple with the reacting gas. The R-type thermocouple was used with a ceramic tip on the gas contacting area. When the temperature rose high enough, the methane concentration dropped rapidly. According to their findings, when the gasifier temperature reached around  $1200^\circ\text{C}$ , the  $\text{CH}_4$  concentration exhibited about a 2.5% value, however, the temperature increased above  $1320^\circ\text{C}$ , the  $\text{CH}_4$  concentration level dropped below 1000 ppm (parts per million) level. Normally a coal gasifier operation requires a methane level less than a few hundred ppm for smooth slag formation and discharge through the slag tap hole (19).

Recent studies (3, 17, 19, 20, 21) demonstrate that during coal gasification, the concentration of CH<sub>4</sub> and other hydrocarbons remain almost constant at low as well as at high temperatures. This is not because of the methanation reaction but is mainly due to the pyrolysis process by which CH<sub>4</sub> is produced, as has been claimed by numerous researchers (20-23). However, a slight change in CH<sub>4</sub> production during coal gasification has been reported, due mainly to the formation and consumption of CH<sub>4</sub> in exothermic reactions at low and high temperatures, respectively (21). Kim et al. (24) have shown that when rising temperatures reach the range of 750 to 850°C, CH<sub>4</sub> concentration starts decreasing from 16.7 to 8.9%. However, an opposite trend is observed for the rest of the hydrocarbons such that their concentrations increase with the increase of temperature. This may be because of the use of low oxygen-to-coal ratio which causes reduction in the reaction of volatiles; the rising gasifier temperature in turn increases the contents of hydrocarbons. It is also common knowledge that during coal gasification, methane is produced by the heterogeneous and homogeneous exothermic reactions (methanation and methane steam reforming). However, the combustion reaction starts consuming methane as a result of which CH<sub>4</sub> concentration does not change significantly with the variation of temperature (25, 26).

#### **2.4 Tunable Diode Laser Technology**

Heppner (10) demonstrates that tunable diode laser technology has the potential to be used in harsh environments. The reason the instrumentation equipment is not influenced by harsh environments is because tunable diode laser technology is non-invasive and the interaction with severe conditions is done only by the laser. There is, however, one main difficulty which occurs during gasification measurement with this

laser diagnostic. Heppner (10) describes this challenge: ‘The pressures at which the gasifier will operate broaden the absorption spectra of the constituents, making it difficult to achieve a clear wavelength at which absorption takes place’ (p.3).

Stanford’s High Temperature Gas Dynamics Laboratory has addressed this issue and has produced a probe that can accurately measure temperature and flow constituents at 147 psi at 80°F to match the density of 734 psi at 2240°F. The Stanford probe makes use of a wavelength-multiplexed approach that produces light at different wavelengths (10). The precise temperature can then be calculated by measuring the ratios of absorption from the different wavelengths provided by the laser.

## **2.5 Modeling of Temperature in Entrained Flow Gasifier**

### **2.5.1 Polynomial Model**

A polynomial model is described as a compilation of essential mathematical and statistical methods helpful for improving and optimizing processes in which a response of interest is affected by several inputs (27). This collection of techniques can be used to investigate the relationships between the response and the independent variables. The graphical perspective of the mathematical model is reflected in the term *Response Surface Methodology*. The relationship between the response and the input is given in equation (2.1):

$$\eta = f(x_1, x_2, \dots, x_n) + \varepsilon \quad (2.1)$$

where  $\eta$  is the response,  $f$  is the unknown function of response,  $x_1, x_2, \dots, x_n$  denote the independent variables (also called *natural variables*),  $n$  is the number of the independent

variables and finally  $\varepsilon$  is the statistical error that represents other sources of variability not accounted for by  $f$ . It is generally assumed that  $\varepsilon$  has a normal distribution with mean zero and variance.

After selection of the design, the model equation is defined and its coefficients are identified (28). The equation used in polynomial model is generally a full quadratic or a diminished form of this equation. The second order model can be written as follows:

$$y = \beta_0 + \sum_{j=1}^k \beta_j X_j + \sum_{j=1}^k \beta_{jj} X_j^2 + \sum \sum_{i < j} \beta_{ij} X_i X_j \quad (2.2)$$

where  $\beta_0$ ,  $\beta_i$ ,  $\beta_{ii}$  and  $\beta_{ij}$  are regression coefficients for intercept, linear, quadratic and interaction coefficients respectively and  $X_i$  and  $X_j$  are coded independent variables.

The matrix notation of the model is given in equation 2.3,

$$y = X\beta + \varepsilon$$

$$\begin{bmatrix} y_1 \\ y_2 \\ \cdot \\ \cdot \\ \cdot \\ y_n \end{bmatrix} = \begin{bmatrix} 1 & x_{11} & x_{12} & \cdot & \cdot & x_{1k} \\ 1 & x_{21} & x_{22} & \cdot & \cdot & x_{2k} \\ \cdot & \cdot & \cdot & \cdot & \cdot & \cdot \\ \cdot & \cdot & \cdot & \cdot & \cdot & \cdot \\ \cdot & \cdot & \cdot & \cdot & \cdot & \cdot \\ 1 & x_{n1} & x_{n2} & \cdot & \cdot & x_{nk} \end{bmatrix} \begin{bmatrix} \beta_0 \\ \beta_1 \\ \cdot \\ \cdot \\ \cdot \\ \beta_k \end{bmatrix} + \begin{bmatrix} \varepsilon_1 \\ \varepsilon_2 \\ \cdot \\ \cdot \\ \cdot \\ \varepsilon_n \end{bmatrix} \quad (2.3)$$

The system of equations given above is typically solved using the method of least square which is a multiple regression technique. In the method of least square, it is assumed that random errors are identically distributed with a zero mean and a common unknown variance and they are independent of each other. The difference between the

observed and the fitted value ( $\bar{y}$ ) for the  $i$  th observation  $\varepsilon_i = y_i - \bar{y}$  is called residual and is an estimate of corresponding  $\varepsilon_i$ . The criteria for choosing the  $\beta_j$  estimates is that they should minimize the sum of the squares of the residuals which is often called the sum of squares of the errors and is denoted by SSE. Thus,

$$\text{SSE} = \sum_{j=1}^n \varepsilon_i^2 = \sum_{j=1}^n (y_i - \bar{y}_i)^2 \quad (2.4)$$

The residuals may be written as

$$\varepsilon = y - X\beta \quad (2.5)$$

and the SSE is

$$\text{SSE} = \varepsilon^T \varepsilon = (y - X\beta)^T (y - X\beta) \quad (2.6)$$

Differentiating the SSE with respect to  $\beta$ , a vector of partial derivatives can be written as:

$$\frac{\partial}{\partial \beta} (\text{SSE}) = -2X^T(y - X\beta) \quad (2.7)$$

Equating this derivative to zero,  $X\beta = y$  is found and this over-determined system of equations could be solved directly to obtain the coefficients of  $\beta$  by the following:

$$\mathbf{X}^T\mathbf{X}\boldsymbol{\beta} = \mathbf{X}^T\mathbf{y} \quad (2.8)$$

The formal solution of these equations is then

$$\boldsymbol{\beta} = (\mathbf{X}^T\mathbf{X})^{-1}\mathbf{X}^T\mathbf{y} = \mathbf{C}\mathbf{X}^T\mathbf{y} \quad (2.9)$$

where

$$\mathbf{C} = (\mathbf{X}^T\mathbf{X})^{-1} \quad (2.10)$$

Where C is a square matrix (28). After the regression coefficients were obtained, the estimation response could be easily calculated using model equation.

### 2.5.2 Power Law

Chavan et al. (29) have recommended that the power law or another term, ‘multivariate regression model (MVR)’ is a well-known method for developing multi-input single-output regression models. It can also be employed for developing multivariable nonlinear regression models. In this study, power law models were developed using Matlab software program for temperature estimation of coal gasification in entrained flow gasifier.

The power law model comprises two types of models, namely power-nonlinear and power-linear regression, respectively. The power law with nonlinear regression model (MNR) with two or more predictor variables ( $x_1, x_2, \dots, x_n$ ) is given as



$$y = a_0 x_1^{a_1} x_2^{a_2} x_3^{a_3} \dots x_{n-1}^{a_{n-1}} x_n^{a_n} \quad (2.11)$$

where  $a_i$  ( $i=0,1,2,\dots,n$ ) represent constants to be estimated. The multipower linear regression (MLR) can be stated as

$$y = a_0 + a_1 x_1 + a_2 x_2 + \dots + a_{n-1} x_{n-1} + a_n x_n + e \quad (2.12)$$

where  $e$  represents the residual. The MLR problem is easier to solve than the MNR problem. It is, however, possible to convert equation 2.12 into a multivariable linear regression problem by taking logarithms of both sides:

$$\log(y) = \log(a_0) + a_1 \log(x_1) + \dots + a_{n-1} \log(x_{n-1}) + a_n \log(x_n) \quad (2.13)$$

The constants of equation 2.14 can be now estimated using the standard MLR strategy.

### 2.5.3 Estimation of Sensitivity Coefficients of Nonlinear Model

Fang and Gentner (30) state that most of the existing sensitivity analysis methods imply the assumption of independence in their development. In other words, there is no generally applicable method for sensitivity analysis when correlation is encountered. Without considering correlation, sensitivity analysis will likely lead to incorrect conclusions and the ultimate purpose for conducting the sensitivity analysis will be irrelevant. That is why it is important to develop a generally applicable method for sensitivity analyses for correlated model inputs (30).

Based on computational experimental design, parameter sensitivity can be assessed by building response surface models. Using response surface models, the estimated coefficients of the response surface model are used as measures of parameter sensitivity (31). When model inputs are correlated, random samples can be generated based on nonparametric statistical methods for building response surface models. However, as Davis and Helton (32) first discovered, the coefficients of a response surface model can not be used as a reliable measure of parameter sensitivity when model inputs are correlated.

Another computation based approach for conducting sensitivity analysis is based on ‘one-parameter-at-a-time’ sampling to generate sequential random samples for estimation of sensitivity coefficients of input parameters (33). The one-parameter-at-a-time sequential sampling method is convenient and easy to implement when input parameters are independent. Measures of sensitivity are directly estimated with the sampled model inputs and corresponding model outputs.

The objectives of this study are to develop an algorithm for generating sequential random samples of multinormal distributions for estimation of sensitivity coefficients of selected input parameters based on the one-parameter-at-a-time method, and to study the effects of correlation in the sensitivity analysis for Australian bituminous coal.

In a sequential random sample, the difference of two vector immediate neighbor vectors is only the random number of one parameter. In addition, the difference of model outputs corresponding to a pair of immediate neighbor vector is caused by the change of only one model input parameter. Therefore, sensitivity coefficients can be estimated

based on the differences of model outputs and inputs (30). The expression of sensitivity analysis can be written follows:

$$\widehat{SC}_i = \frac{1}{n} \sum_{j=1}^n \frac{\Delta y_{ij}}{\Delta x_{ij}} \quad (2.14)$$

Where  $\widehat{SC}_i$  is the estimated sensitivity coefficient of model input  $x_i$ ,  $\Delta x_{ij}$  and  $\Delta y_{ij}$  are respectively, the  $j$  th differences of  $x_i$  and model output  $y$  caused by the change of  $x_i$ , and  $n$  is the sample size. The estimated sensitivity coefficients are global. Essentially, eq. (2.14) is the Monte Carlo integration approximation of the integral:

$$\int_{-\infty}^{\infty} \dots \int_{-\infty}^{\infty} \frac{\partial y}{\partial x_i} f(x) dx_1 \dots dx_p \approx \frac{1}{n} \sum_{j=1}^n \frac{\Delta y_{ij}}{\Delta x_{ij}},$$

Where  $f(x)$  is assumed to be a multinormal distribution function.

Sobol (33) approaches this method with another way and points out that when the  $k$  input parameters of the model are mutually independent, such a sequential random sample is not difficult to generate. Firstly, an order to sample the numbers for the parameters are determined. Second, independently  $k$  random numbers are generated to form the first random vector. Third, according to the sampling order, independently a random number for the specific parameter is generated to replace the corresponding one in the preceding random vector to form a new vector (26, 34). The global sensitivity is given by the following formula:

$$\widehat{SC}_{ji} = \sqrt{\sum_{k=1}^k (SC_{ji}^{(k)})^2} \quad (2.15)$$

Where k is the total number of available patterns and  $SC_{ij}$  refers to sensitivity of j th output with respect to i th input. The sensitivities were later normalized to get the percentage sensitivity as given below:

$$\% \widehat{SC}_{ji} = \left( \frac{SC_{ji}}{\sum_{i=1}^j SC_{ji}} \right) * 100 \quad (2.16)$$

## **CHAPTER 3**

### **SIMULATION SETUP AND PROCEDURE**

The ChemCAD simulation program was used to determine coal conversion, cold-gas efficiency, coal gasification products, and the adiabatic flame temperature. The latter occurs exclusively in the presence of adiabatic conditions, which in turn are created solely by the Gibbs free reactor. This reactor offers the additional advantages of preventing heat loss to the outside. The application of the ChemCAD and the design of the Gibbs free reactor will be explained in the following pages.

#### **3.1 Shell Gasification Diagram Setup**

The Gibbs reactor was selected as the entrained flow gasifier because it provides the adiabatic conditions for coal gasification. Before coal particles are fed into the reactor, a slurry system was formed with coal and water. Then the upper side went through the vertical reactor with nitrogen and oxygen streams. The temperature of coal and water were held as 313 K and this value did not change during the simulation runs. In addition, the temperature of oxygen and nitrogen were kept constant as 333 K. The flow of coal for both types was set to 1000 kg/h. The development of the Shell gasification diagram and the Gibbs free reactor design were displayed with detailed explanations. The reason of the selection of Gibbs free reactor is that it does not require the stoichiometric ratio of components which consist of coal gasification.

### 3.2 The Gibbs Free Reactor

The Gibbs reactor model is often preferred to simulate reactors for the purpose of heat and material balances. Product rates, compositions, and thermal conditions are calculated by the minimization of Gibbs free energy, subject to an overall mass balance. All components in the component list (for the current flowsheet) are considered in the Gibbs free energy minimization calculation unless specifically excluded (identified as inert).

The minimum information required by the Gibbs reactor is the identity of the feed and product streams for standard database components. Temperature and/or pressure may be set if different from those derived from the feed stream(s). The other conspicuous characteristic of this reactor is stated that no reaction stoichiometry is required when the reactions are identified in the program. Although the reactor could be operated isothermally at a specified temperature, or at the feed temperature, it was designed in adiabatic conditions in this study. Finally, heat may be added or removed, and temperature limits are definitely imposed (35).

For user-supplied or pseudo-components, the free energy of formation, molecular weight and heat capacity must be supplied. For solid components, the free energy of formation, the heat of formation, molecular weight, and heat capacity must be present in the database. Apart from this, it is important to point out that several overall constraints are imposed on the reaction. The gasifier temperature approach to chemical equilibrium for the entire reacting system can be specified. In this case, the chemical equilibrium is determined at  $T + \Delta T$ , while the properties are computed at  $T$ , where  $T$  is the reactor temperature and  $\Delta T$  is the approach to chemical equilibrium.

### 3.3 Methods and General Assumptions

#### 3.3.1 Method and Approach

The Gibbs reactor is based on the principal that at chemical equilibrium the total Gibbs energy of the system has its minimum value. In an attempt to minimize the total energy of the system, individual equilibria constants are not examined. Rather, the possible reaction species are noted, and the distribution of these species is established using a general mathematical technique to give a minimum free energy for the system. Thus, for any reaction system, all important species are expatiated and solution is carried out without prior knowledge of the chemistry of the system. The solution so achieved will satisfy all expected equilibria and be accurate within the limits of the thermodynamic data (36). To obtain the same solution using individual equilibrium constants would require knowledge of the reactions involved (the equilibrium reactor uses this method). Free energy minimization is accomplished with these steps:

- a) Develop expressions for the free energy of the system.
- b) Write an expression for the free energy of a mixture of assumed composition, i.e., assumed concentrations of the various species to be deliberated.
- c) The free energy of the equilibrium mixture (composition unknown) is expressed in terms of the assumed mixture and in unknown increments which represent the changes needed to bring the assumed mixture composition to the final equilibrium composition. The expression used involves the first two terms of a Taylor series and is termed a 'quadratic approximation'.
- d) The expanded function, i.e., quadratic approximation, is minimized to simplify the equations.

e) As a result of the manipulations involved, a system of linear simultaneous equations is obtained in as many unknowns. When solved, the system yields a new composition that represents a new approximation of the composition which gives minimum free energy.

f) The procedure is repeated until the calculated and prior compositions are identical.

At this point, the free energy of the system is at a minimum.

The above approach for computing fugacity is effective only if the equation of state we use is adequate. This may not be true for two reasons. First, the equation may not adequately represent the compound itself, even in the pure state. Second, the mixing rules of the equation may not sufficiently interpret or quantify what happens to a molecule when it is in solution. This can happen for many reasons but frequently it is due to the failure to adequately model intermolecular forces. In such a case, an alternative approach is taken (36). Define activity,  $\alpha_i$ , as follows:

$$\alpha_i = \frac{f_i^-}{f_i^\circ} \quad (3.1)$$

where  $f_i^-$  is the fugacity of the component in solution and  $f_i^\circ$  represents the fugacity of the component at some arbitrarily defined standard state. The activity coefficient ( $\gamma$ ) is also defined as

$$\gamma_i = \frac{a_i}{x_i} = \frac{f_i^-}{x_i f_i^\circ} \quad (3.2)$$



Thus, equation 3.2 can be written as,

$$f_i^- = x_i \cdot \gamma_i \cdot f_i^o \quad (3.3)$$

From the Gibbs-Duhem relations, it can be demonstrated for one mole of solution:

$$\Delta(G_i^- - G_i^o) = \sum_i x_i RT \ln \gamma_i \quad (3.4)$$

Where  $x_i$  is the molar liquid fraction of  $i^{\text{th}}$  component,  $R$  is the ideal gas constant,  $T$  is temperature and  $\gamma_i$  defines the activity coefficient.

$$\Delta(G_i^- - G_i^o) = \text{Total excess Gibbs free energy}$$

The difference between the Gibbs free energy of the component in the solution and the Gibbs free energy of the component in the standard state, is called the excess Gibbs free energy. The term  $\Delta(G_i^- - G_i^o)$  is the change in excess Gibbs free energy for the entire solution.

We can thus, approach  $\gamma_i$ , by relating it to the excess Gibbs free energy of solution,  $\cong G^E$ . However, since  $\cong G^E$  cannot be directly measured, this is virtually always taken as a theoretical framework or starting point. In the final analysis, the value of  $\gamma_i$ , must be directly correlated over narrow data ranges. This is done through the use of binary interaction parameters or BIPs. ChemCAD provides a BIP database, as well as a

data regression facility through which these BIPs can be directly correlated from phase equilibrium data. Thus, activity coefficients are a function not only of the component for which they are computed, but also of the nature and quantity of the other components in the solution. In addition, the activity coefficients themselves are computed semi-empirically, i.e., the approach has a theoretical basis but the application is dependent on parameters correlated over specific data ranges.

At equilibrium, all net driving forces are zero and, thus, all thermodynamic properties such as U (free energy), A (Hemholtz free energy), G (Gibbs free energy), etc., are minimized. Mathematically, for any quantity, the first derivative of that quantity equals zero at either a maximum, a minimum, or an inflection point. Since the second law of thermodynamics states that energy always flows downhill, the free energy functions U, A, and G should be minimized.

$$dU = dA = dG = 0 \quad (3.5)$$

Here, there are some options:

Since  $dU = TdS - PdV$ , if S and T are fixed (i.e., known, measured), U can be minimized.

Since  $dA = -PdV - SdT$ , if V and T are fixed, A is minimized as well. Since  $dG = VdP - SdT$ , if P and T are fixed, G may be minimized. For all purposes it is best to attempt to

minimize G because T and P are easily measured. For a closed two-phase system,

$$dG = dG_1 + dG_2 \quad (3.6)$$

For any given phase,

$$\text{Phase 1 : } dG_1 = \sum_1^l G_{1l}^- dn_{1l} \quad (3.7)$$

$$\text{Phase 2 : } dG_2 = \sum_1^l G_{2l}^- dn_{2l} \quad (3.8)$$

Where  $G_{1l}$  defines the Gibbs energy of first component in liquid phase  $G_{2l}$  explains the Gibbs energy of second component in liquid phase. Therefore,

$$dG = \sum_1^l G_{1l}^- dn_{1l} + \sum_1^l G_{2l}^- dn_{2l} \quad (3.9)$$

Conservation of mass requires that  $dn_1 = -dn_2$ . Hence,

$$dG = \sum_1^l (G_{2l}^- - G_{1l}^-) dn_2 \quad (3.10)$$

In order for equation 3.10 to be generally valid, it cannot depend on any particular choice of the  $dn_i$ . Thus, the total Gibbs free energy will be a minimum ( $dG = 0$ ) for an arbitrary choice of the  $dn_i$  only if

$$G_{2i}^- = G_{1i}^- \quad (3.11)$$

for all components. Thus, at equilibrium the partial molar Gibbs free energy of each component must be the same in each phase present in the system. In other words,

$$f_{1i}^- = f_{2i}^- \quad (3.12)$$

Therefore, partial Gibbs free energy of any component in the system can be used to specify the characterization of the other components due to the equality of fugacity. This approach is beneficial to convert the chemical properties of components, especially, when the equation is written by another fugacity term in order to find the target point.

### 3.3.2 Overall Assumptions

In this simulation, Australian bituminous (type 1) and Indonesian roto coal (type 2) in the entrained flow gasifier have been evaluated and different parameters such as system pressure, oxygen-to-coal feed ratio and steam-to-coal feed ratio were utilized to predict not only the adiabatic flame temperature of gasifier but also the amount of product gases. The compositions of coal types are annotated in this chapter. The boundary conditions were taken around the gasifier. The Shell gasification diagram was drawn in Figure 3.1 and a simulation using ChemCAD has been performed. Some suppositions, which are necessary to build up the properties of various streams and gasifier type, were made and explained below before designing the reactor.

An entrained flow gasifier which exists on a large scale because of envisaged products is characterized by coal particles dragged along with gas stream. Large scale coal particles generally mean lower specific costs and heat integration is easier. Small coal particles, typically 100  $\mu\text{m}$ , were used in this simulation. The coal gasification was performed at a high temperature to achieve high efficiency. Since the entrained flow gasifier operates at a high temperature, it results in a CO- and H<sub>2</sub>- rich gas (inevitably

also CO<sub>2</sub>). It was assumed to operate under pressure (typically 20-80 bar) with pure oxygen.

The two-phase flow was assumed to be steady-state and one dimensional. The gas phase reactions were assumed to reach equilibrium. The heterogeneous reactions between coal, steam and oxygen were considered as irreversible surface reactions. It was assumed that a pulverized coal was gasified with oxygen in a vertical reactor with co-current flow, and that the coal particles were moved by N<sub>2</sub> and injected to the so-called burner in the gasifier. The burner intends to realize a thorough mixing of coal and oxygen.

### **3.4 Simulation Procedure**

Gasification of Australian bituminous coal and Indonesian roto coal were performed by using ChemCAD simulation and design program. As mentioned before, one of the aims of this study was to ascertain the gasification products composition on a dry basis by moles %. Carbon monoxide, carbon dioxide, methane and hydrogen were the expected gasification products. The other gas products such as SO<sub>2</sub> and NO<sub>x</sub> were assumed as negligible. Finally, the essential gasification characteristics—coal conversion and cold gas efficiency—which give a general idea on the gasifier performance were merely examined.

Table 3.1 indicates the coal characteristics of Australian bituminous coal and Indonesian roto Coal, respectively. The proximate analysis and ultimate analysis based on weight % were tabulated for two different coal types. These findings were taken from previous studies (35, 37). The amount of carbon in Indonesian roto coal was higher than the amount of carbon in Australian bituminous coal.

However, the percentage of oxygen and hydrogen by weight in Indonesian roto coal were lower than those of the Australian coal type. Table 3.2 interprets ash contents of the two types of coal.

The first step to integrate the coal gasification and coal properties into ChemCAD program was to select the engineering unit selection. Here, the Alt SI engineering system was chosen for all simulation runs. The unit of temperature was Kelvin, the unit of pressure of all stream were selected as bar. MJ/h unit system was integrated to enthalpy of Shell gasification diagram. Finally, the unit of mass flow rate of the streams were kg/h as seen in Figure 3.2.

Another important step was to create a component which did not exist in the ChemCAD component database. Firstly, this simulation program actually does not perceive these two types of coal even though the gasification products such as methane, sulfur dioxide or carbon monoxide exit the component database. Australian and Indonesian coals needed to be introduced into the simulation program. As illustrated in Figure 3.3, from the toolbar of the program, 'create new component' is chosen with the assistance of the thermophysical part and component database section. After clicking on the new data component heading, new component section appears as seen in Figure 3.4 which demonstrates the introduction of Indonesian coal into the program. The heart of this step is to select the combustion solid for new components (see Figure 3.4) due to the fact that coal typically is a combustible fuel.

After the combustion solid is pointed out in the database, the next step is to introduce the coal properties of various coal types into the database. The coal properties of Indonesian roto coal by weight are displayed in Figure 3.5. The same procedure is also

applied for Australian bituminous coal. Figure 3.5 provides two options for users. The coal properties basically can be written either by weight or by stoichiometric terms. Thus, the coal properties of those coal types were written by weight percentage. If the heat capacity of coal or the solid heat capacity are known for each new component, it would be better to add into the solid component part located the bottom of this section. If not, the heat capacity or solid heat capacity of coals can be written in terms of properties of carbon element as well.

The ChemCAD program is now aware of these new components before coal gasification as exhibited in Figure 3.6. The chemical formulas are already presented in the database. When these types of coal are wanted to use for simulation, it is enough to write these components' name in the 'select component button' for users.

For example, if the user wants to change the properties of components, it is very easy to do in the program. Figure 3.7 displays the edit/view, plot or print for all components exist in the database. The components used during coal gasification can be selected from the component list and all their properties can also be seen from view/edit component data. If a new component is introduced into component list, all necessary characteristics should be written in the component data section. After ChemCAD identifies the new component in the database, the user may use the synonyms and formulas of those components as seen in Figure 3.8. The numbers located to the left side of each component show the element or molecular code. For instance, the code of nitrogen is 46, or code 2 describes the methane component in the database. The new code is always denoted when a new component is put in the component list. The code of Australian bituminous coal is automatically dedicated as 8003 (see Figure 3.8).

The other important component characteristics can be categorized as minimum required data, basic data, density data and heat capacity data. For each new component of simulation program, these properties must be found and introduced into the database as well. In this study, some of the properties of Australian bituminous coal and Indonesian roto coal such as polynomial heat capacity coefficients and heat of formation could not be found and were treated as carbon characteristics. Figure 3.9 demonstrates the minimum required data of Australian bituminous coal and before running a simulation, these essential terms must be put in the edit component section. The critical temperature and critical pressure were taken by 2778 K and 551 bar, respectively. Acentric factor of Australian coal was kept constant as 1.700 and specific gravity at 60 F was held as 2.38. Figure 3.10 illustrates the basic data of Australian bituminous coal. The normal boiling point and melting point were fixed as 4232 K and 4250 K, respectively. Finally, the molecular weight was taken 100 kg basis for both coal types. Liquid density and solid density were dedicated by ChemCAD (see Figure 3.11). The equation numbers for both phase were exhibited as 100 but the user does not see that equation clearly. Low and high temperature values, unfortunately, were taken from carbon features because of the fact that these terms could not be found in literature.

Gibbs free reactor provides an opportunity for users who want to perform the coal gasification simulation in ChemCAD program. It does not require the stoichiometric ratio for gasification and combustion reactions. ChemCAD determines the reactions and enthalpies of all reactions itself. Hence, the only requirement for set-up gasification is to select the reactants and products from the component database. Figure 3.12 displays the selected components for coal gasification. These different components are always seen in



each streams. The 'clear' and 'delete' options in the select components section also provide convenience for evaluating the design of diagram.

The evaluation of particle size is also possible for coal gasification. In this study, coal particle size is held at 100 micron. However, it is not an input parameter and this value did not change during the simulation. Then, the type of stream which is considered as solid combustion is chosen. Here, the coal stream is described as stream 2 and in the select streams part, this value should be written as shown in figures 3.13 and 3.14. The next step is to evaluate the thermophysical settings. Figure 3.15 is the main window for thermodynamic settings. All thermodynamic assumptions, equations and rules such as Henry law and Raoult's law are calculated in this section.

Figures 3.16 and 3.17 also explain what model are used in this simulation. Global K model is supposed as ideal vapor pressure or in other term as Raoult's law. No vapor phase association is another assumption for this part. Finally, latent heat is preferred as global enthalpy model. The Gibbs free energy reactor design is the last design configuration. Figure 3.18 and 3.19 indicate the operating conditions of Gibbs free reactor. The pressure drop is the same and kept constant as 1.5 bar. However, the pressure is being changed for every new parameter. The adiabatic conditions are taken into consideration due to the main purpose of this study is estimation of adiabatic flame temperature. Air/oxygen calculation is also determined by the program. The users only need to introduce which streams belong to fuel or air. Convergence parameters include minimum and maximum temperatures and they are 298 K and 3050 K, respectively. Then, the second screen named component element matrix occurs as shown in Figure

3.20. The matrix system explains the molecular composition of each reactant and products obtained in the coal gasification.

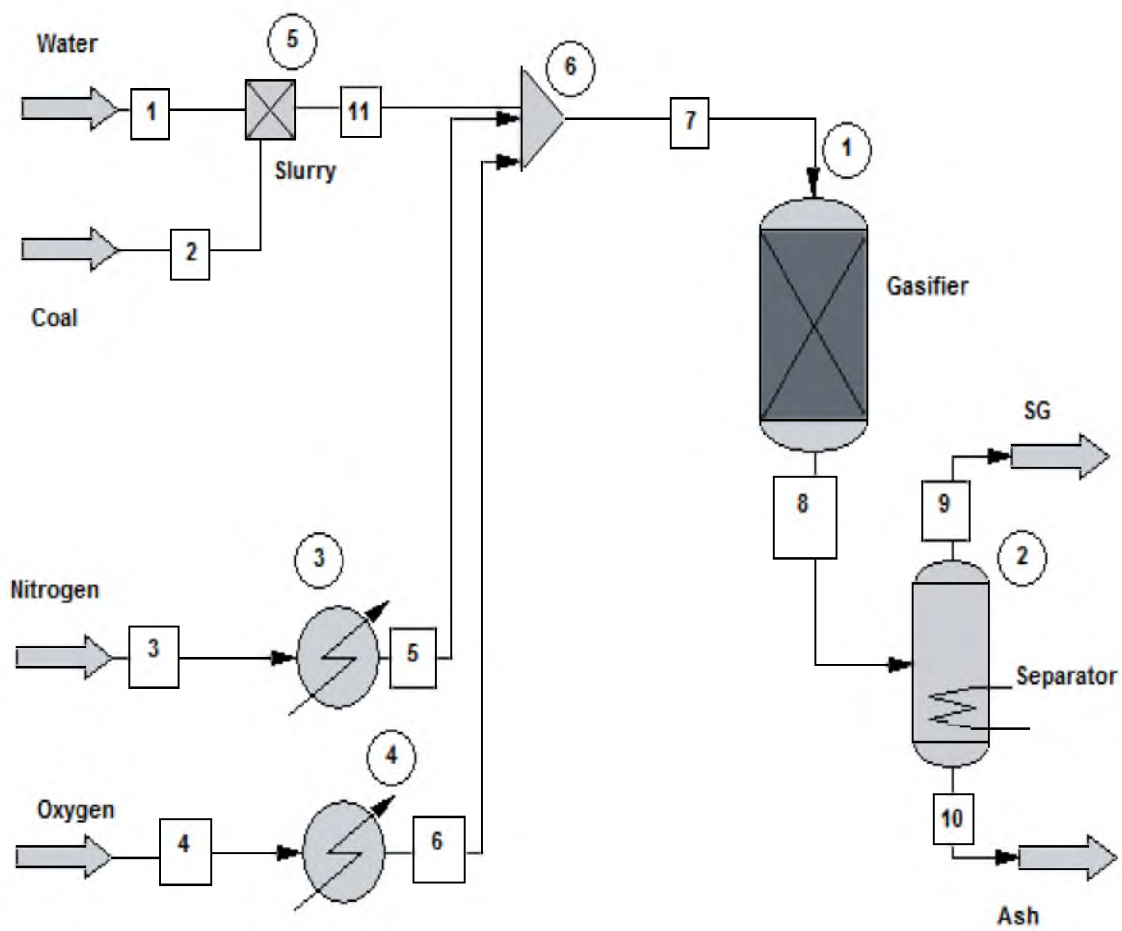
The Gibbs free energy reactor has an important advantage compared to other gasifier reactors. It does not require the stoichiometric ratio of reactions and enthalpy of formation as well. The reactions take place in the Gibbs free energy reactor and the composition of products gases or adiabatic flame temperature is the final state. The users can read the last values from stream 9 by clicking on it.

Table 3.1- Coal Properties, Proximate and Ultimate Analysis of Coal Types (34, 36)

	Parameter		
	Proximate Analysis(%weight)	COAL TYPE 1 Australian Bituminous	COAL TYPE 2 Indonesian Roto
Moisture		3.7	2.5
Volatile matter		29.6	48
Fixed Carbon		62.9	48
Ash		3.8	1.5
	Ultimate Analysis Dry base (%weight)		
Carbon		72.3	85
Hydrogen		4.3	1.9
Oxygen		13.7	4.1
Nitrogen		0.4	1.4
Sulphur		0.2	0.24
Chlorine		0.05	0.008
Ash		8.3	7.5
LHV		20.16414 (MJ/kg)	18.751(MJ/kg)

Table 3.2 - Ash Contents of Coals by Weight (34, 36)

	Ash Content weight % of Type 1 and Type 2	
	Australian Bituminous	Indonesian Roto
Al <sub>2</sub> O <sub>3</sub>	23	15.15
SiO <sub>2</sub>	55	37.93
Fe <sub>2</sub> O <sub>3</sub>	19.4	21.47
MgO	3.5	12.02
K <sub>2</sub> O	1.1	2.57



**Figure 3.1.** Shell gasification diagram

Engineering Unit Selection -

Units selection		Options and references	
Time	h	Liq. Density / Conc.	kg/m <sup>3</sup>
Mass/Mole	kg	Vapor Density	kg/m <sup>3</sup>
Temperature	K	Thickness	m
Pressure	bar	Diameter	m
Enthalpy	MJ	Length	m
Work	MJ	Velocity	m/sec
Liquid Volume	m <sup>3</sup>	Area	m <sup>2</sup>
Liquid Vol. Rate	m <sup>3</sup> /h	Heat Capacity	kJ/kg-K
Crude Flow Rate	m <sup>3</sup> /h	Specific Heat	kJ/kg
Vapor Volume	m <sup>3</sup>	Heat Trans. Coeff.	W/m <sup>2</sup> -K
Vapor Vol. Rate	m <sup>3</sup> /h	Therm. Conduct.	W/m-K
		Viscosity	N-s/m <sup>2</sup>
		Surf. Tension	N/m
		Solubility Par.	(J/m <sup>3</sup> ) <sup>-0.5</sup>
		Dipole Moment	C.m
		Cake Resistance	m/kg
		Packing DP	mm water/m
		Currency	\$
		Currency factor	1
		ALT SI	Save Profile
			Load Profile

English   Alt SI   SI   Metric   LoadDefault   SaveDefault   Cancel   OK

**Figure 3.2** Engineering unit selection

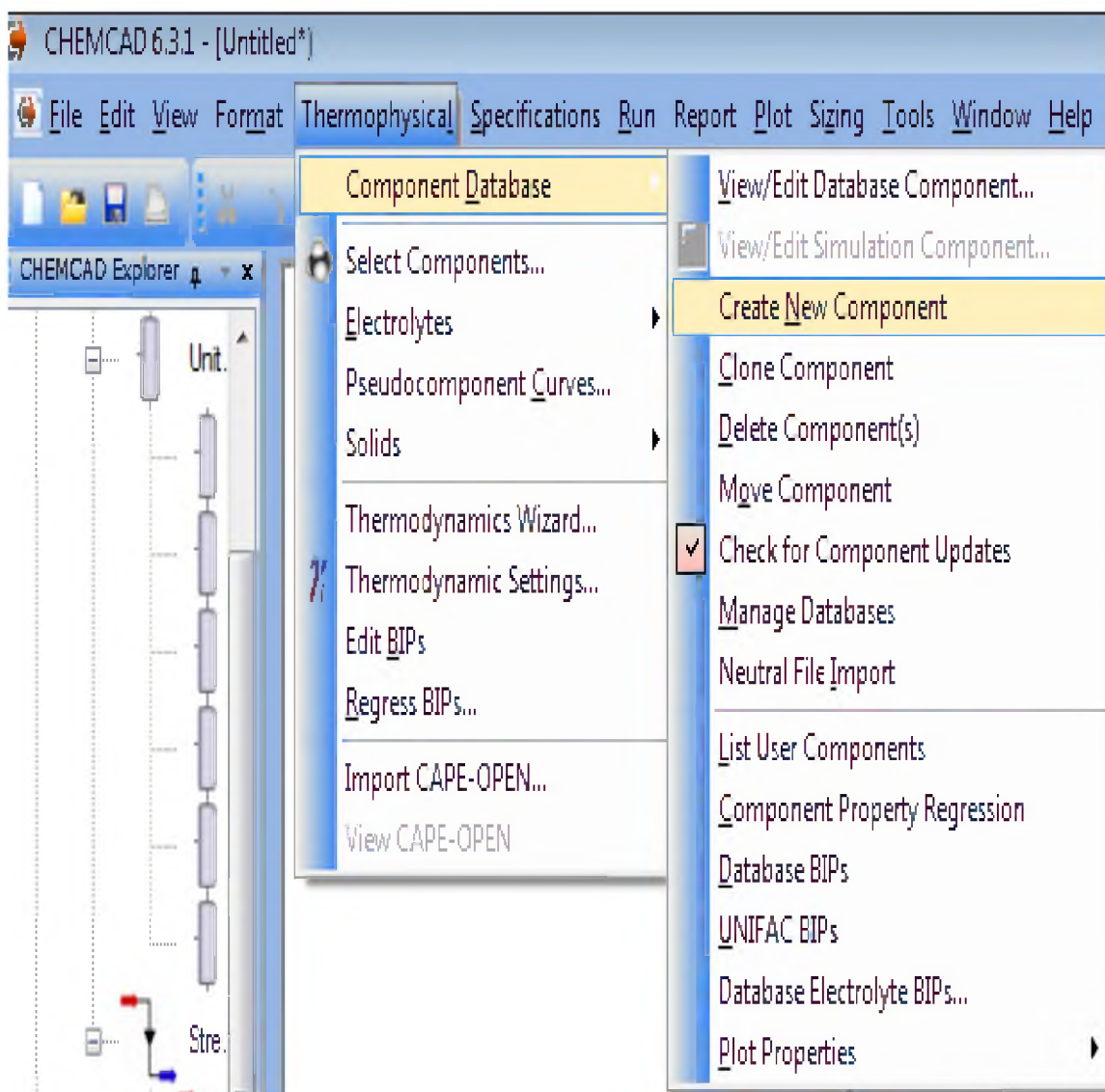
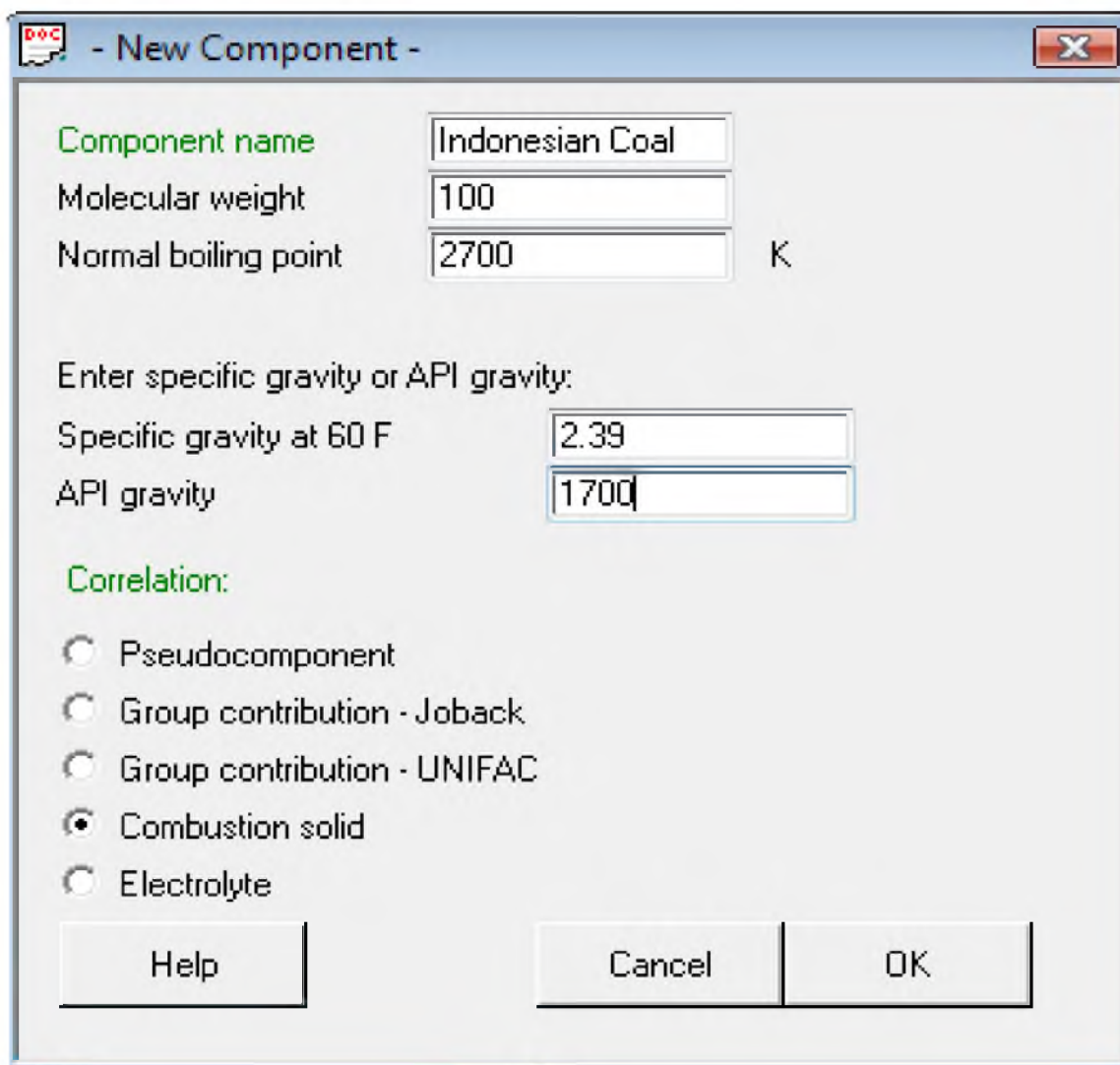


**Figure 3.3** Creating new component for simulation



**- New Component -**

Component name: Indonesian Coal

Molecular weight: 100

Normal boiling point: 2700 K

Enter specific gravity or API gravity:

Specific gravity at 60 F: 2.39

API gravity: 1700

**Correlation:**

- Pseudocomponent
- Group contribution - Joback
- Group contribution - UNIFAC
- Combustion solid
- Electrolyte

Buttons: Help, Cancel, OK

**Figure 3.4** Tool for new component expression

**- Combustion Solid -**

Solid Element Analysis

Element analysis basis: Weight %

Atom	Weight % or stoichiometrics	Atom	Weight % or stoichiometrics
C	85	Mg	0.9
H	2.1	Si	3.15
O	4.4	Al	1.125
S	0.24	Fe	1.575
N	1.4	K	0.225

Basis for heating value:

Net heating value  
 Gross heating value

Heating value:  kJ/kg

Solid heat capacity:  kJ/kg-K

**Figure 3.5** Introduction of coal properties



The image shows a software dialog box titled "- View/Edit Component Formulas -". It contains the following fields and controls:

- Standard Name:** A text field containing "Indonesian Coal".
- Formula 1:** A text field containing the chemical formula  $C7.07676H2.08354O0.267198S0.00748596N0.0999522Mg0.037029$ .
- Formula 2:** An empty text field.
- Formula 3:** An empty text field.
- Formula 4:** An empty text field.
- Buttons:** "Help", "Cancel", and "OK". The "Cancel" button is highlighted with a dotted border.

**Figure 3.6** View or edit Indonesian roto coal's formula

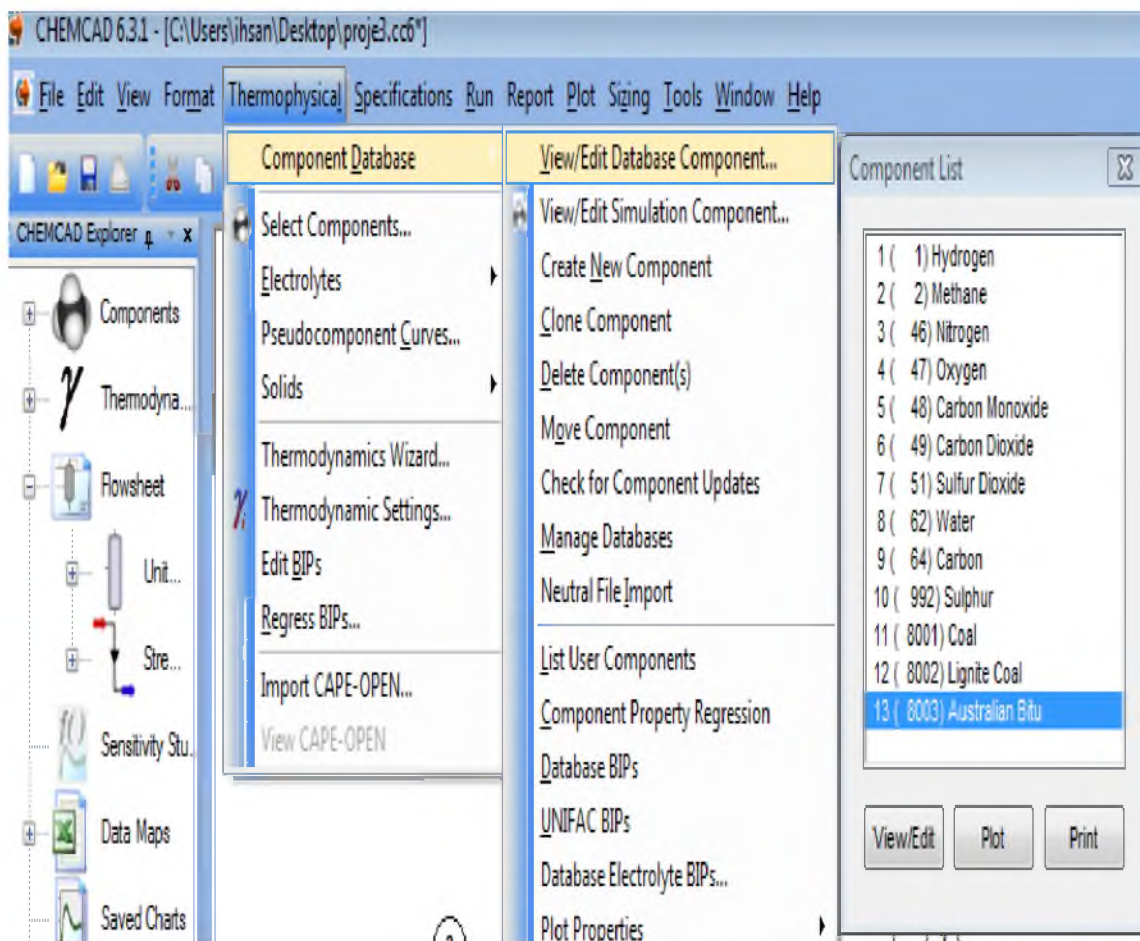


**Figure 3.7** Component list

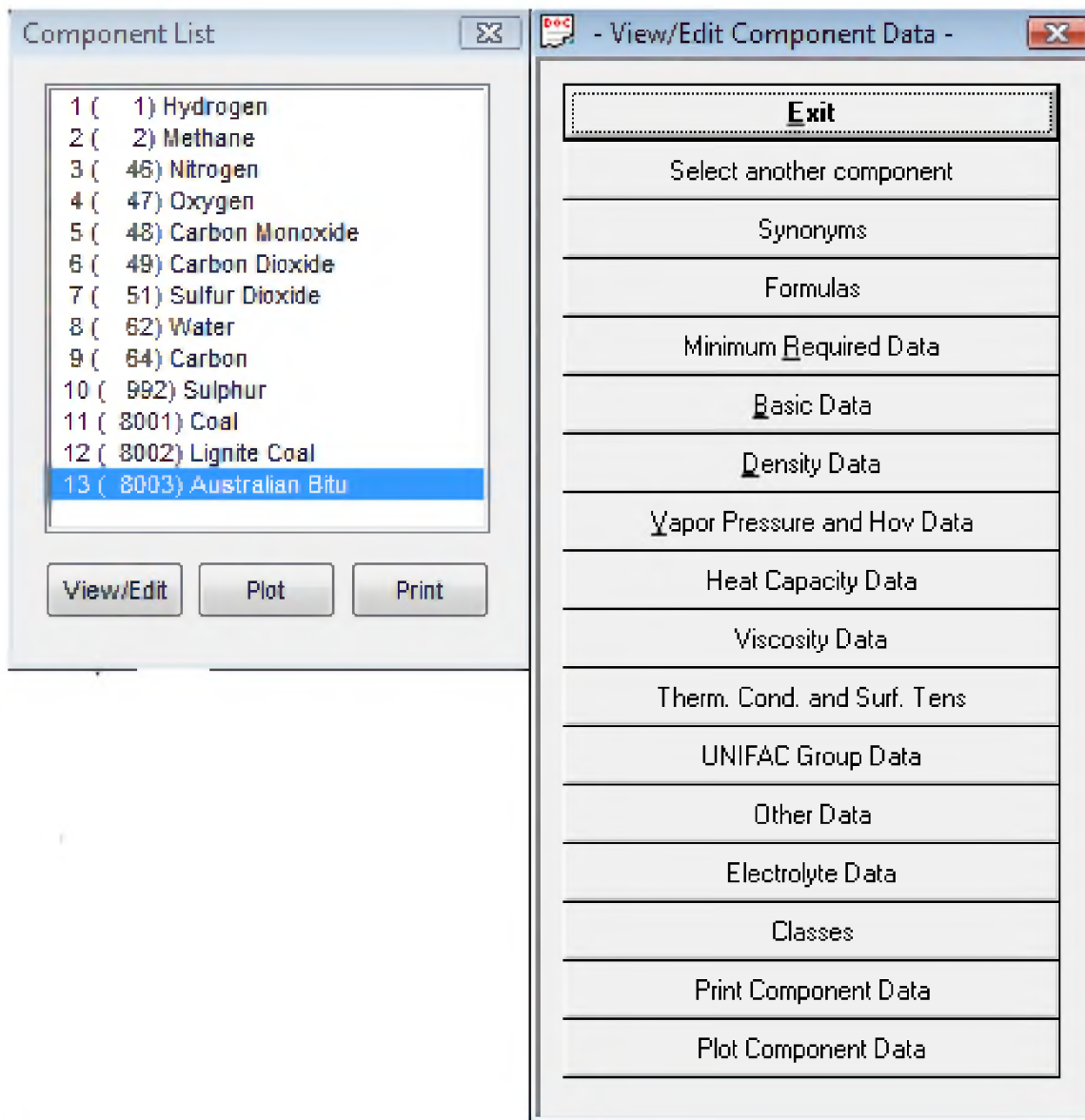


**Figure 3.8** View/Edit component data

Australian Bitu

Molecular weight	<input type="text" value="100"/>	
Critical T	<input type="text" value="2778.33"/>	K
Critical P	<input type="text" value="551.581"/>	bar
Acentric factor	<input type="text" value="1.7001"/>	
SG at 60 F	<input type="text" value="2.38"/>	

Polynomial Ideal Gas Heat Capacity (cal/mol-K)

Coefficient: A	<input type="text" value="4.99686"/>
Coefficient: B	<input type="text" value="-4.194e-005"/>
Coefficient: C	<input type="text" value="-3.0623e-008"/>
Coefficient: D	<input type="text" value="4.6342e-011"/>
Coefficient: E	<input type="text" value="-1.05292e-014"/>
Coefficient: F	<input type="text" value="7.13592e-019"/>

Help Cancel OK

**Figure 3.9** Minimum required data

- Basic Data -

Australian Bitu Component ID:

Molecular weight	<input type="text" value="100"/>	
Critical T	<input type="text" value="2778.33"/>	K
Critical P	<input type="text" value="551.581"/>	bar
Critical V	<input type="text" value="0.0187969"/>	m <sup>3</sup> /kmol
Acentric factor	<input type="text" value="1.7001"/>	
Normal boiling point	<input type="text" value="4232"/>	K
Melting point	<input type="text" value="4250"/>	K
Heat of Fusion	<input type="text" value="1.052e+008"/>	J/kmol

Enter either ideal gas or solid data

	Ideal Gas		Solid	
Heat of formation	<input type="text"/>	J/kmol	<input type="text" value="-3.03648e+009"/>	J/kmol
Gibbs of formation	<input type="text"/>	J/kmol	<input type="text" value="2.32601e+009"/>	J/kmol

Solubility parameter	<input type="text" value="76880.5"/>	(J/m <sup>3</sup> ) <sup>0.5</sup>
Dipole moment	<input type="text"/>	C.m

**Figure 3.10** Basic data of Australian bituminous coal

Australian Bitu

Liquid Density  
(kmol/m<sup>3</sup>)

Equation No.

Low T (K)  Low value

High T (K)  High value

Solid Density  
(kmol/m<sup>3</sup>)

Equation No.

Low T (K)  Low value

High T (K)  High value

Coefficients: A

B

C

D

E

Coefficients: A

B

C

D

E

**Figure 3.11** Library density data

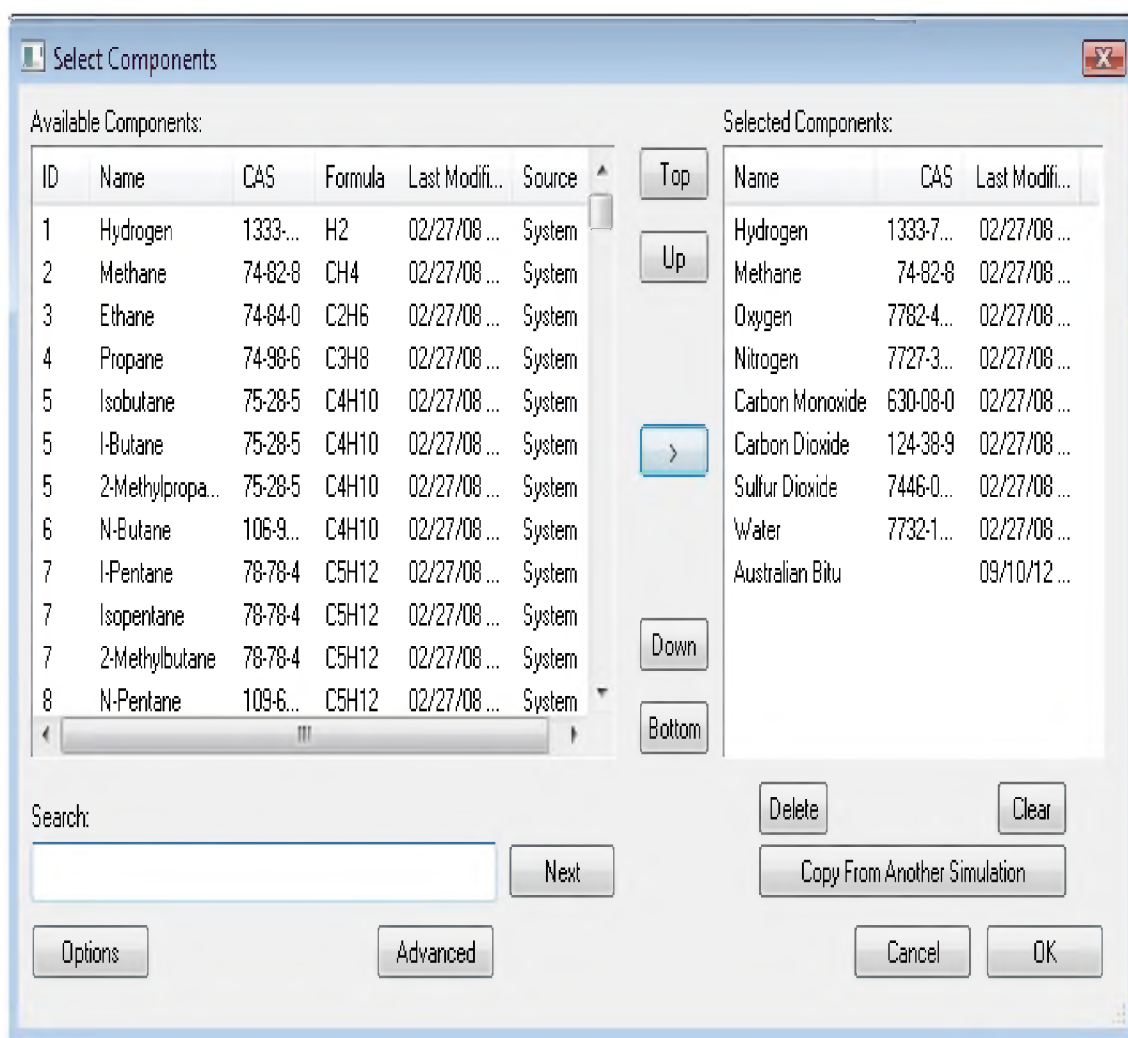


**Figure 3.12** Select components section

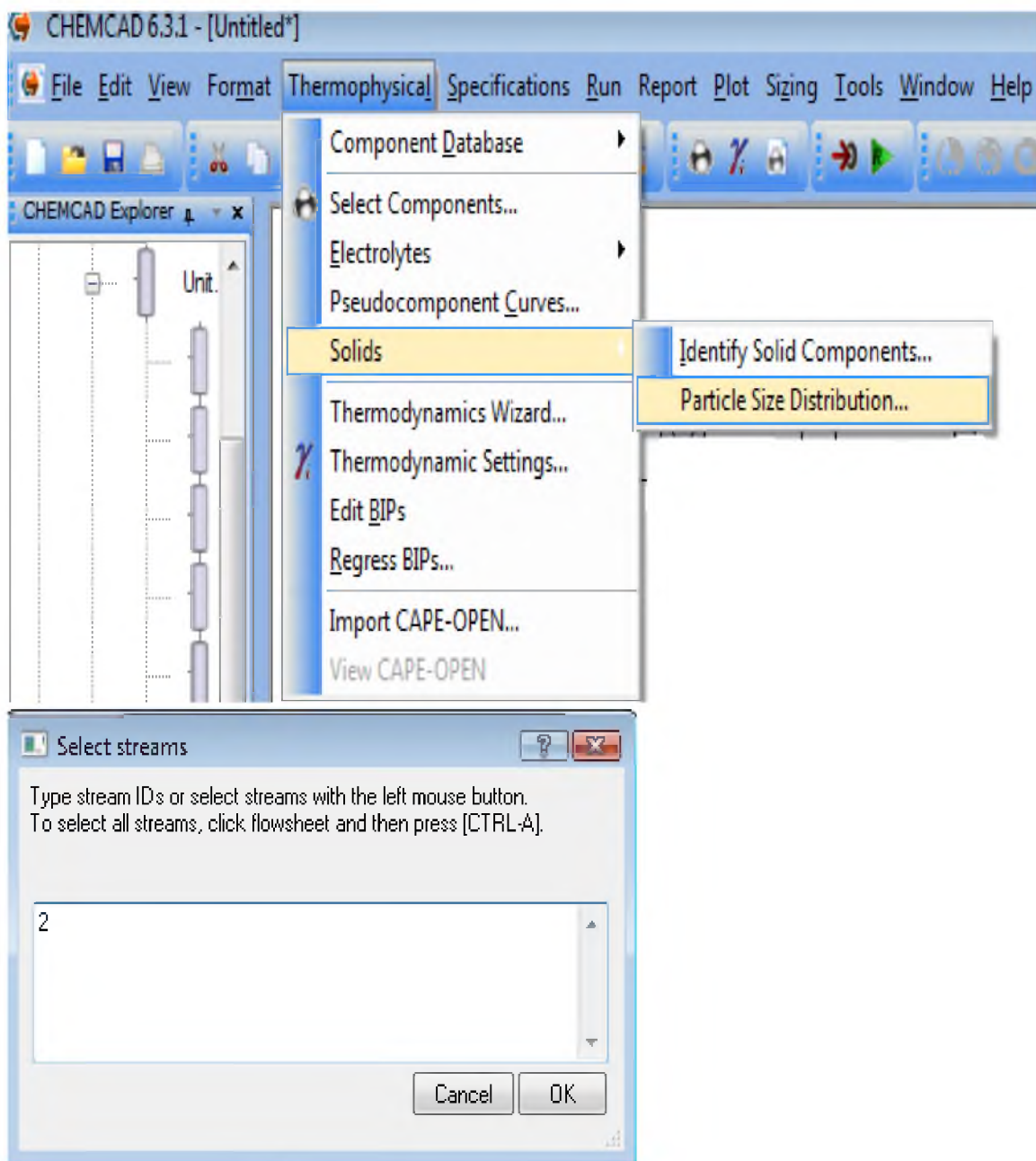


**Figure 3.13** Particle size distribution



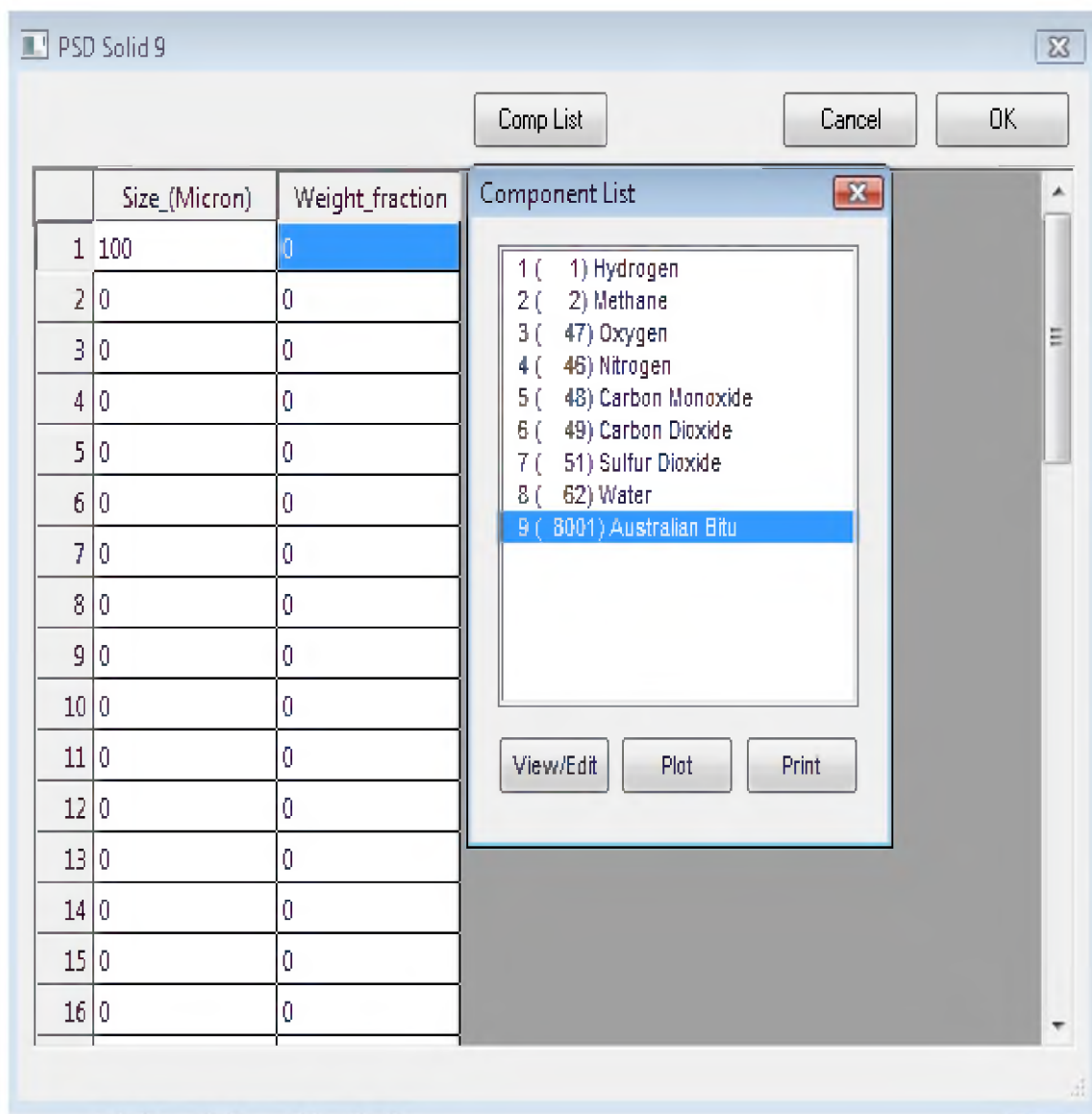


**Figure 3.14** Particle size of coal type

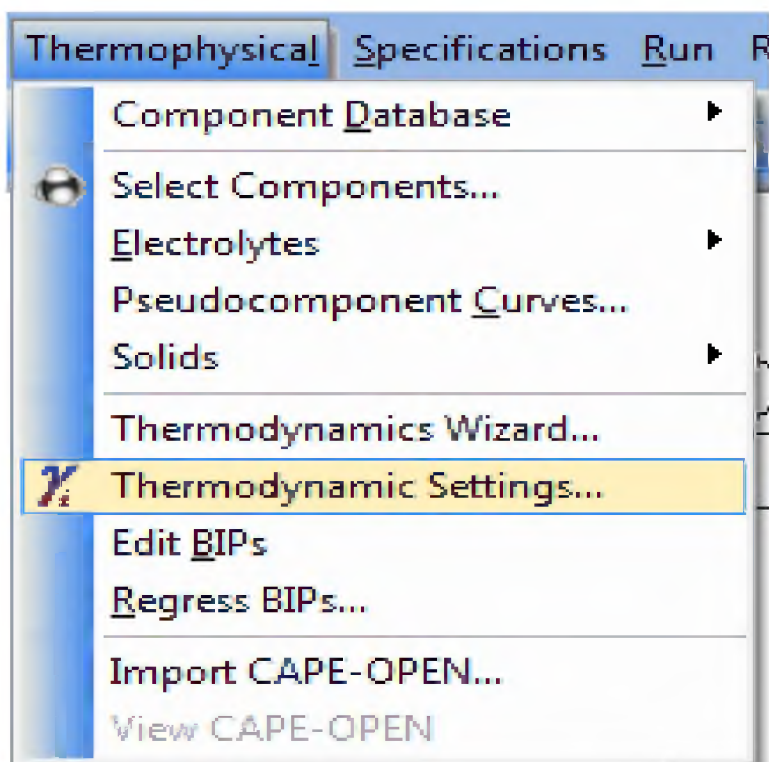


**Figure 3.15** Thermodynamic settings

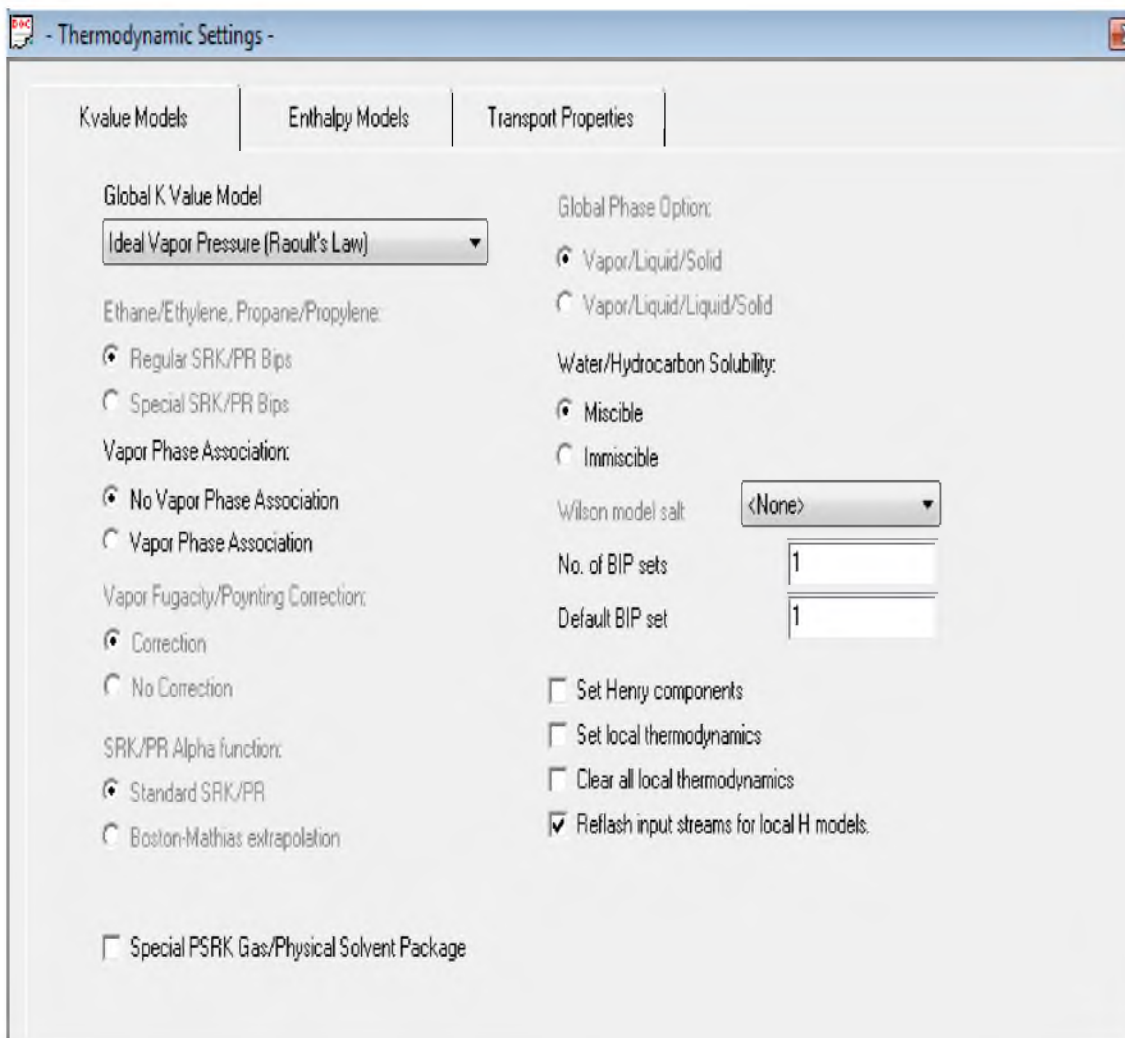


**Figure 3.16** K value models

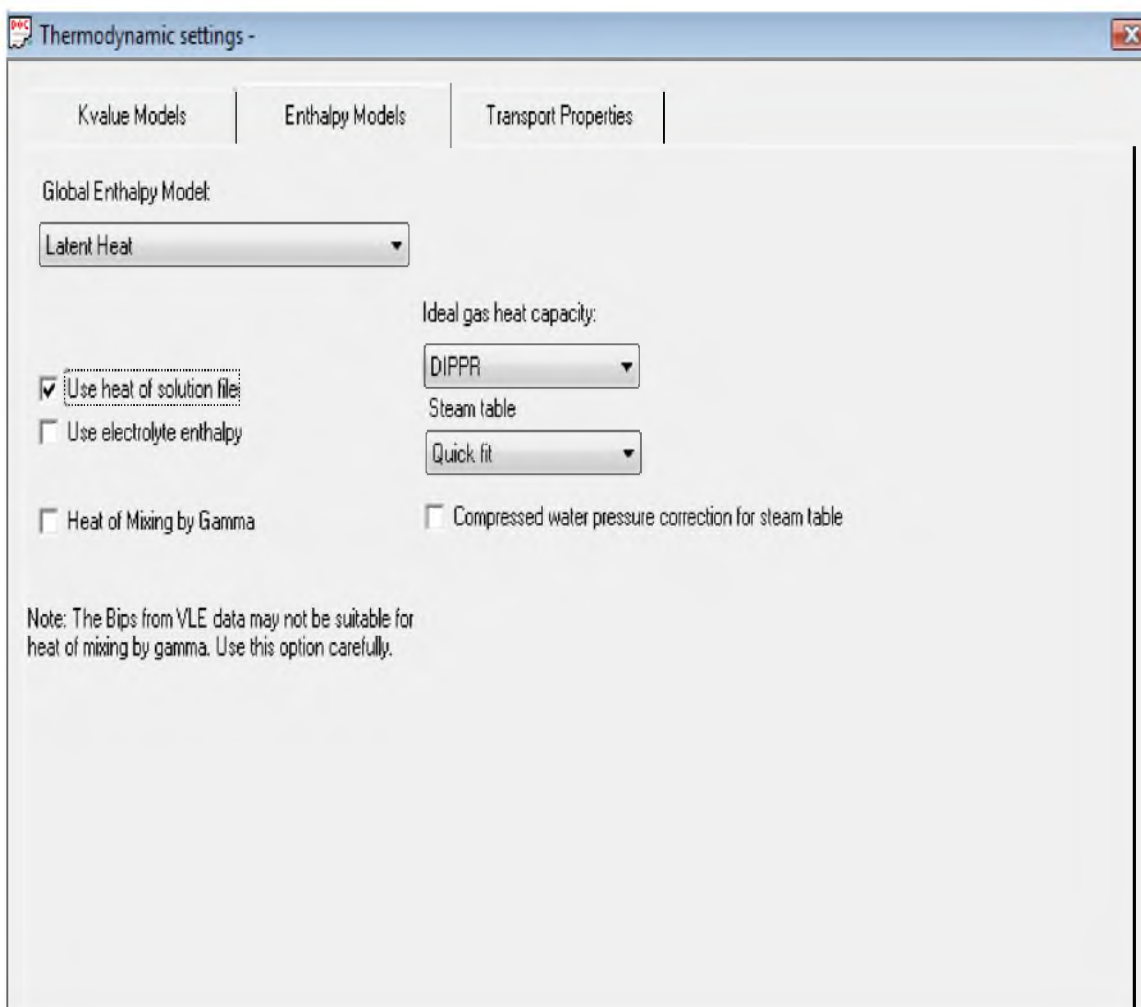


**Figure 3.17** Enthalpy models

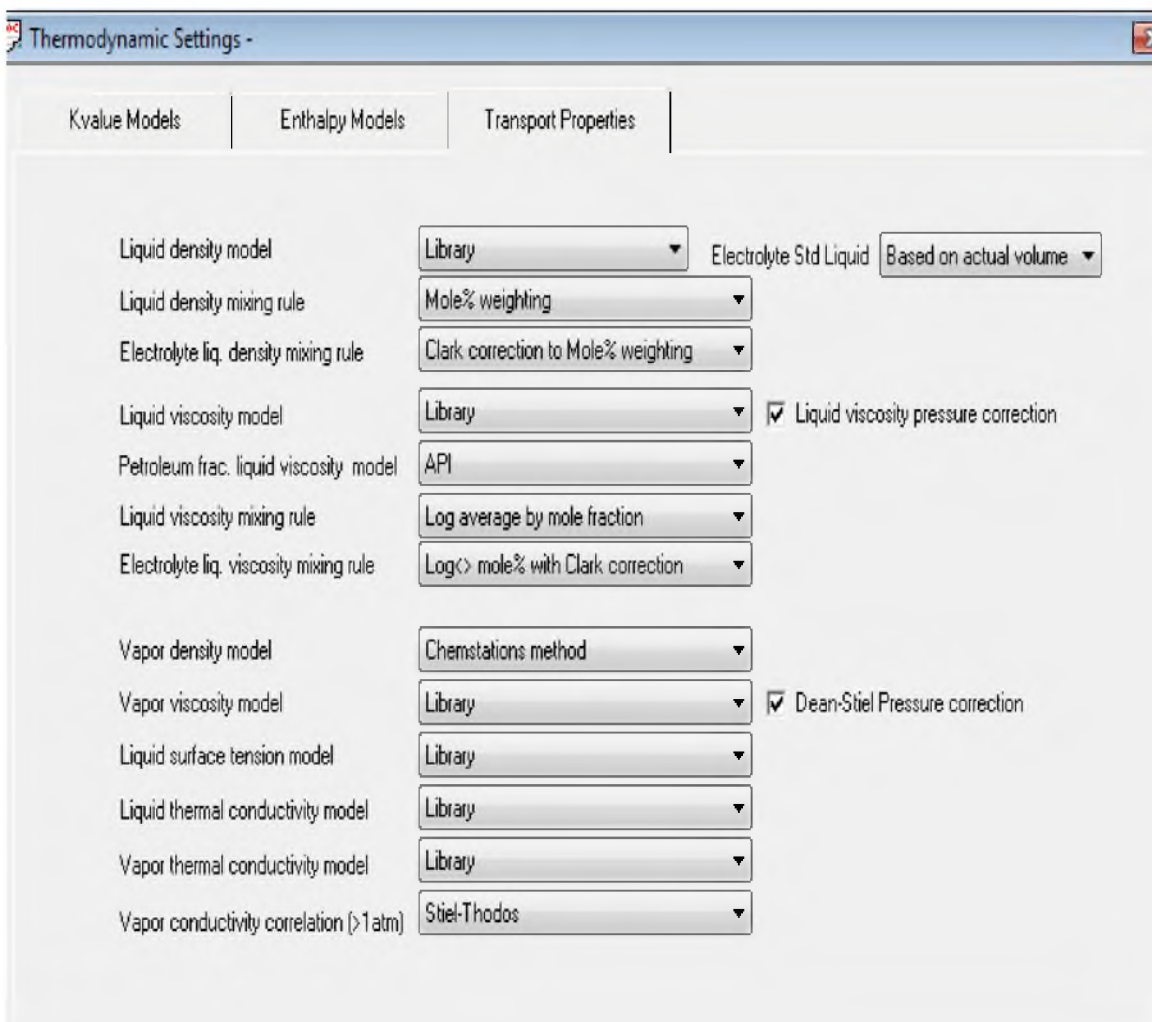


**Figure 3.18** Transport properties

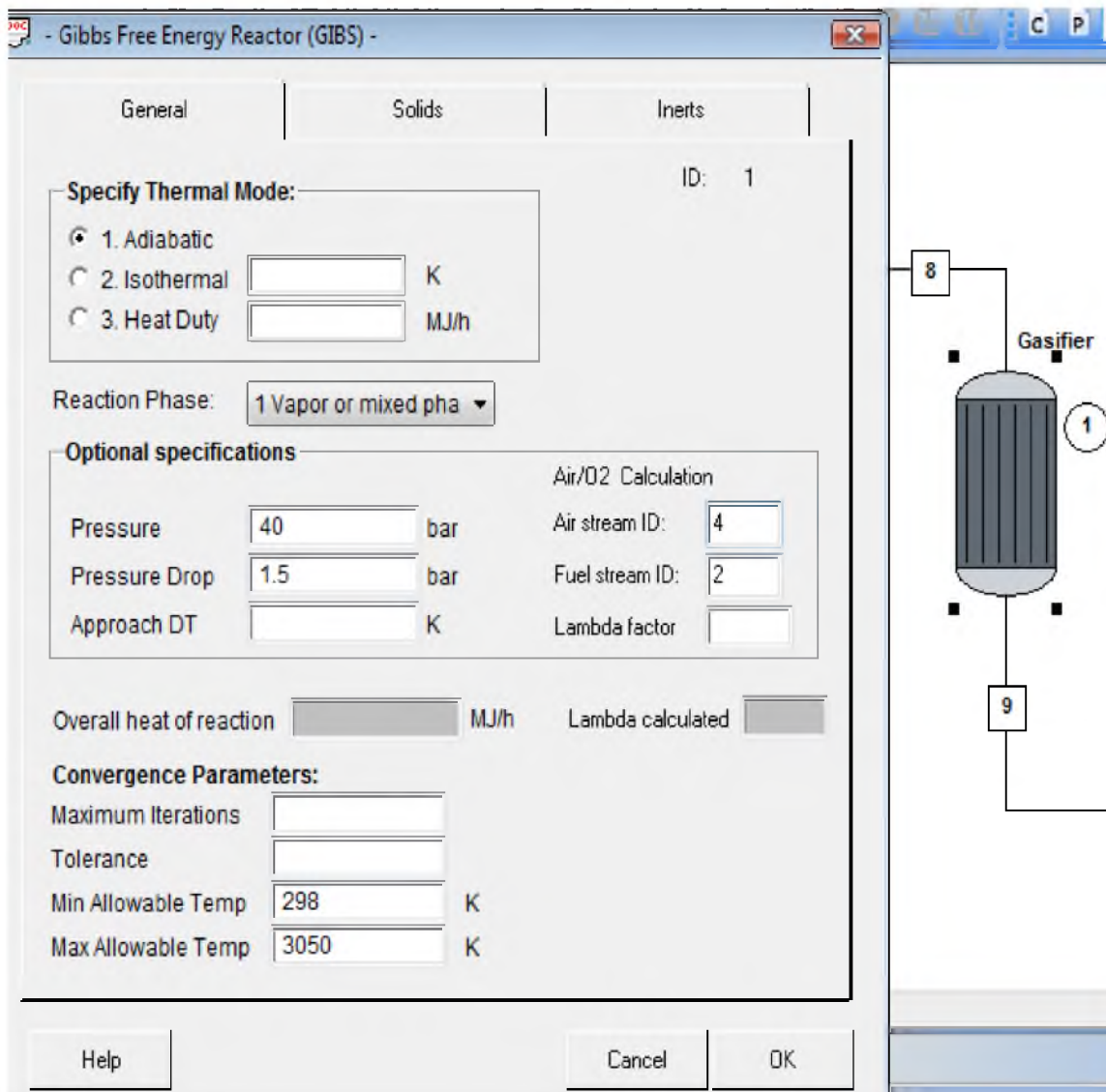


**Figure 3.19** Gibbs free energy reactor

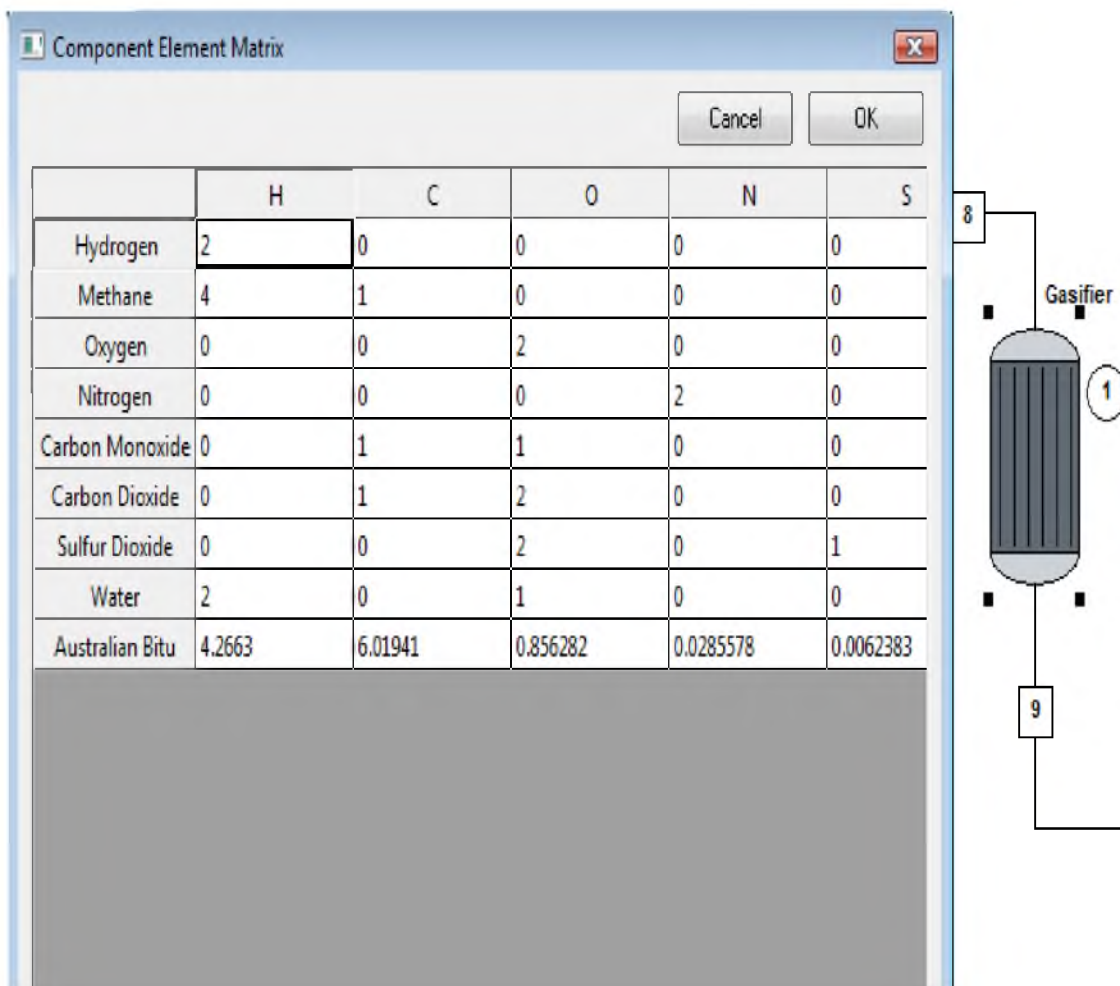


**Figure 3.20** Component element matrix

## CHAPTER 4

### RESULTS: SIMULATION OF COAL GASIFICATION

#### 4.1 Influence of Steam-to-Coal Ratio and Pressure on Gasification

The simulation procedure consists of three main parts. In the first part, steam-to-coal feed ratio (kg/kg) and system pressure were changed while the temperature of coal, temperature of oxygen, oxygen-to-feed ratio held constant. The feed rate of coal also was assumed to be 1000 kg/h. The temperature of coal and water were fixed as 313 K and formed the slurry before reaching the gasifier. The oxygen-to-coal ratio was kept as 1.0 kg/kg of feed ratio. The temperature of oxygen was set at 333 K for all the simulation runs.

Figure 4.1 and Figure 4.2 illustrate the *adiabatic flame temperature* based on steam-to-coal ratio and pressure. The flame temperature was determined using different system pressure and steam-to-coal feed ratio by kg/kg. Type 1 describes the Australian bituminous coal and type 2 denotes the Indonesian roto coal. The highest adiabatic flame temperature of Australian bituminous coal was found at 2223 K with a steam-to-coal feed ratio of 0.0092 by kg/kg as shown in Figure 4.1. The flame temperature decreases with rising pressure and steam-to-coal ratio. Although an increase in steam-to-coal feed ratio promotes the char-steam reaction, the temperature decreases because the char-steam reaction is highly endothermic and lowers the reaction temperature.



Figure 4.2 demonstrates the temperature profile of Indonesian roto coal (type 2) with varying pressure and steam-to-coal feed ratio (kg/kg). At steam-to-coal feed ratio of 0.0092 kg/kg, the maximum adiabatic flame temperature was obtained at 2367 K. The reason that adiabatic flame temperature of Indonesian roto coal is higher than that of Australian bituminous coal is due to different carbon and oxygen percentages of coal properties. The unreacted carbon was clearly observed in simulation result with steam-to-coal ratio up to 0.2 and with increasing pressure. This observation caused a negative result in entrained flow gasifier on temperature. The simulation temperature was different than the expected result for that reason.

Figure 4.3 and Figure 4.4 state *the concentration of  $H_2$*  on a dry basis for type 1 and type 2, respectively. Even though the amount of  $H_2$  increased until reaching steam-to-coal ratio of 0.82, it decreased slightly after this point as can be seen in Figure 4.3. Both the higher amount of steam and the lower temperature resulting from it contribute to this trend. This increasing line tends to promote the coal-steam and water gas shift reactions. It is possible to produce the hydrogen gas level 33-36 by moles % with these parameters. Other gasification parameters were assumed constant like other simulation runs. The production of  $H_2$  with high efficiency is very important for industry because hydrogen product is generally evaluated in producing electricity and chemical products.

*The concentration of carbon monoxide* on a dry basis by moles % with different steam-to-coal ratio and pressure has been mentioned in Figure 4.5 for type 1 and, in Figure 4.6 for type 2. With increasing steam-to-coal ratio and pressure, the molar concentration of CO decreases considerably. In the small amount of steam-to-coal ratio and pressure, the maximum CO was observed as 56% and 58.1% by moles in Figure 4.5

and Figure 4.6, respectively. The results are pretty close to each other and the reason for this high quantity is due to the high carbon content of both coal types. In addition to this observation, the decreasing line was obtained with increasing feed ratio and pressure. From the figures, it is possible to say that there is an inverse relation between CO concentration and variable parameters. This decreasing line tends to retard the coal-carbon dioxide and coal-hydrogen reactions.

*The concentration of CO<sub>2</sub>* was as shown in Figure 4.7 for type 1 and in Figure 4.8 for type 2. The concentration of CO<sub>2</sub> intensified with ascending steam-to-coal feed ratio (kg/kg) and steam pressure. The maximum amount of CO<sub>2</sub> was found at 28% and 25% by moles, respectively. This increasing line tends to promote the coal-steam and water gas shift reactions. Thus, it is concluded that the steam-to-coal ratio has a great effect on production of CO and CO<sub>2</sub>. However, it can be seen that there is a inverse proportion of CO<sub>2</sub> and CO after simulation of coal types.

Figure 4.9 and Figure 4.10 indicate *the molar concentration of methane (CH<sub>4</sub>)* based on steam-to-coal feed ratio and system pressure. It can be seen that when water was employed instead of superheated steam, the methane concentration reached a negligible level. Methane formation, coal with hydrogen, is generally obtained at high pressures and low temperatures and is thus, mainly important in lower temperature gasification systems. Methane formation is also an exothermic reaction that does not consume oxygen and, therefore, increases the efficiency of gasification and the final heating value of the synthesis gas. In addition to this, most of the cases or simulation experiments exhibit that methane concentration is negligible because of very low concentrations. The maximum methane production on a dry basis by moles was detected as 0.161% with minimum

steam-to-coal feed ratio (kg/kg) and pressure in Figure 4.9. Similarly, for the Indonesian roto coal, the maximum value was found as 0.142% by moles on a dry basis.

According to literature, these results are quite similar for methane concentration with industry. In reality, concentration of  $\text{CH}_4$  can not be a significant level in order to be used for producing energy. The graphs also indicate that the concentration of  $\text{CH}_4$  begins to increase with heightening steam-to-coal feed ratio and pressure but not a significant amount. With new technology, the gasifier temperature basically might be accurately measured using methane concentration in ppm level because only a tiny amount of methane is needed for analyzer. However, this attempt requires a new gasification process and more experiments in the laboratory to gain consistent about the results and to find a logical correlation between  $\text{CH}_4$  and flame temperature as well.

The carbon conversion range with different steam-to-coal ratio and pressure for two types of coal is demonstrated in Figure 4.11 and Figure 4.12. Carbon conversion steps up slightly with increasing steam-to-coal feed ratio and pressure for both coal types. However, the effect of pressure is fairly at a negligible level. The steam-to-coal ratio showing a maximum carbon conversion ranges from 0.70 to 0.80 at the oxygen-to-coal ratio of 1.

After that value, the conversion goes down slightly. That is due to the fact that the fraction of steam contributing to the equilibrium reaction of the pyrolysis step is almost constant, and this amount of steam keeps promoting carbon-steam reactions to the direction of  $\text{CO}$  and  $\text{H}_2$  formation while increasing steam-to-coal ratio.

Although an increase in the steam-to-coal ratio promotes the char-steam reaction, the gasifier temperature decreases because the steam reaction is highly

endothermic and lowers the temperature. A maximum carbon conversion with respect to steam-to-coal ratio exists, because of two opposite effects on the equilibrium reaction.

#### **4.2 Influence of Oxygen-to-Coal Ratio and Pressure on Gasification**

Another important input parameter is oxygen-to-coal feed ratio (kg/kg) for temperature distribution in an entrained flow gasifier. Oxygen is the main source to complete the kinetic reaction in the gasifier. If the oxygen concentration is not enough for coal gasification, the unreacted coal will be observed at the end of the reaction. Thus, oxygen concentration directly affects the concentrations of CO, CO<sub>2</sub> and methane. The concentration changes are caused by the competitive interactions between the combustion and gasification reactions, the rates of which are very sensitive to the temperature variations produced. Since a higher oxygen feed rate increases the temperature of the system, the oxidation reactions occur to a greater extent.

Figures 4.13 and 4.14 demonstrate the effect of oxygen-to-coal feed ratio and pressure *on adiabatic flame temperature*. The temperature of oxygen in the bottom stream was hold constant at 333 K. The temperature of water and coal were fixed 313 K. Steam-to-coal feed ratio was assumed 0.8 kg/kg for each simulation run in order to point out the importance of oxygen-to-coal feed ratio. Due to the exothermic coal combustion, the flame temperature rises as oxygen-to-coal ratio and pressure increase. Adiabatic flame temperature increased until oxygen-to-coal ratio of 2.0 for type 1 shown in Figure 4.13. At that point, the total gasification completed because of the concentration of reactants. After this point, the temperature rapidly decreased. The reason for this decline is that the product gases start to absorb the heat from inside the gasifier and the excess

oxygen absorbs some of that heat. A similar tendency arose for Indonesian coal (type 2) can be seen in Figure 4.14. The maximum flame temperature was found for type 2 at 2650 K. This result is higher than that of the first type of coal (Australian coal). It is highly possible that the reason for this difference is due to carbon composition of coals.

Carbon monoxide is the dominant output parameter in coal gasification product. CO is important because it is actually a syngas component with hydrogen and sometimes methane. More carbon monoxide means more syngas which creates more electric power and energy used in industry. Under this background for CO, *simulation results of carbon monoxide* are indicated below in Figure 4.15 for type 1 and in Figure 4.16 for type 2. With increasing oxygen-to-coal feed ratio (kg/kg) and pressure, the concentration of CO in molar basis goes up considerably with increasing pressure and oxygen-to-coal ratio. Coal-carbon dioxide and coal-oxygen reactions cause this trend.

The maximum composition of CO was attained 55.7% on a dry basis for Australian bituminous coal and 55.9% on a dry basis for Indonesian roto coal. The unreacted coal has just been obtained at the beginning of the reaction in the entrained flow gasifier. Until reaching an oxygen-to-coal feed ratio of 0.2, the unreacted coal was collected at the bottom of the stripper in the Shell gasification process illustrated in Figure 3.1.

*The concentration of hydrogen* on a dry basis by moles are shown in Figure 4.17 for type 1 and Figure 4.18 for type 2, respectively. Although an increase in the oxygen-to-coal feed ratio tends to increase the temperature, which in turn reverses the water gas shift reaction, it also tends to moderate the coal-steam and hence, the coal-carbon dioxide reactions during the gasification period. Eventually, a point is reached beyond which a

significant change in the carbon monoxide and a somewhat lower yield of H<sub>2</sub> gas is observed. The decreasing line of H<sub>2</sub> was acquired with increasing oxygen-to-coal ratio (kg/kg) and pressure for both charts, but it is insensitive to this parameter while the amount of CO and CO<sub>2</sub> change significantly. The molar composition of H<sub>2</sub> (see Figure 4.17) only diminished from 44.1% to 36.4% with increasing oxidant ratio and from 38.5% to 36.0% for type 2 as shown in Figure 4.18.

Figure 4.19 and Figure 4.20 display *the carbon dioxide molar composition* with respect to oxygen-to-coal ratio and pressure. The normal level in a coal gasification for CO<sub>2</sub> was identified around 18.1 by moles % with same input parameters. The results indicate a consistent implication between CO<sub>2</sub> concentration and input parameters. According to graphs, the amount of CO<sub>2</sub> decreases considerably with increasing oxygen-to-coal feed ratio (kg/kg) and pressure. The oxidant concentration is a key parameter for chemical reactions in order to produce carbon dioxide. The maximum and minimum CO<sub>2</sub> concentration for type 1 was achieved at 18.1% and 6.2%, respectively. Similarly, for type 2, CO<sub>2</sub> production varied from 16.2% to 4.5% as can be seen in Figure 4.20.

Another concentration profile describes the methane product. *The mole fraction of methane* with different oxygen-to-coal feed ratio has been stated in Figure 4.21 for Australian coal and Figure 4.22 for Indonesian roto. The content of methane was considered as a pure matter and no other components which consist of methane were taken into account. Figure 4.21 shows that with increasing oxygen-to-coal ratio and pressure, the concentration of CH<sub>4</sub> began to decrease and then after oxygen-to-coal feed ratio of 0.92, the stable line which describes the methane fraction has been observed. In addition to this observation, as expected, the methane concentration profile was at a small

level or in other words, the molar percentage of  $\text{CH}_4$  in both graphs is less than that of other products of coal gasification.

Using methane concentration in ppm level, gasifier temperature is accurately measured, the temperature distribution is definitely identified in every height of gasifier. In the next chapter, this subject was taken into account and a model which describes the relationship the methane and temperature was developed based on simulation results.

There are also other important coal characteristics which explain the quality of coal and performance conditions including carbon conversion and cold gas efficiency. It is very important to know these essential properties of coal in order to estimate the behaviour of coal gasification products and gasifier conditions. Carbon conversion, defined by the ratio of carbon in gas phase to that contained in coal, is an essential factor in improving the performance of coal gasification. Carbon conversion was calculated using solid-gas reactions between char and gasification reagents. Equation 1.3 was used to determine the carbon conversion by percentage for this chapter. It is known that, in adiabatic conditions, the reaction temperature of coal gasification and carbon conversion depend mainly on both oxygen-to-coal ratio and steam-to-coal ratio. The carbon conversion is plotted as a function of oxygen-to-coal ratio and system pressure in Figure 4.23 for type 1 and Figure 4.24 for type 2. Due to the exothermic coal combustion, the carbon conversion intensifies with increasing oxygen-to-coal feed ratio. The oxygen-to-coal ratio is critical to the conversion, since the heat resulting from combustion reactions supports the endothermic gasification reactions.

The unreacted coal were also observed in small oxygen-to-coal feed ratio since there was not enough oxygen which reacts with hydrocarbon compounds in the gasifier.

These results are quite reasonable once the previous reporters support proportionally between oxygen feed rate and coal conversion, which is in line with the present results. Therefore, the carbon conversion is influenced by the oxygen-to-coal ratio rather than the steam-to-coal ratio.

Finally, the last two graphs, Figure 4.25 and Figure 4.26, display the cold gas efficiency of coal types with different oxygen-to-coal feed ratio (kg/kg) and system pressure (bar). The formula of cold gas efficiency was given in Chapter 1 (see Equation 1.2 and 1.3). The lower heating value of carbon dioxide was not considered because it does not react with oxygen to produce heat and never affects the release of heat to the gasifier. The figures demonstrate that the cold gas efficiency decreases with increasing oxygen-to-coal ratio and pressure. It can be concluded that the highest cold gas efficiency occurs at the minimum oxygen-to-coal feed ratio and the lowest cold gas efficiency is obtained at the maximum oxygen-to-coal feed ratio and pressure. However, the pressure does not have a great influence on the cold gas efficiency. Therefore, it can be said that pressure is insensitivity to the cold gas efficiency.

### **4.3 Influence of Oxygen-to-Coal and Steam-to-Coal Ratios on Gasification**

The purpose of last part of Chapter 4 is to investigate the effect of oxygen-to-coal feed ratio and steam-to-coal feed ratio on gasifier performance. It is clearly seen in sections 4.1 and 4.2 that the effect of pressure on adiabatic flame temperature and coal compositions is not as much as steam-to-coal ratio or the amount of air inside the gasifier. The differences of neighbour data in the graphs are negligible when the pressure is taken into account as an input parameter. The other input parameters, oxygen-to-coal ratio and



steam-to-coal ratio have great influence on the flame temperature and concentrations of coal types in the entrained flow gasifier.

In this study, the system pressure was held at 40 bar and was not changed during the simulation. The coal feed rate was supposed at 1000 kg/h and the amount of steam and oxygen were changed in order to determine the flame temperature of coal types and other coal characteristics. Since the initial temperatures of coal and water do not have enormous effects on the outlet temperature of coal gasification, they were maintained at 313 K. Another aim of this work is to figure out the importance of oxygen-to-fuel ratio on the temperature of coal gasification. It is known that with increasing oxygen-to-fuel ratio, the temperature increases considerably. This is due to exothermic combustion reactions which occur in the combustor zone inside the gasifier. As seen in the previous studies, the oxygen-to-coal ratio also is the dominant factor on the conversion of coal rather than steam-to-coal ratio. However, the steam-to-coal has an important effect on product gas compositions. For example, the methanation reactions do not consume oxygen, and the level of air in the gasifier does not alter significantly with the changing the methane concentration.

After maintaining the input parameters, the simulation begins to calculate the adiabatic flame temperature and coal characteristics. Figure 4.27 and 4.28 demonstrate the effect of oxygen-to-coal ratio and steam-to-coal ratio on the adiabatic flame temperature in the entrained flow gasifier for Australian bituminous coal and Indonesian roto coal, respectively. The graphs illustrate that the adiabatic flame temperatures rise significantly with increasing oxygen-to-coal feed ratio while they decrease with increasing steam-to-coal ratio. The reason for this tendency can be explained as the

oxygen directly affects the combustion reactions which are highly exothermic reactions. It leads to an increase the reaction temperatures inside the gasifier. On the other hand the steam does not severely affect the oxidation reactions. Moreover, the char-steam reactions are obtained in the reduction zone and the endothermic reactions take place in that region. Therefore, it causes to the flame temperature to decrease due to the need for heat. Another observation from the figure is that the adiabatic flame temperature of Indonesian roto coal is higher than that of Australian bituminous coal due to the coal properties such as carbon percentage.

Figure 4.29 and Figure 4.30 indicate the *molar composition of carbon monoxide* with varying the oxygen-to-coal ratio and steam-to-coal ratio at 40 bar. The concentration of CO increases considerably when the oxygen-to-coal ratio goes up inside the gasifier. The char-O<sub>2</sub> reactions which take place in the combustor zone is the dominant factor in producing the carbon monoxide product gas. Nevertheless, the steam-to-coal ratio causes a negative effect on CO production. The decreasing line occurs with increasing steam-to-coal ratio. This is due to the fact that the carbon monoxide reacts with water to form carbon dioxide gas. Therefore, it is concluded that CO/H<sub>2</sub> syngas ratio ascends when the oxygen-to-coal feed ratio increases in the entrained flow gasifier.

*The concentrations of hydrogen* product gas for Australian bituminous coal and Indonesian roto coal based on oxygen-to-coal and steam-to-coal ratio are exhibited in Figure 4.31 and Figure 4.32, respectively. When the amount of steam-to-coal increases for both types, hydrogen production rises inside the gasifier. The char-steam and water-gas shift reactions contribute to this tendency. On the other hand, the oxygen-to-coal feed ratio is insensitive to the fraction of hydrogen. A remarkable change in the concentration

of hydrogen is obtained during the gasification. The critical point for hydrogen and other hydrocarbon productions demonstrates that the amount of oxygen which react with fuel is not enough in the combustor zone. The maximum oxygen-to-coal ratio by kg/kg roughly corresponds to stoichiometric ratio of 0.5. It means the gasification reactions have not completed due to lack of oxygen capacity.

The same observation was made for *carbon dioxide concentration* after finishing coal gasification simulation. The amount of carbon dioxide increases with increasing steam-to-coal feed ratio. However, the CO<sub>2</sub> product gas decreases slightly with rising oxygen-to-coal ratio. The highest steam-to-coal ratio produce the maximum value of carbon dioxide compared to small amount of steam-to-coal. In general, the lower CO<sub>2</sub> production is preferred for syngas efficiency and cold gas efficiency. The cost goes up in order to separate and clean up CO<sub>2</sub> from the entrained flow gasifier. In addition, it can be predicted that the syngas composition which contains hydrogen and carbon monoxide product gases is higher at the lowest steam-to-coal ratio than that at the highest steam-to-coal feed ratio.

Figure 4.33 and 4.34 illustrate the mole fractions of CO<sub>2</sub> product gas for Australian coal and Indonesian roto coal. As can be seen from the figures, the oxygen effect on CO<sub>2</sub> production is insensitive compared to steam-to-coal feed ratio. The gasification reactions which take place in the reduction zone are more effective for determining the CO<sub>2</sub>. The amount of volatile matter and fixed carbon of these coal types also limit the syngas content and carbon dioxide composition in the gasifier. Another consideration regarding carbon dioxide production is that the reaction kinetics of coal types can be calculated based on vapor pressure of CO<sub>2</sub> and gasifier temperature.

Previous studies (4, 37) support the relationship between reaction kinetics and CO<sub>2</sub> concentration on the pilot scale in the industry.

*The last gasification product is methane.* Section 4.1 and 4.2 demonstrate that the amount of methane does not change dramatically with varying system pressure. The effect of pressure on methane production can be assumed as negligible level. Therefore, the effect of steam-to-coal and oxygen-to-coal have simultaneously been investigated on methane concentration using ChemCAD simulation program. The concentration of methane with respect to oxygen-to-coal and steam-to-coal ratio is illustrated in Figures 4.35 and 4.36 for Australian bituminous coal and Indonesian roto coal, respectively. The graphs display that the effect of oxidant on methane production is not as strong as the effect of steam. This trend is explicated by the methanation reaction for producing methane does not consume oxygen. Indeed, the range of 0-500 ppm level of methane is considered a reasonable standard indication at the moment. Thus, the optimum relation of methane composition and adiabatic flame temperature are obtained at the highest oxygen-to-coal ratio. Finally, as mentioned in Chapter 2, the gasification temperature can be measured with the help of the methane concentration where the thermocouples show the deviation from standard measurement and break down due to the high temperature conditions.

The influence of steam feed rates on the carbon conversion is presented in Figure 4.37 in various oxygen-to-coal ratios. Although an increase in the steam-to-coal ratio promotes the char-steam reaction, the temperature decreases because the char-steam reaction is highly endothermic and lowers the reaction temperature. A maximum carbon conversion with respect to the steam-to-coal ratio exists, because of the two opposite

effect on the equilibrium reaction (i.e., promotion of char-steam reaction and temperature decreasing). It is observed that the steam-to-coal ratio showing a maximum carbon conversion (99.15%) changes from about 0.70 to 0.80, as the oxygen-to-coal ratio increases from 0.8 to 1.0. The oxygen-to-coal feed ratio is critical to the conversion, since the heat resulting from the combustion reactions support the endothermic gasification reactions. Therefore, the carbon conversion is influenced by the oxygen-to-coal ratio rather than the steam-to-coal ratio.

This analysis demonstrates that the concentration of steam and oxygen in the feed gas are crucial in determining the reactor performance and are sensitive controls for a stable gasification operation. Similar observations have been made by previous investigators. The sensitivity and insensitivity of the distribution of product gas to changes in steam-to-coal and oxygen-to-coal feed ratio were also found by Nguyen et al. (16), and Yoshida et al. (17). Moreover, these and other authors, Pinto et al. (43) and Harris (35), reported proportionality between oxygen feed rate and coal conversion, which is in line with the present results.

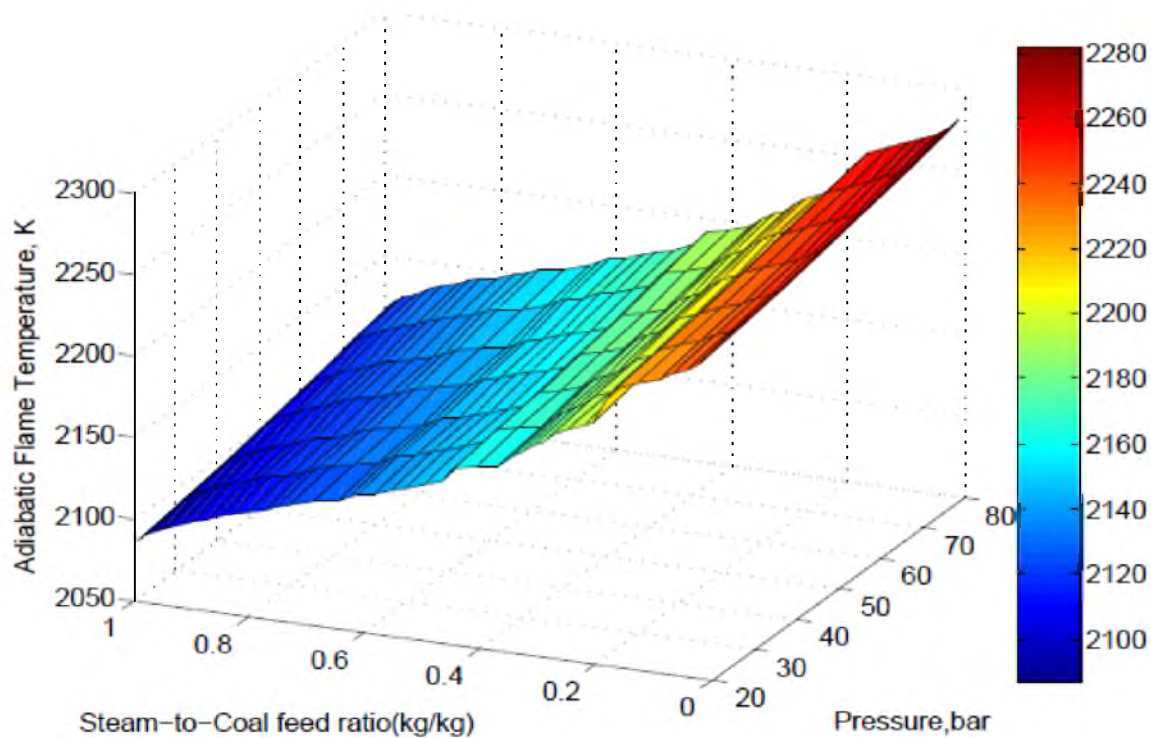


**Figure 4.1.** Effect of steam-to-coal feed ratio and pressure on adiabatic flame temperature of Australian bituminous coal (oxygen-to-coal ratio: 1.0 kg/kg, coal feed rate: 1000 kg/h, temperature of water and coal: 313 K, temperature of oxygen: 333 K)

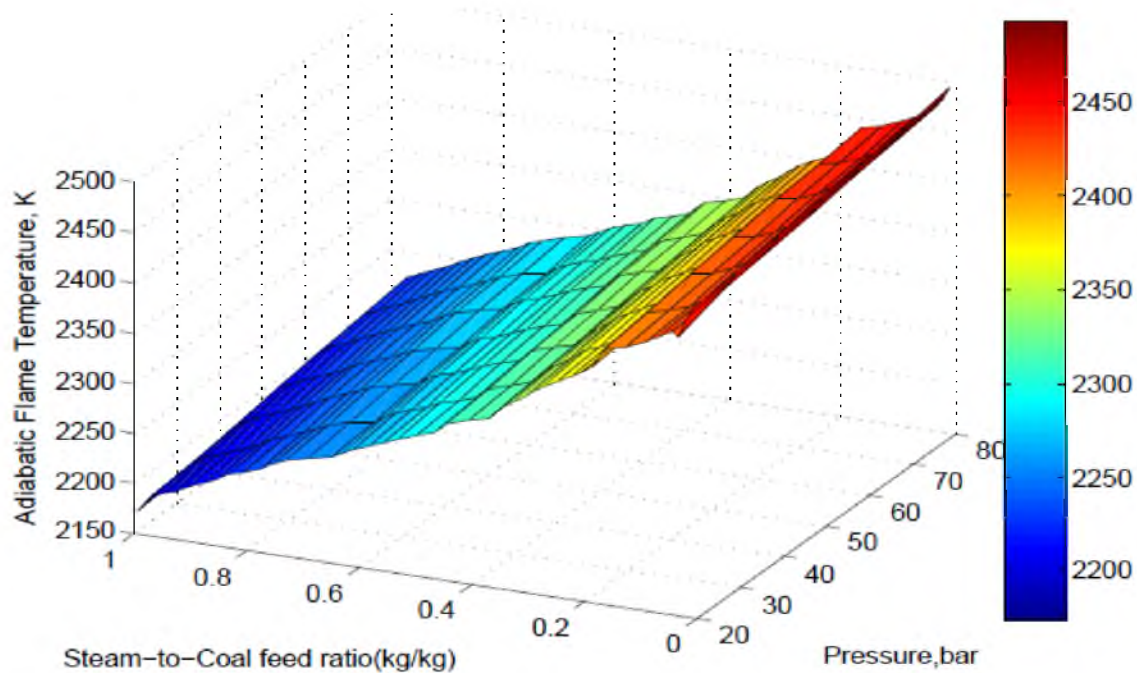


**Figure 4.2.** Effect of steam-to-coal feed ratio and pressure on adiabatic flame temperature of Indonesian roto coal (oxygen-to-coal ratio: 1.0 kg/kg, coal feed rate: 1000 kg/h, temperature of water and coal: 313 K, temperature of oxygen: 333 K)

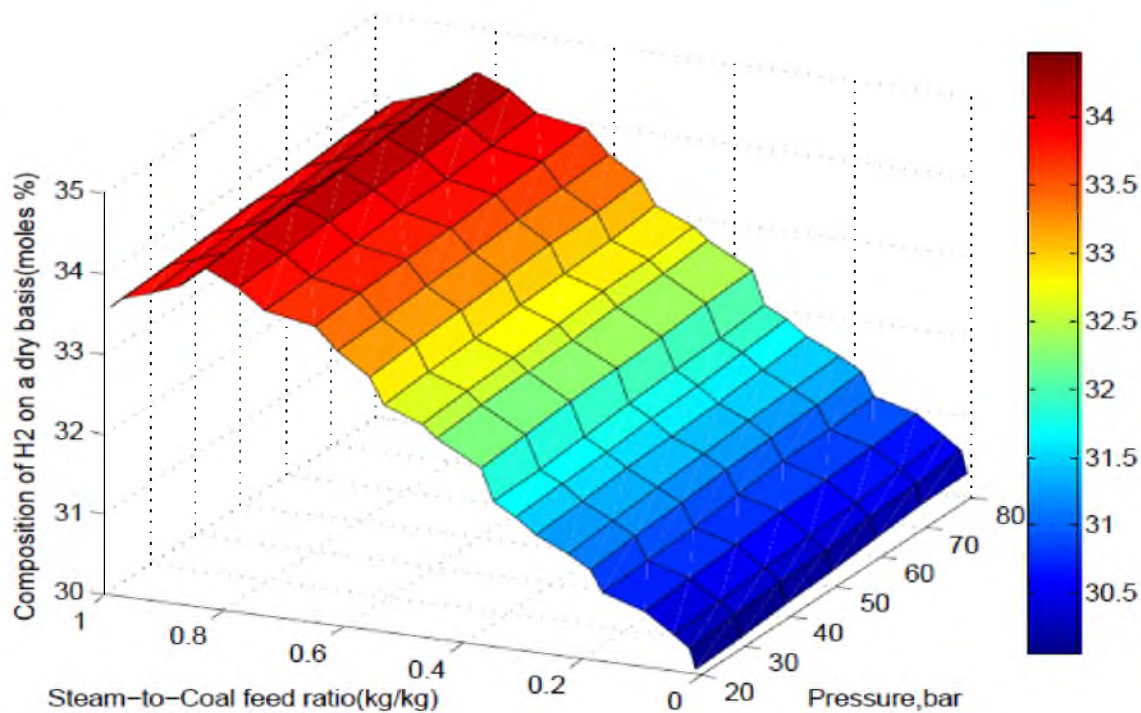


**Figure 4.3.** Effect of steam-to-coal feed ratio and pressure on concentration of  $H_2$  for Australian bituminous coal (oxygen-to-coal ratio: 1.0 kg/kg, coal feed rate: 1000 kg/h, temperature of water and coal: 313 K, temperature of oxygen: 333 K)

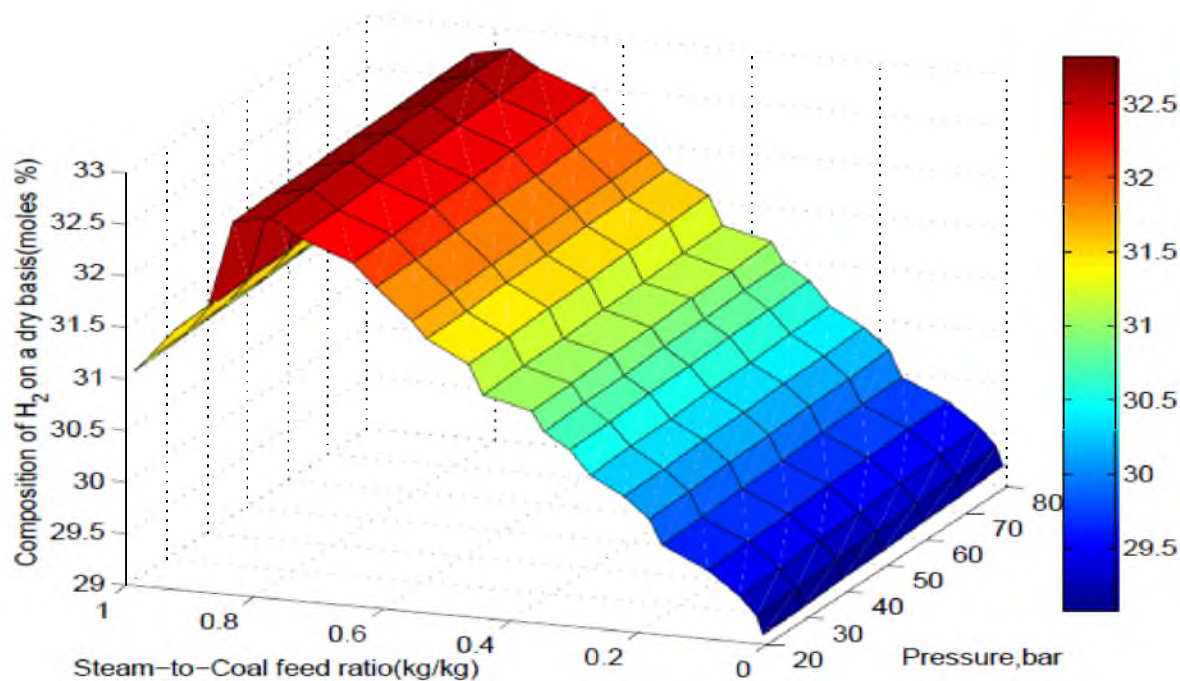


**Figure 4.4.** Effect of steam-to-coal feed ratio and pressure on concentration of  $H_2$  for Indonesian roto coal (oxygen-to-coal ratio: 1.0 kg/kg, coal feed rate: 1000 kg/h, temperature of water and coal: 313 K, temperature of oxygen: 333 K)

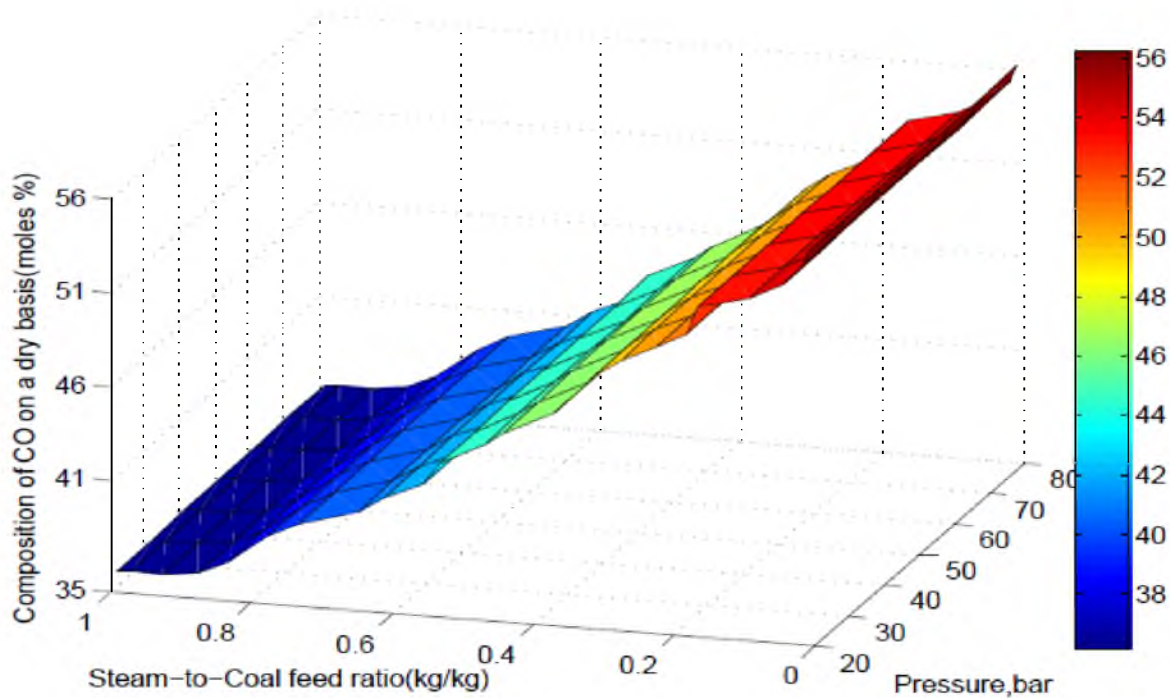


**Figure 4.5.** Effect of steam-to-coal feed ratio and pressure on concentration of CO for Australian bituminous coal (oxygen-to-coal ratio: 1.0 kg/kg, coal feed rate: 1000 kg/h, temperature of water and coal: 313 K, temperature of oxygen: 333 K)

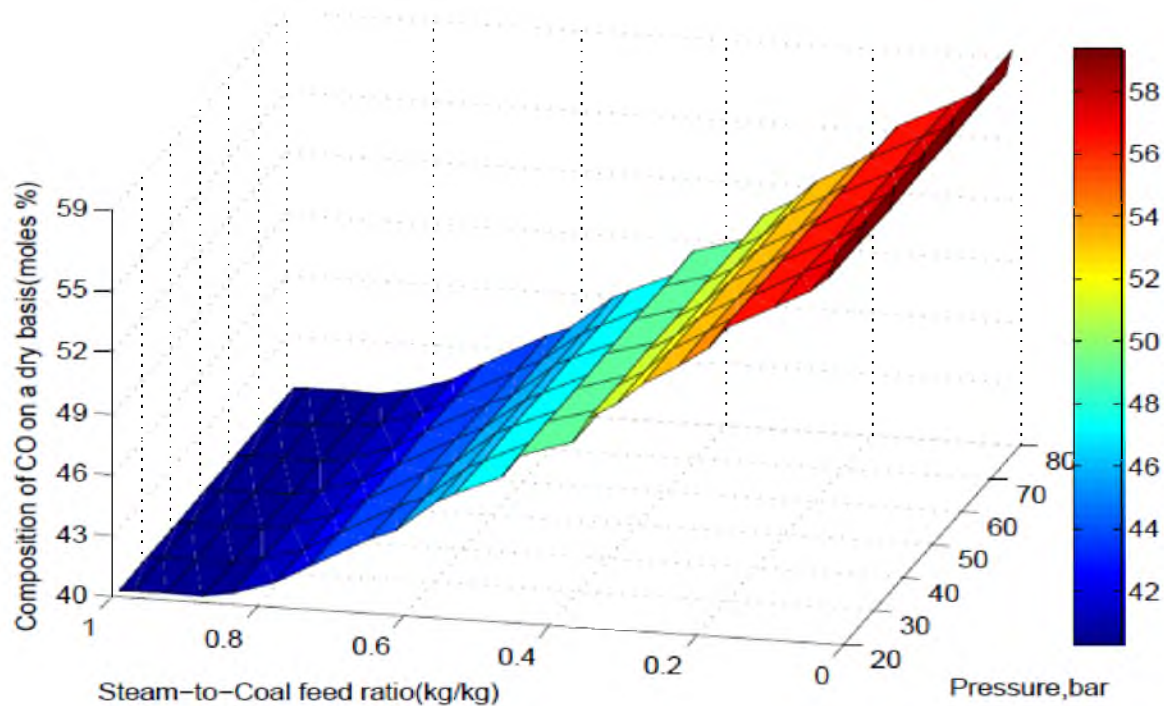


**Figure 4.6.** Effect of steam-to-coal feed ratio and pressure on concentration of CO for Indonesian roto coal (oxygen-to-coal ratio: 1.0 kg/kg, coal feed rate: 1000 kg/h, temperature of water and coal: 313 K, temperature of oxygen: 333 K)



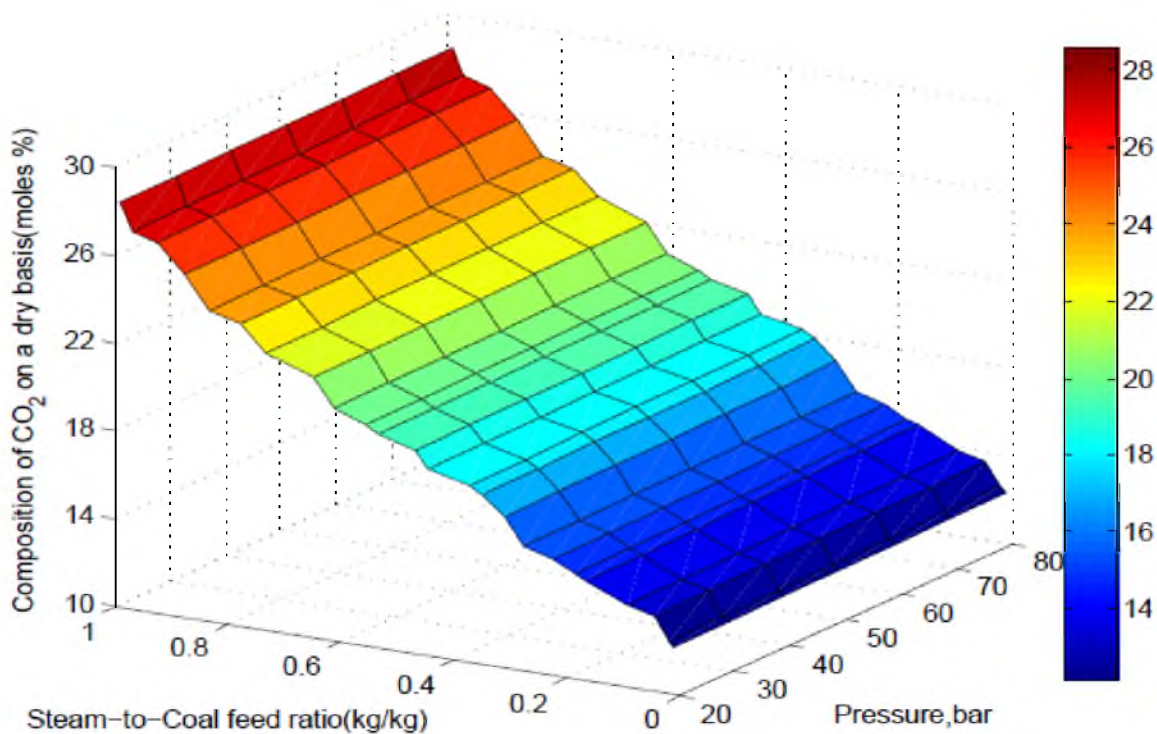


**Figure 4.7.** Effect of steam-to-coal feed ratio and pressure on concentration of CO<sub>2</sub> for Australian bituminous coal (oxygen-to-coal ratio: 1.0 kg/kg, coal feed rate: 1000 kg/h, temperature of water and coal: 313 K, temperature of oxygen: 333 K)

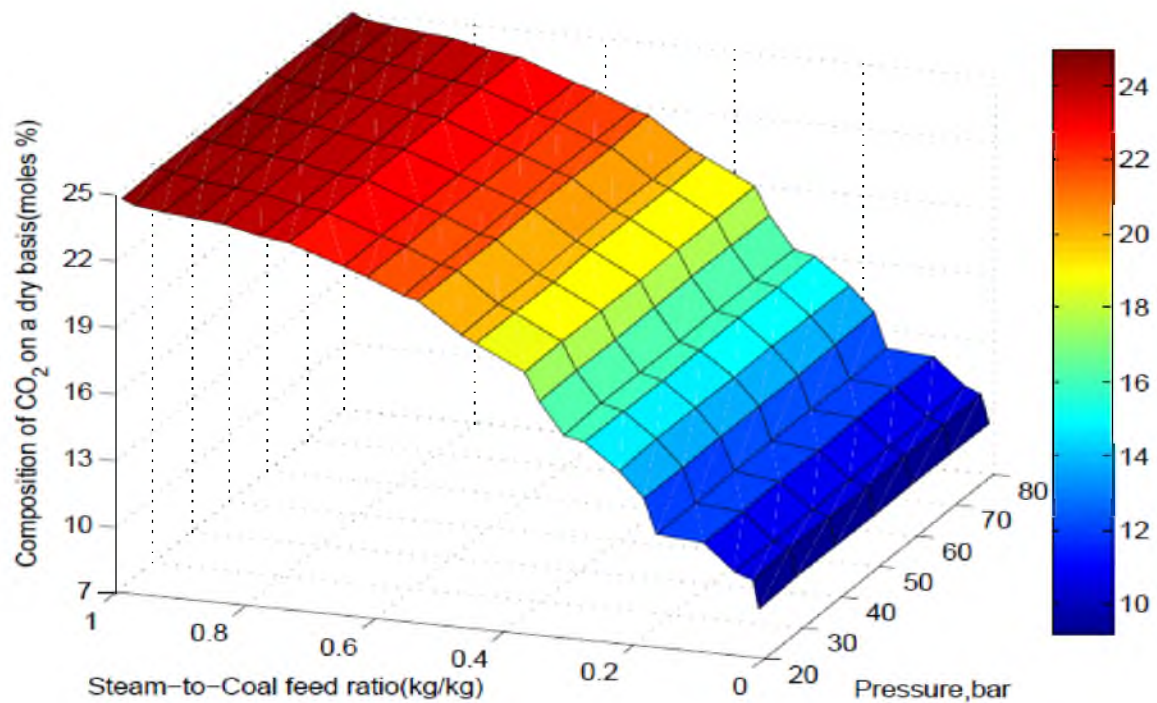


**Figure 4.8.** Effect of steam-to-coal feed ratio and pressure on concentration of CO<sub>2</sub> for Indonesian roto coal (oxygen-to-coal ratio: 1.0 kg/kg, coal feed rate: 1000 kg/h, temperature of water and coal: 313 K, temperature of oxygen: 333 K)

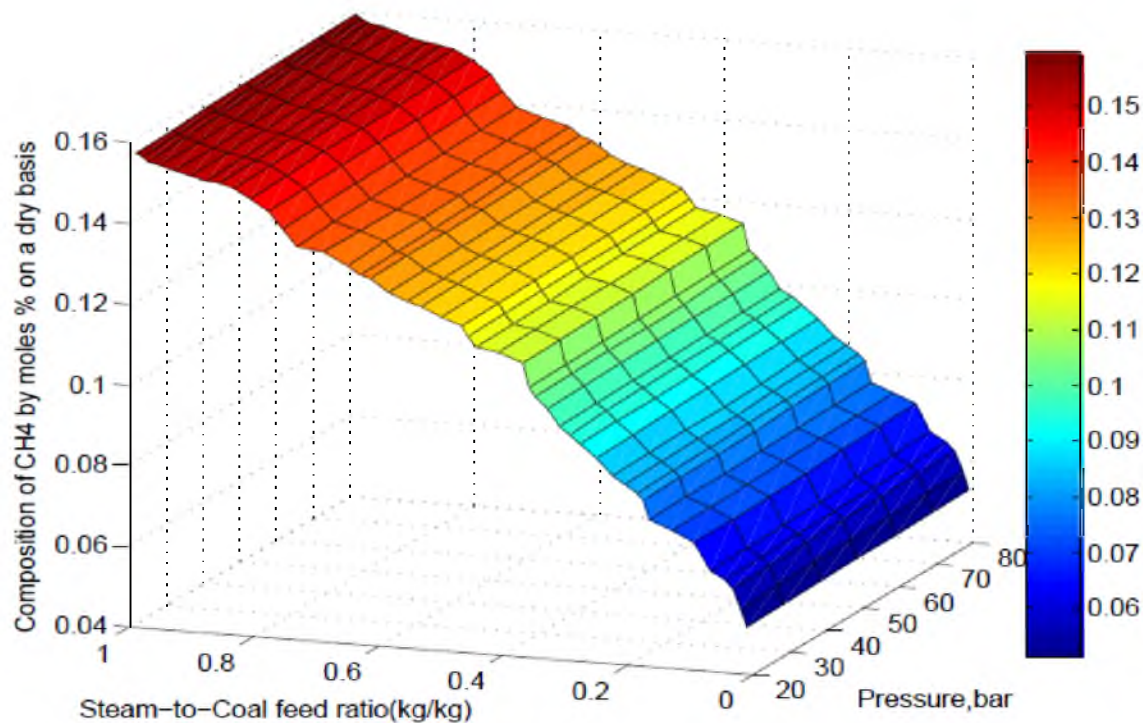


**Figure 4.9.** Effect of steam-to-coal feed ratio and pressure on concentration of CH<sub>4</sub> for Australian bituminous coal (oxygen-to-coal ratio: 1.0 kg/kg, coal feed rate: 1000 kg/h, temperature of water and coal: 313 K, temperature of oxygen: 333 K)

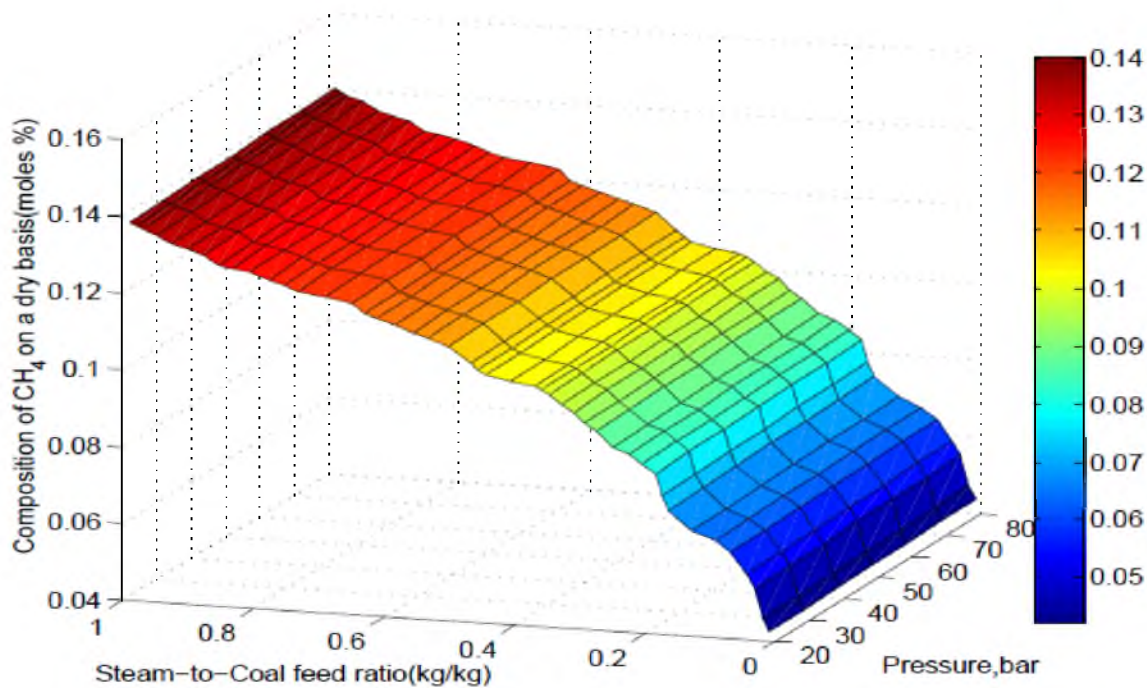


**Figure 4.10.** Effect of steam-to-coal feed ratio and pressure on concentration of CH<sub>4</sub> for Indonesian roto coal (oxygen-to-coal ratio: 1.0 kg/kg, coal feed rate: 1000 kg/h, temperature of water and coal: 313 K, temperature of oxygen: 333 K)

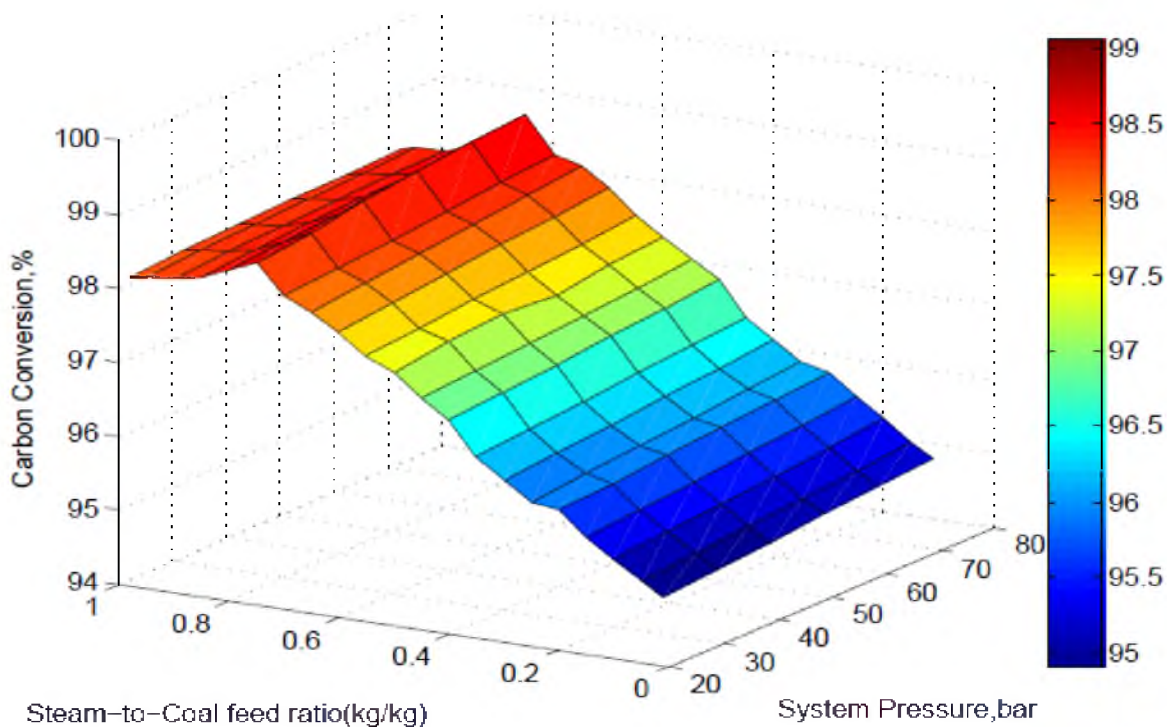


**Figure 4.11.** Effect of steam-to-coal feed ratio and system pressure on carbon conversion for Australian bituminous coal (oxygen-to-coal ratio: 1.0 kg/kg, coal feed rate: 1000 kg/h, temperature of water and coal: 313 K, temperature of oxygen: 333 K)

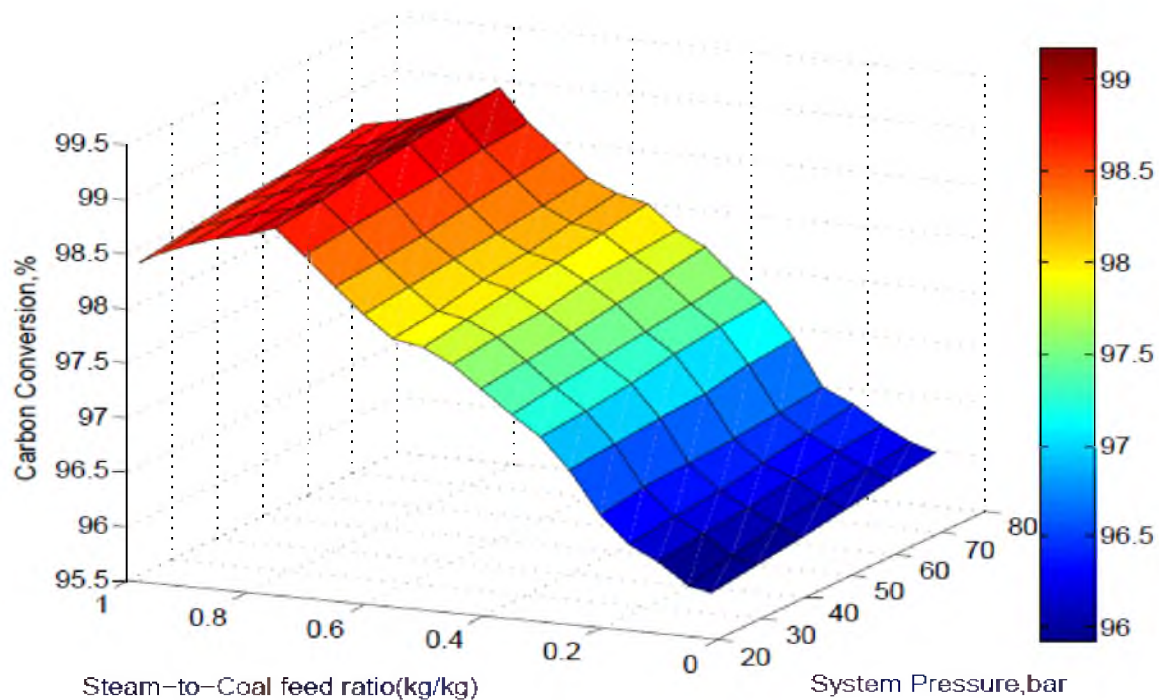


**Figure 4.12.** Effect of steam-to-coal ratio and system pressure on carbon conversion for Indonesian roto coal (oxygen-to-coal ratio: 1.0 kg/kg, coal feed rate: 1000 kg/h, temperature of water and coal: 313 K, temperature of oxygen: 333 K)

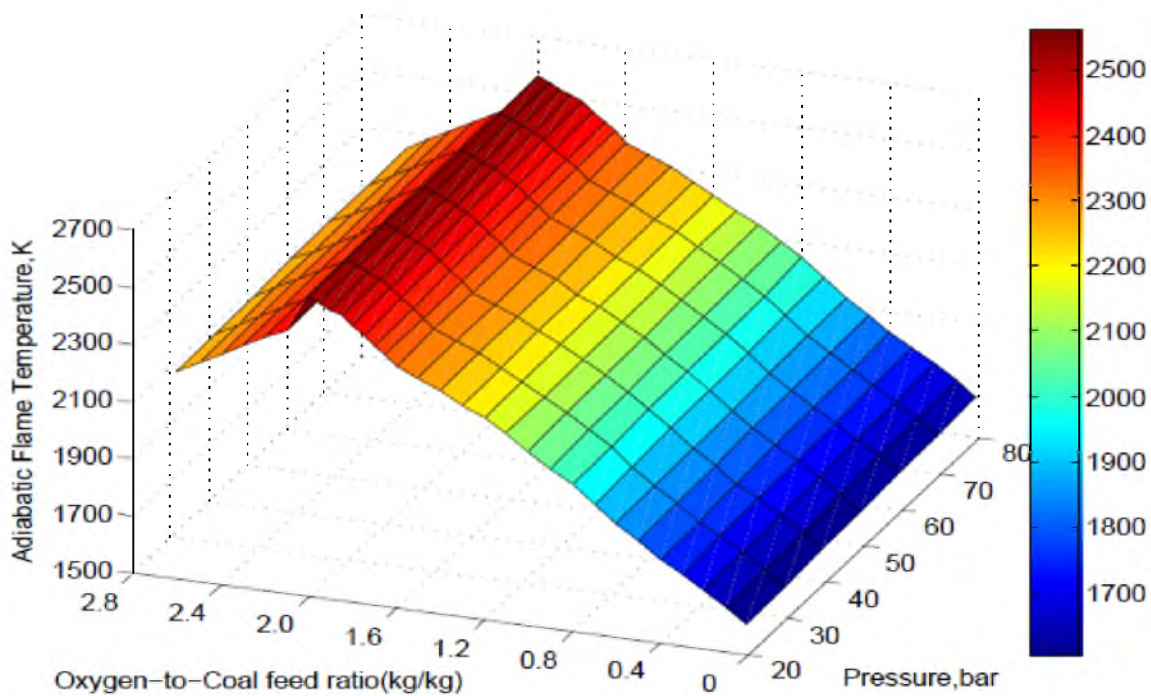


**Figure 4.13.** Effect of oxygen-to-coal feed ratio and pressure on adiabatic flame temperature of Australian bituminous coal (steam-to-coal ratio: 0.8 kg/kg, coal feed rate: 1000 kg/h, temperature of water and coal: 313 K, temperature of oxygen: 333 K)

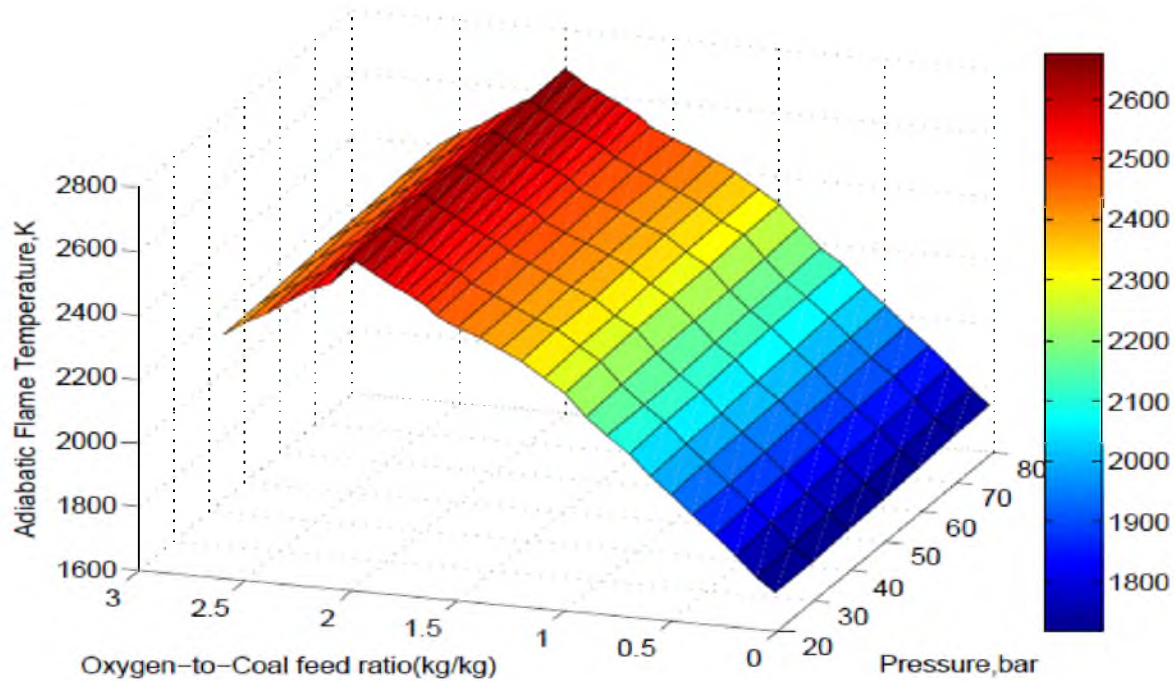


**Figure 4.14.** Effect of oxygen-to-coal feed ratio and pressure on adiabatic flame temperature of Indonesian roto coal (steam-to-coal ratio: 0.8 kg/kg, coal feed rate: 1000 kg/h, temperature of water and coal: 313 K, temperature of oxygen: 333 K)

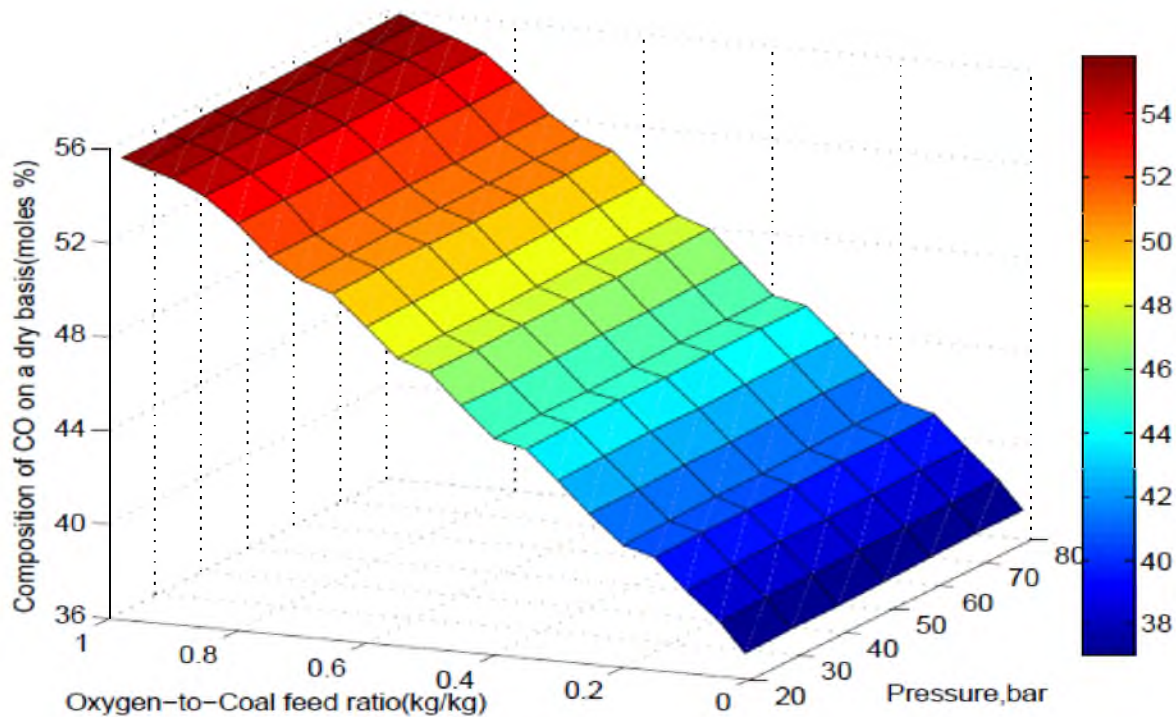


**Figure 4.15.** Effect of oxygen-to-coal feed ratio and pressure on concentration of CO for Australian bituminous coal (steam-to-coal ratio: 0.8 kg/kg, coal feed rate: 1000 kg/h, temperature of water and coal: 313 K, temperature of oxygen: 333 K)

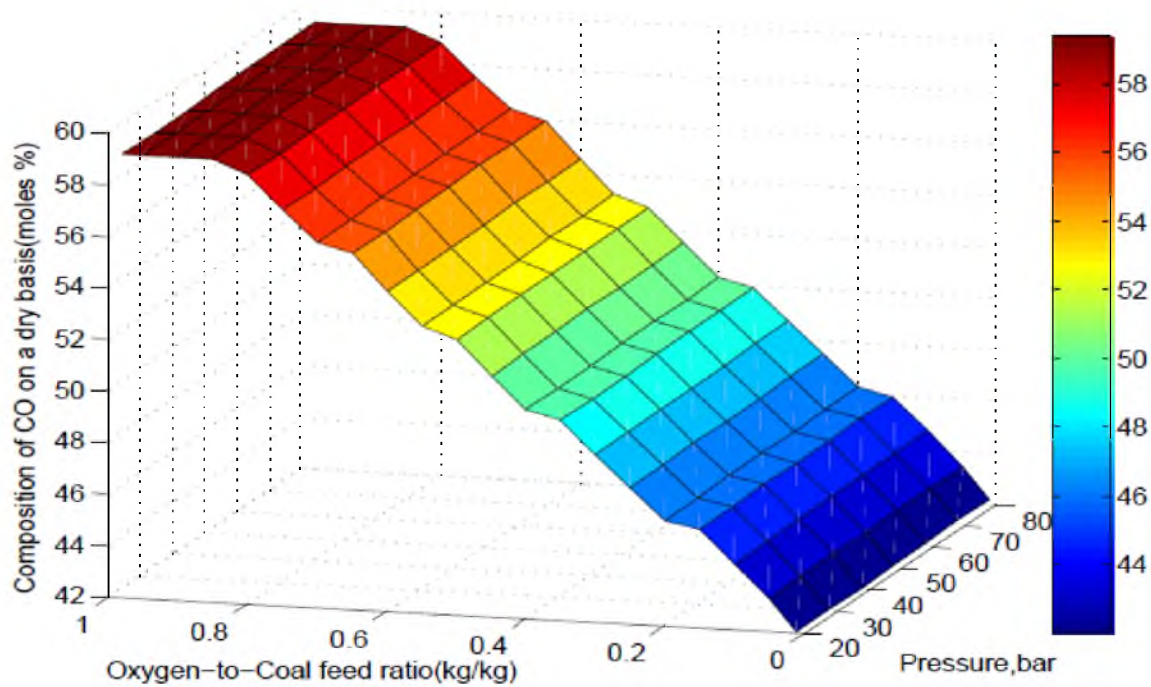


**Figure 4.16.** Effect of oxygen-to-coal feed ratio and pressure on concentration of CO for Indonesian roto coal (steam-to-coal ratio: 0.8 kg/kg, coal feed rate: 1000 kg/h, temperature of water and coal: 313 K, temperature of oxygen: 333 K)

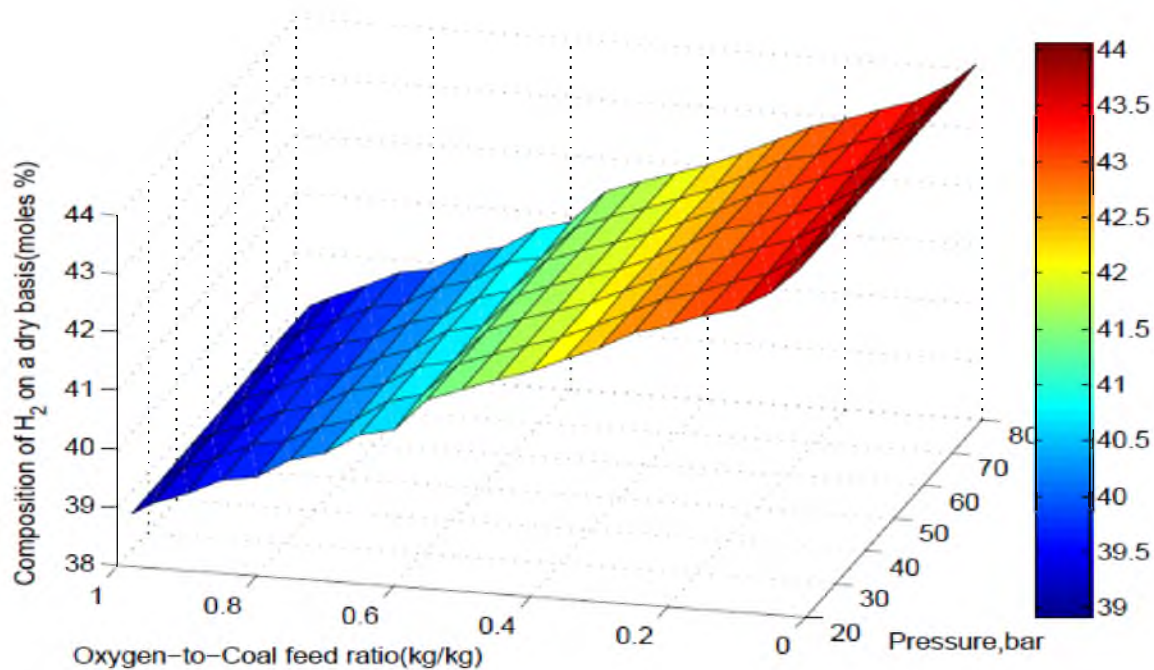


**Figure 4.17.** Effect of oxygen-to-coal feed ratio and pressure on concentration of  $H_2$  for Australian bituminous coal (steam-to-coal ratio: 0.8 kg/kg, coal feed rate: 1000 kg/h, temperature of water and coal: 313 K, temperature of oxygen: 333 K)

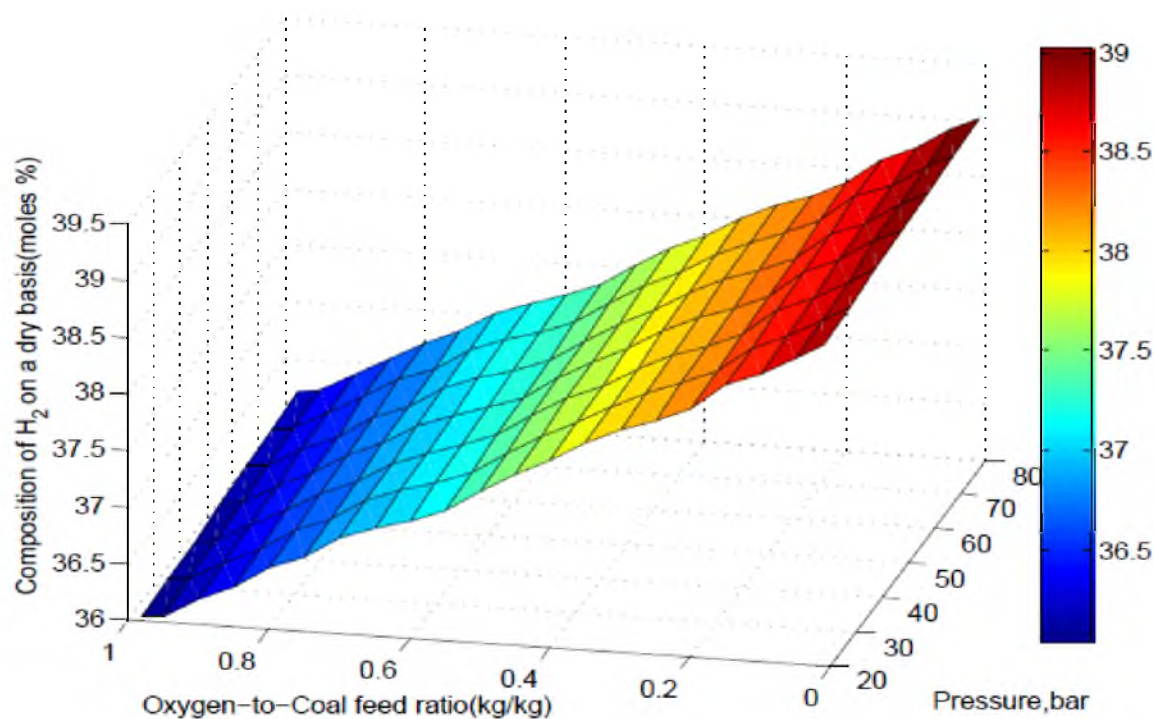


**Figure 4.18.** Effect of oxygen-to-coal feed ratio and pressure on concentration of  $H_2$  for Indonesian roto coal (steam-to-coal ratio: 0.8 kg/kg, coal feed rate: 1000 kg/h, temperature of water and coal: 313 K, temperature of oxygen: 333 K)

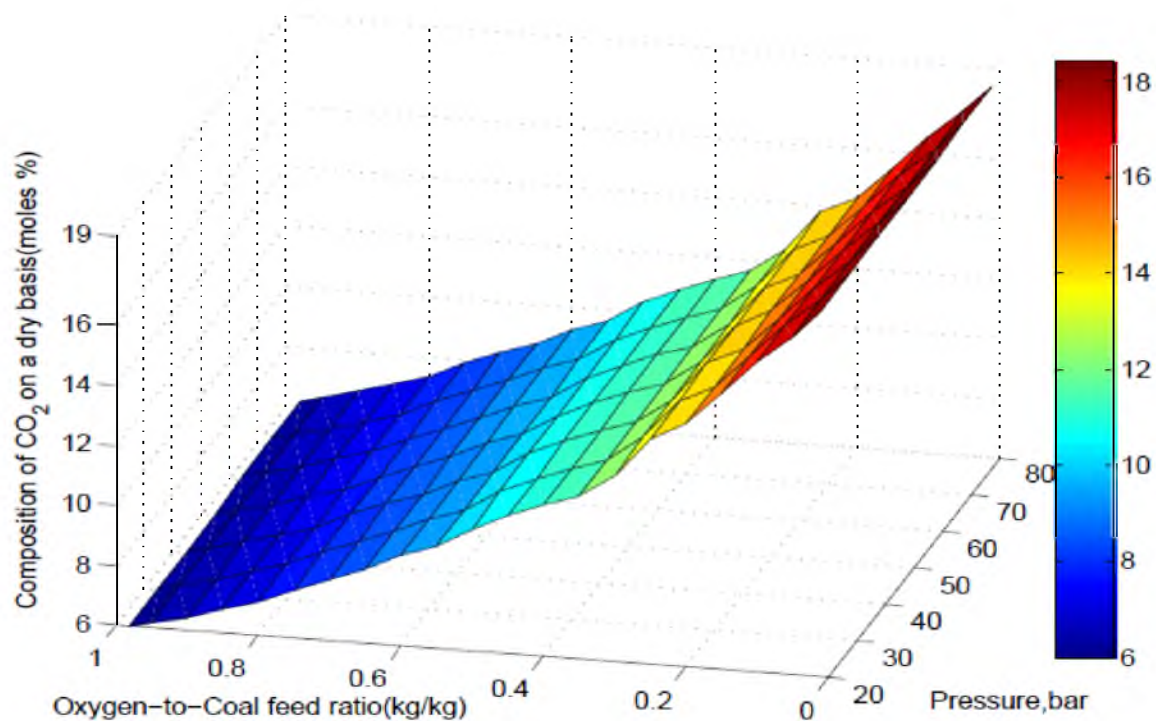


**Figure 4.19.** Effect of oxygen-to-coal feed ratio and pressure on concentration of  $\text{CO}_2$  for Australian bituminous coal (steam-to-coal ratio: 0.8 kg/kg, coal feed rate: 1000 kg/h, temperature of water and coal: 313 K, temperature of oxygen: 333 K)

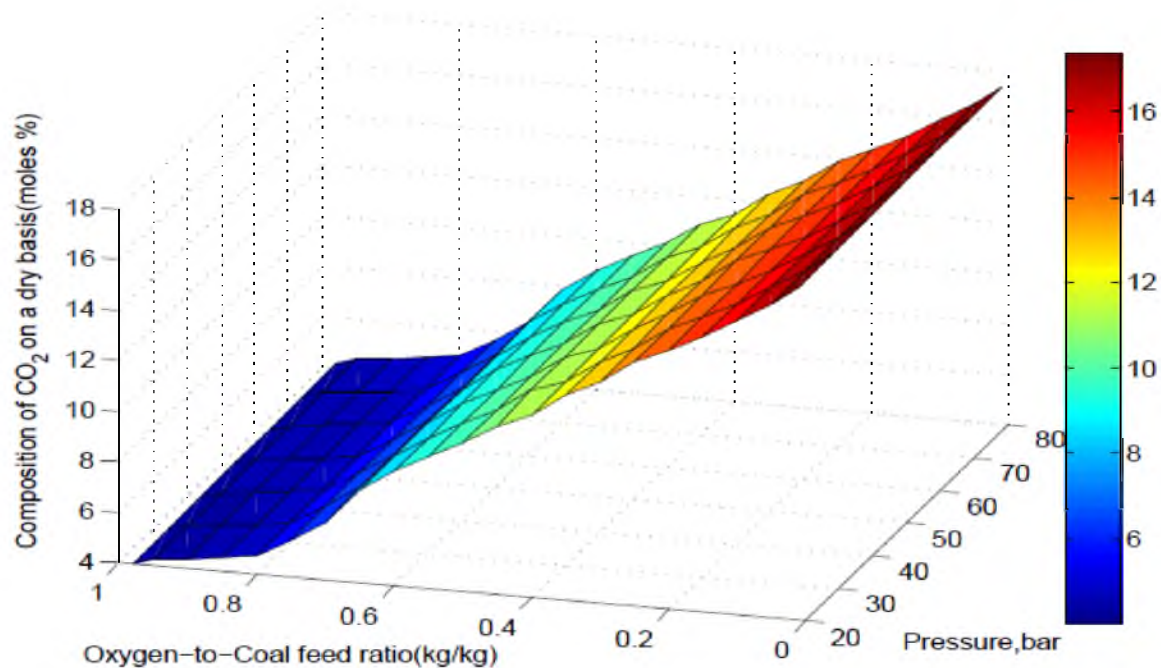


**Figure 4.20.** Effect of oxygen-to-coal feed ratio and pressure on concentration of  $\text{CO}_2$  for Indonesian roto coal (steam-to-coal ratio: 0.8 kg/kg, coal feed rate: 1000 kg/h, temperature of water and coal: 313 K, temperature of oxygen: 333 K)

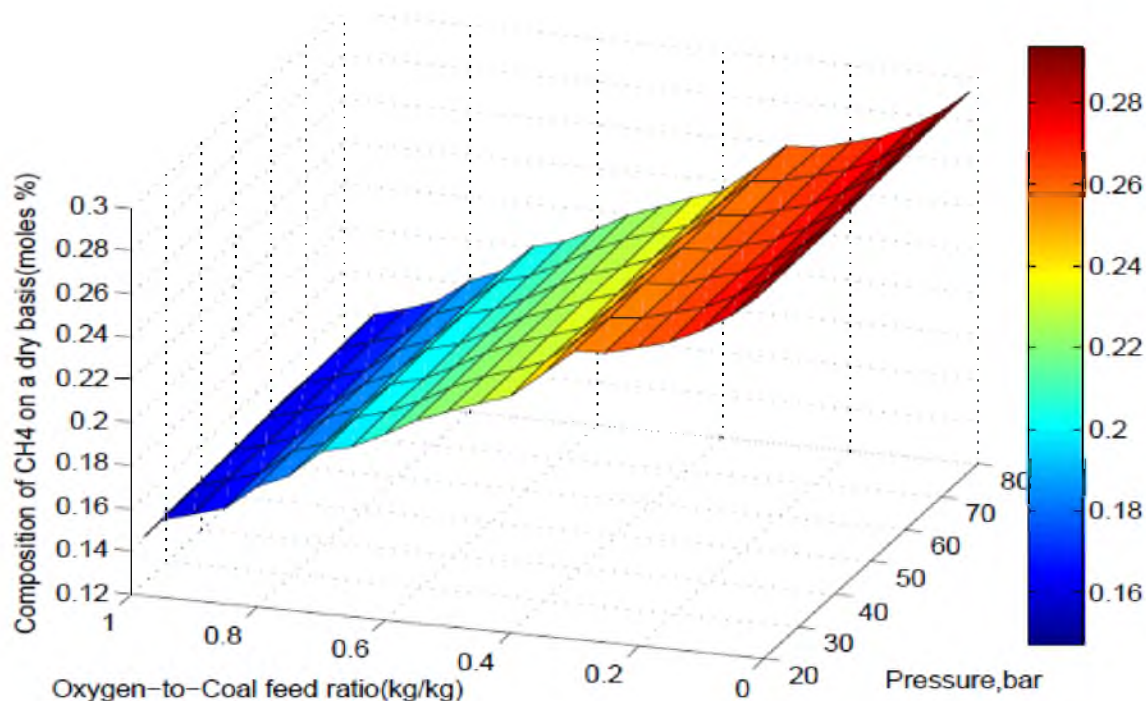


**Figure 4.21.** Effect of oxygen-to-coal feed ratio and pressure on concentration of CH<sub>4</sub> for Australian bituminous coal (steam-to-coal ratio: 0.8 kg/kg, coal feed rate: 1000 kg/h, temperature of water and coal: 313 K, temperature of oxygen: 333 K)

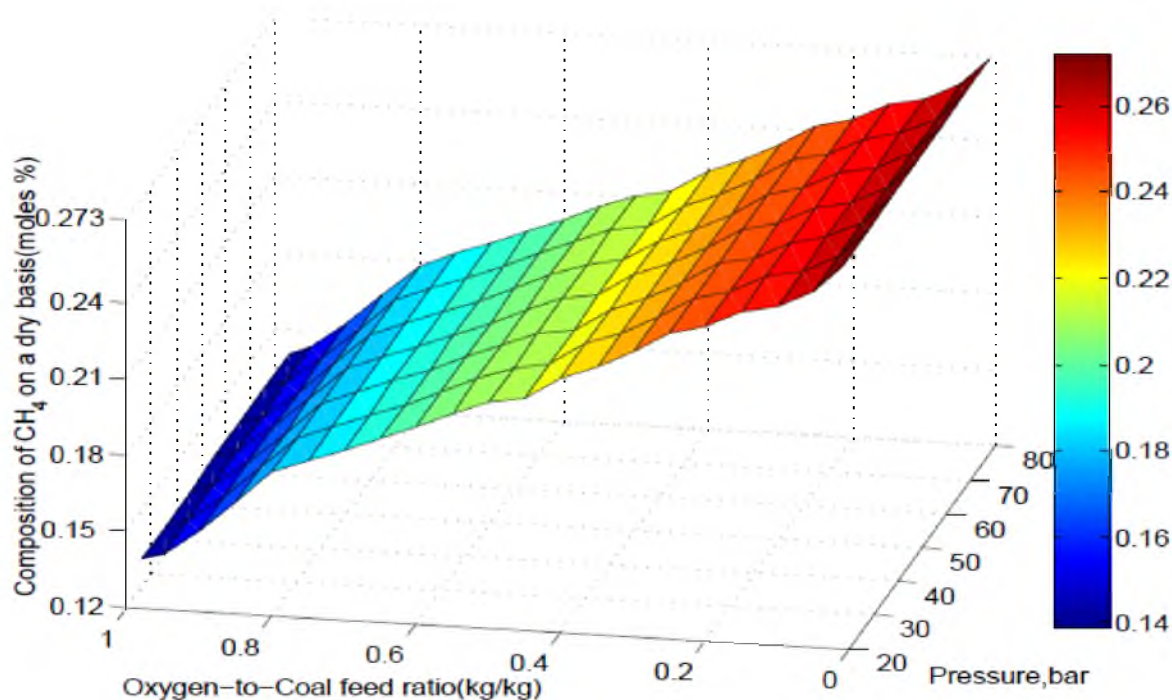


**Figure 4.22.** Effect of oxygen-to-coal feed ratio and pressure on concentration of CH<sub>4</sub> for Indonesian roto coal (steam-to-coal ratio: 0.8 kg/kg, coal feed rate: 1000 kg/h, temperature of water and coal: 313 K, temperature of oxygen: 333 K)



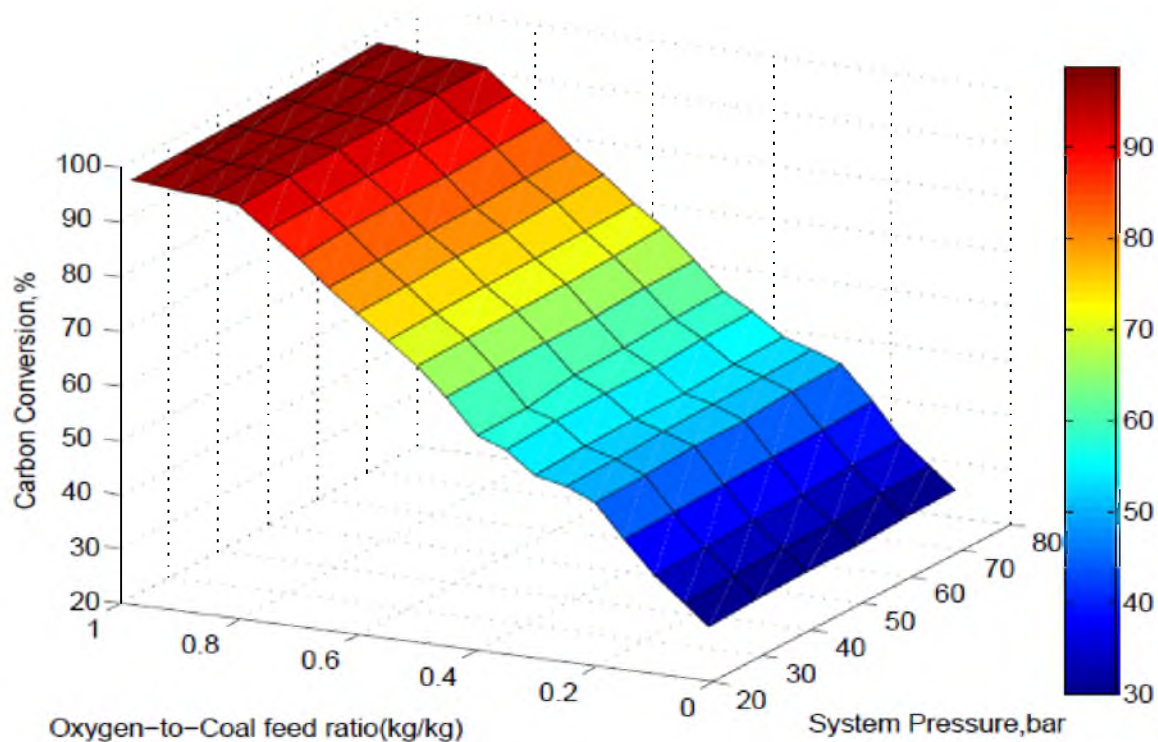


**Figure 4.23.** Effect of oxygen-to-coal feed ratio and system pressure on carbon conversion for Australian bituminous coal (steam-to-coal ratio: 0.8 kg/kg, coal feed rate: 1000 kg/h, temperature of water and coal: 313 K, temperature of oxygen: 333 K)

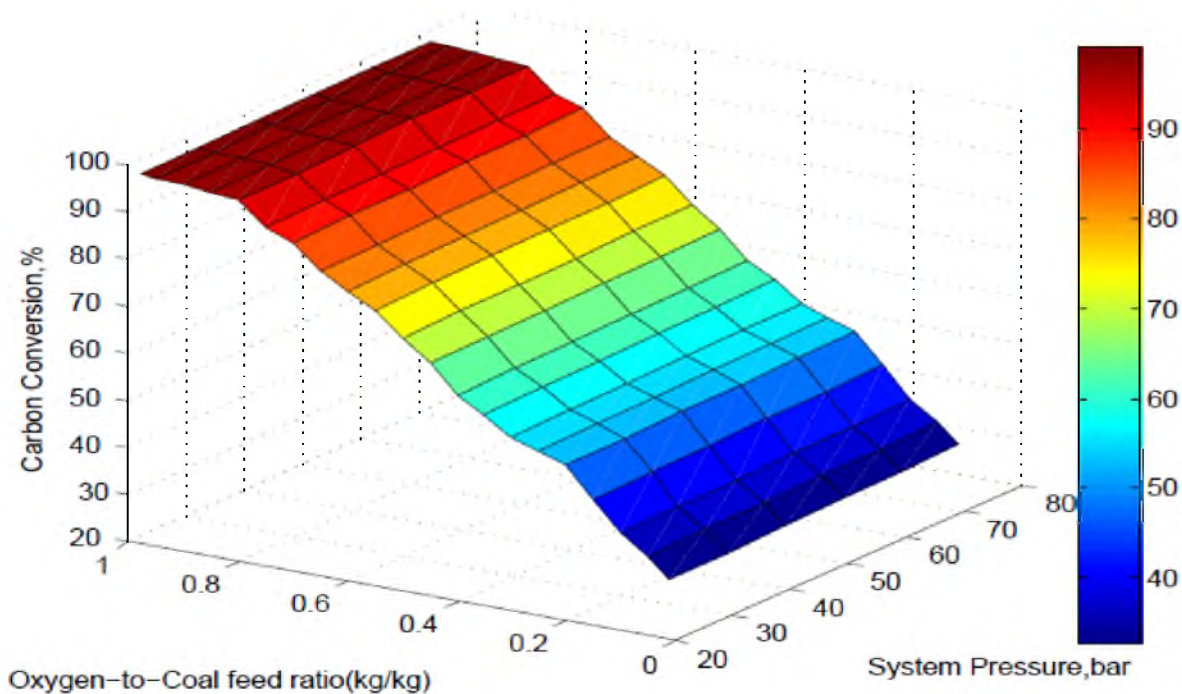


**Figure 4.24.** Effect of oxygen-to-coal feed ratio and system pressure on carbon conversion for Indonesian roto coal (steam-to-coal ratio: 0.8 kg/kg, coal feed rate: 1000 kg/h, temperature of water and coal: 313 K, temperature of oxygen: 333 K)

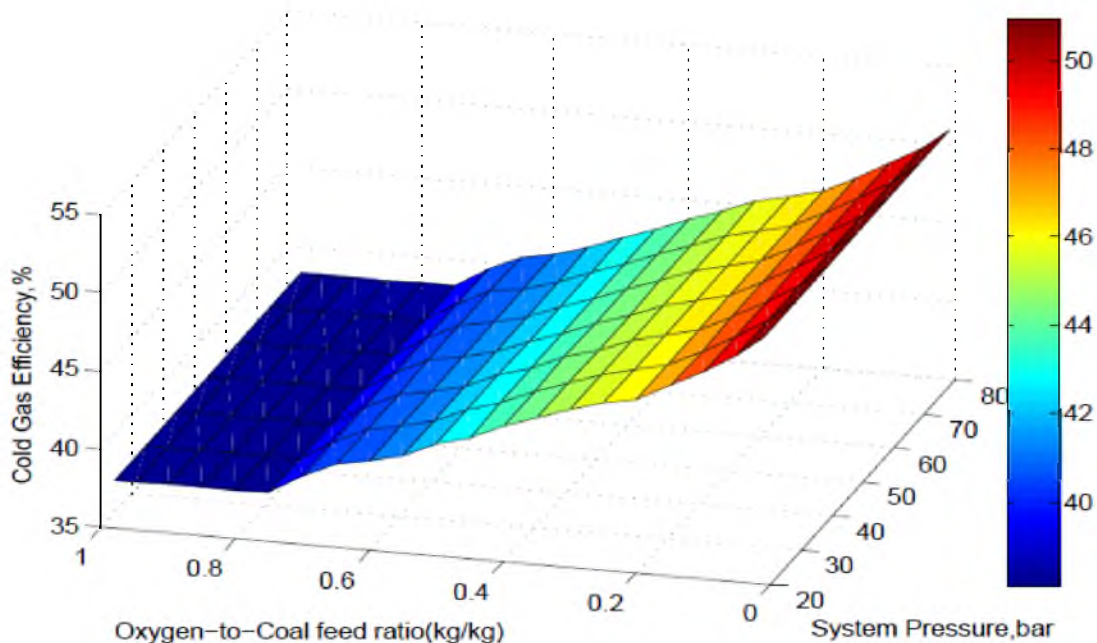


**Figure 4.25.** Effect of oxygen-to-coal feed ratio and system pressure on cold gas efficiency for Australian bituminous coal (steam-to-coal ratio: 0.8 kg/kg, coal feed rate: 1000 kg/h, temperature of water and coal: 313 K, temperature of oxygen: 333 K)

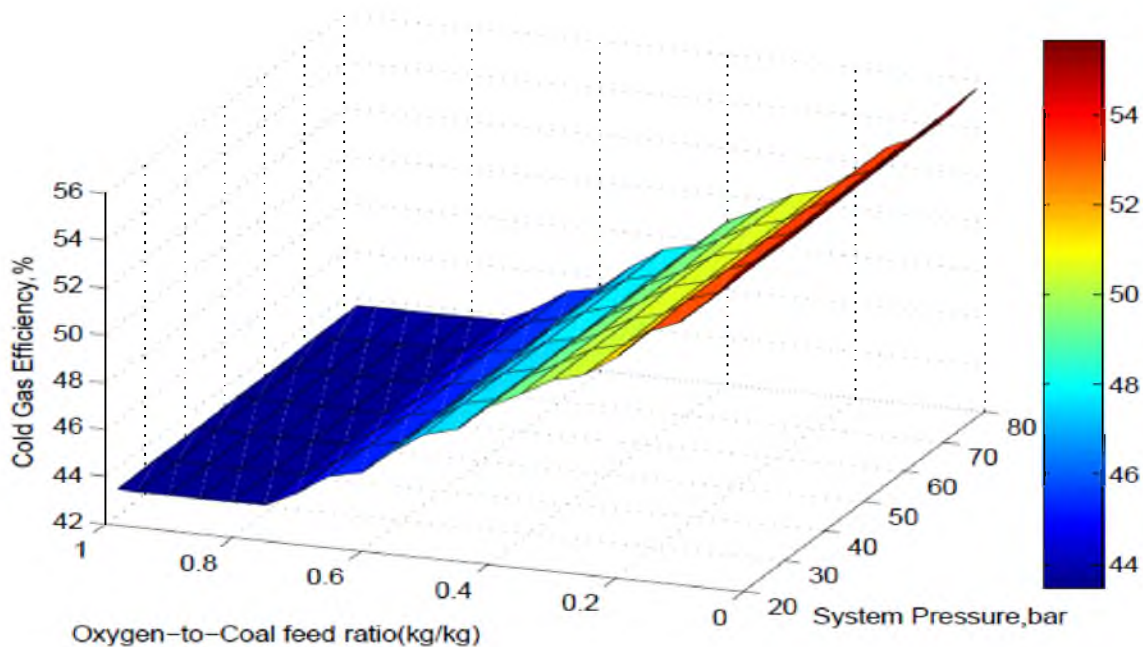


**Figure 4.26.** Effect of oxygen-to-coal feed ratio and system pressure on cold gas efficiency for Indonesian roto coal (steam-to-coal ratio: 0.8 kg/kg, coal feed rate: 1000 kg/h, temperature of water and coal: 313 K, temperature of oxygen: 333 K)

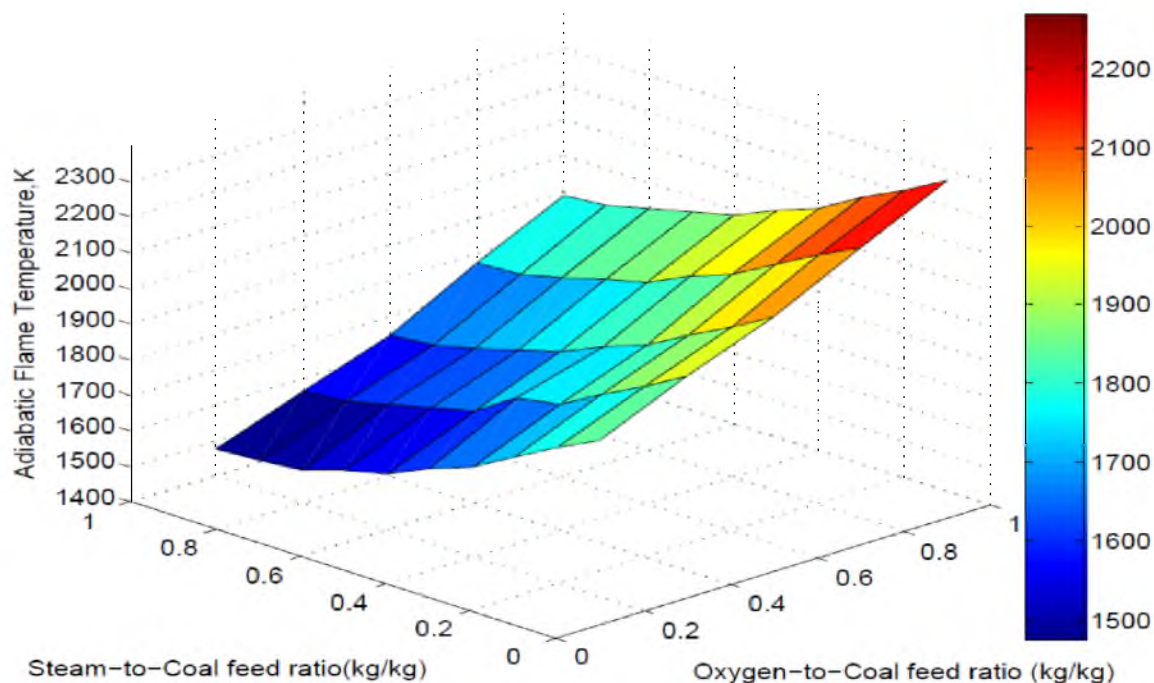


**Figure 4.27.** Effect of oxygen-to-coal ratio and steam-to-coal ratio on adiabatic flame temperature for Australian bituminous coal (coal feed rate: 1000 kg/h, temperature of water and coal: 313 K, temperature of oxygen: 333 K)

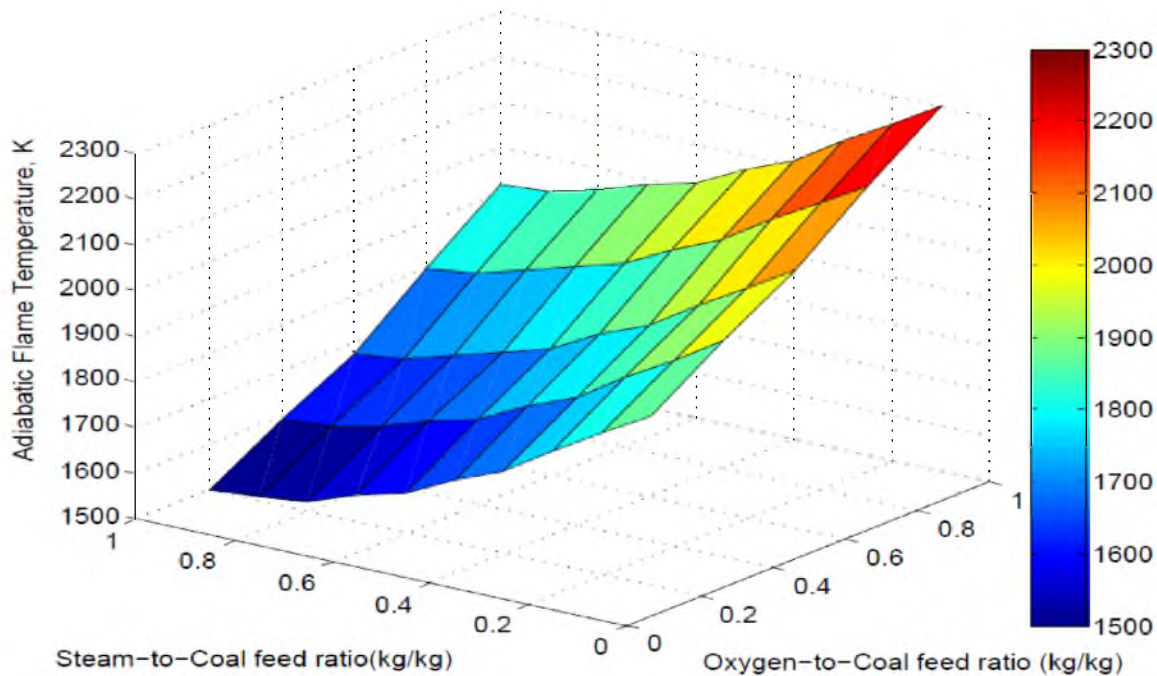


**Figure 4.28.** Effect of oxygen-to-coal ratio and steam-to-coal ratio on adiabatic flame temperature for Indonesian roto coal (coal feed rate: 1000 kg/h, temperature of water and coal: 313 K, temperature of oxygen: 333 K)

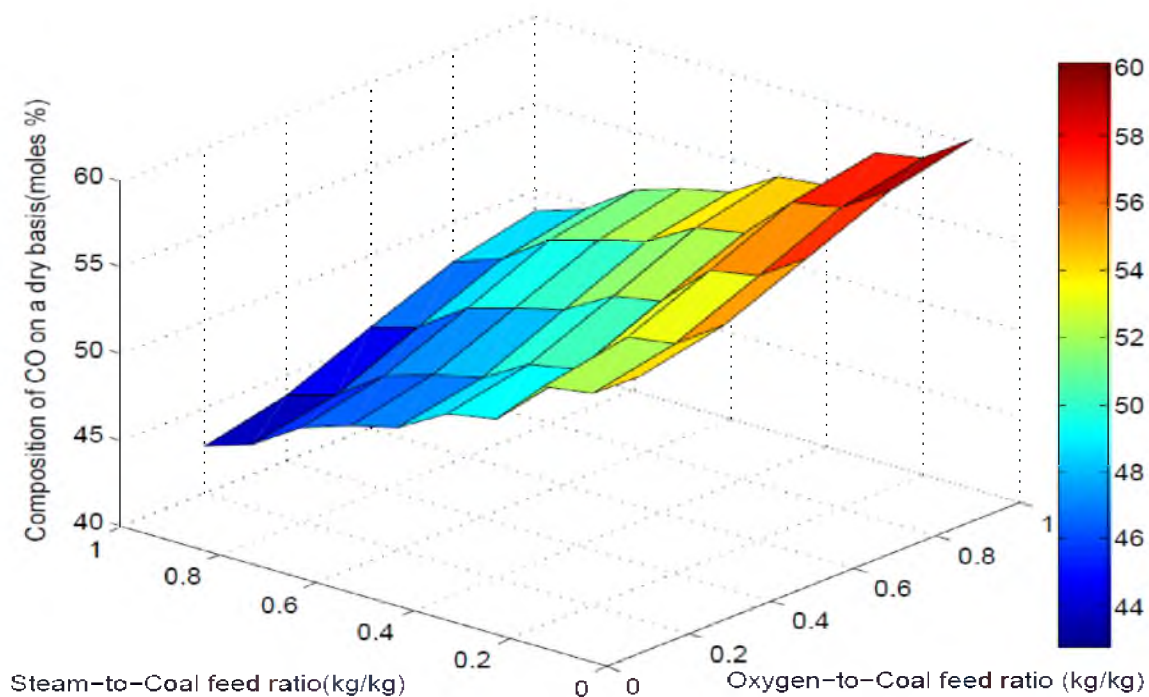


**Figure 4.29.** Effect of oxygen-to-coal ratio and steam-to-coal ratio on CO production for Australian bituminous coal (coal feed rate: 1000 kg/h, temperature of water and coal: 313 K, temperature of oxygen: 333 K)

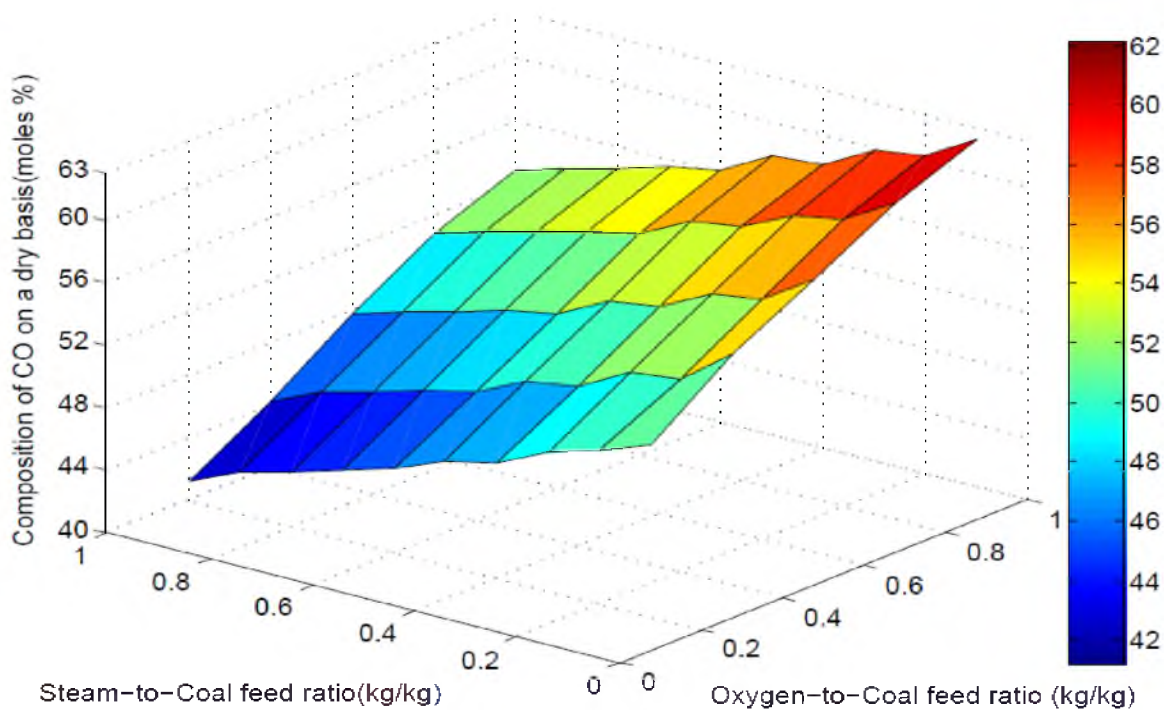


**Figure 4.30.** Effect of oxygen-to-coal ratio and steam-to-coal ratio on CO production for Indonesian roto coal (coal feed rate: 1000 kg/h, temperature of water and coal: 313 K, temperature of oxygen: 333 K)

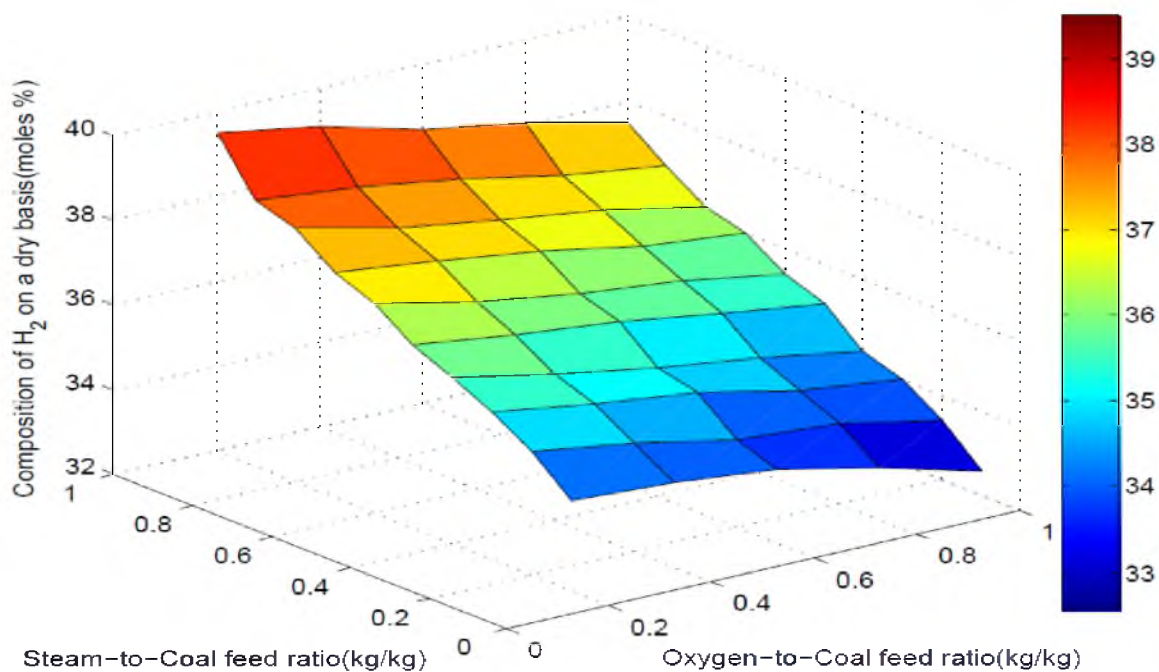


**Figure 4.31** Effect of oxygen-to-coal ratio and steam-to-coal ratio on H<sub>2</sub> production for Australian bituminous coal (coal feed rate: 1000 kg/h, temperature of water and coal: 313 K, temperature of oxygen: 333 K)

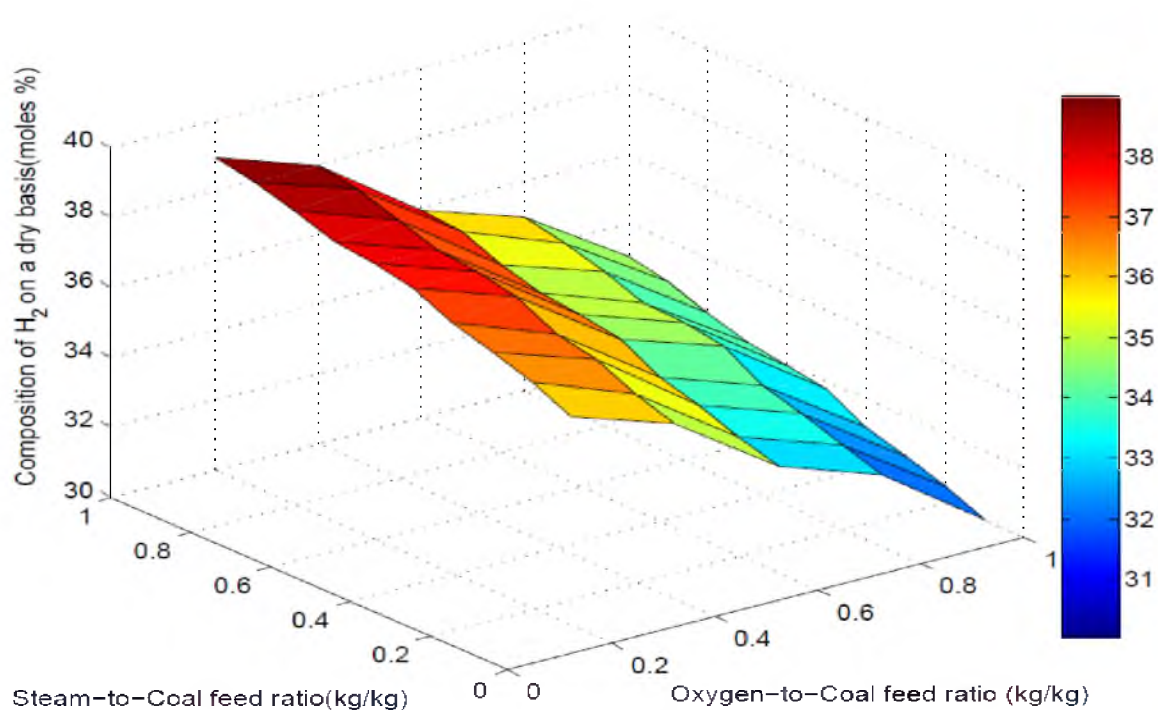


**Figure 4.32** Effect of oxygen-to-coal ratio and steam-to-coal ratio on H<sub>2</sub> production for Indonesian roto coal (coal feed rate: 1000 kg/h, temperature of water and coal: 313 K, temperature of oxygen: 333 K)

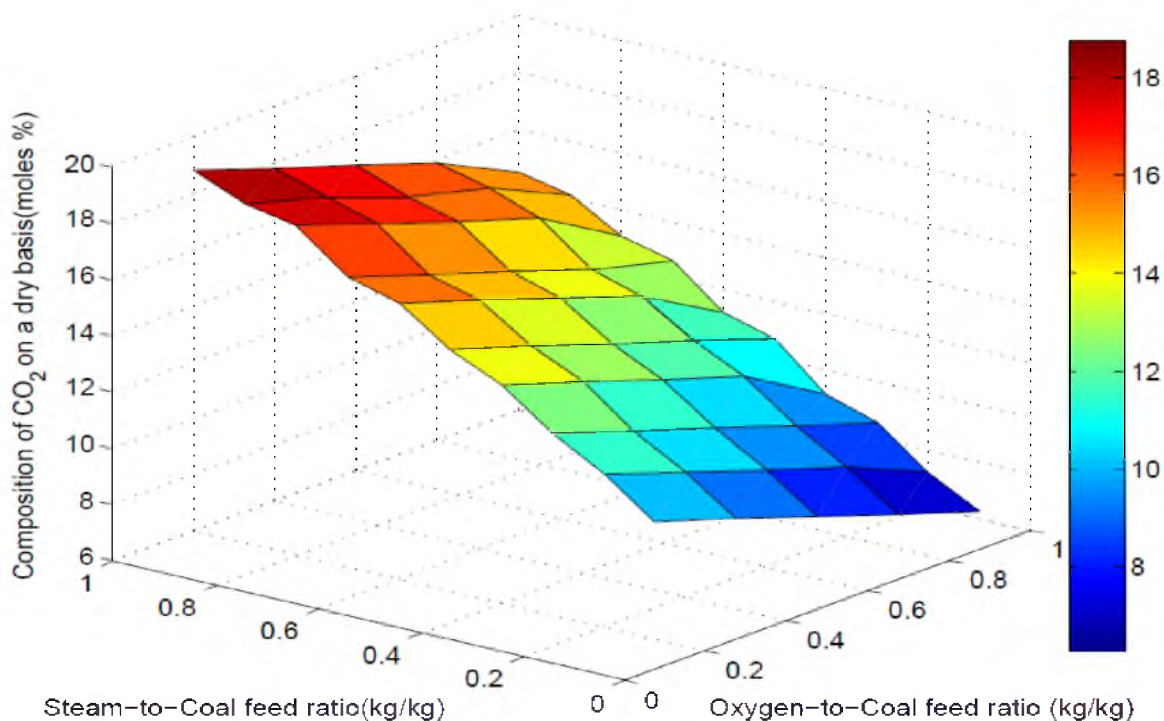


**Figure 4.33** Effect of oxygen-to-coal ratio and steam-to-coal ratio on CO<sub>2</sub> production for Australian bituminous coal (coal feed rate: 1000 kg/h, temperature of water and coal: 313 K, temperature of oxygen: 333 K)

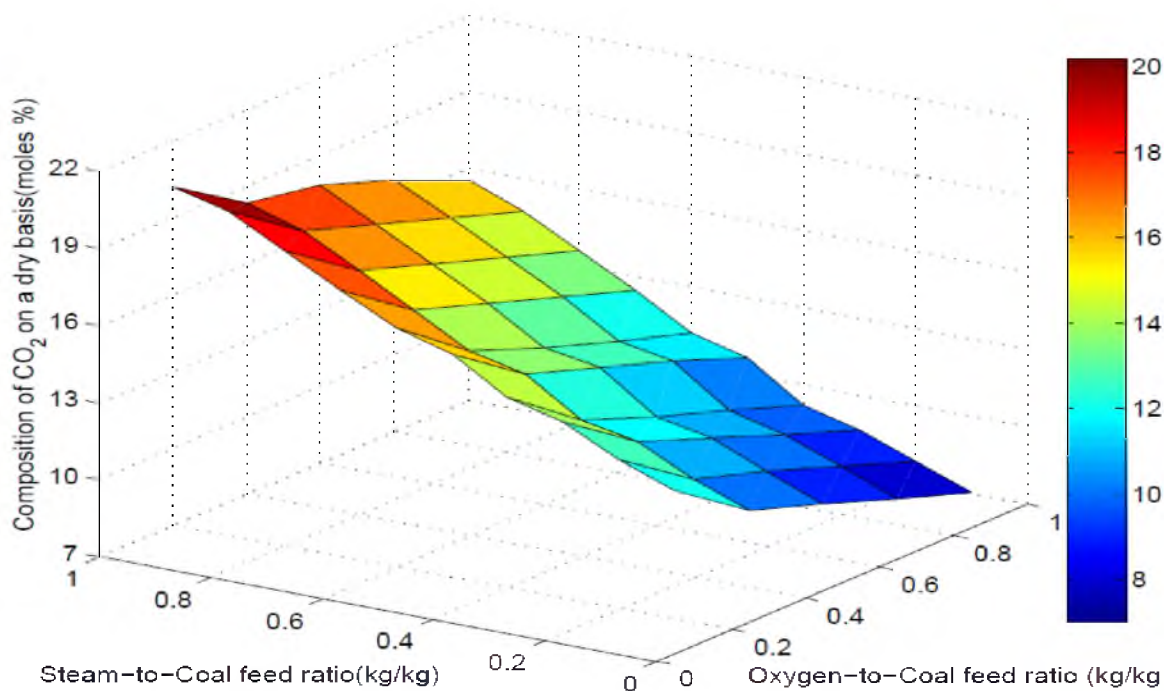


**Figure 4.34** Effect of oxygen-to-coal ratio and steam-to-coal ratio on CO<sub>2</sub> production for Indonesian roto coal (coal feed rate: 1000 kg/h, temperature of water and coal: 313 K, temperature of oxygen: 333 K)

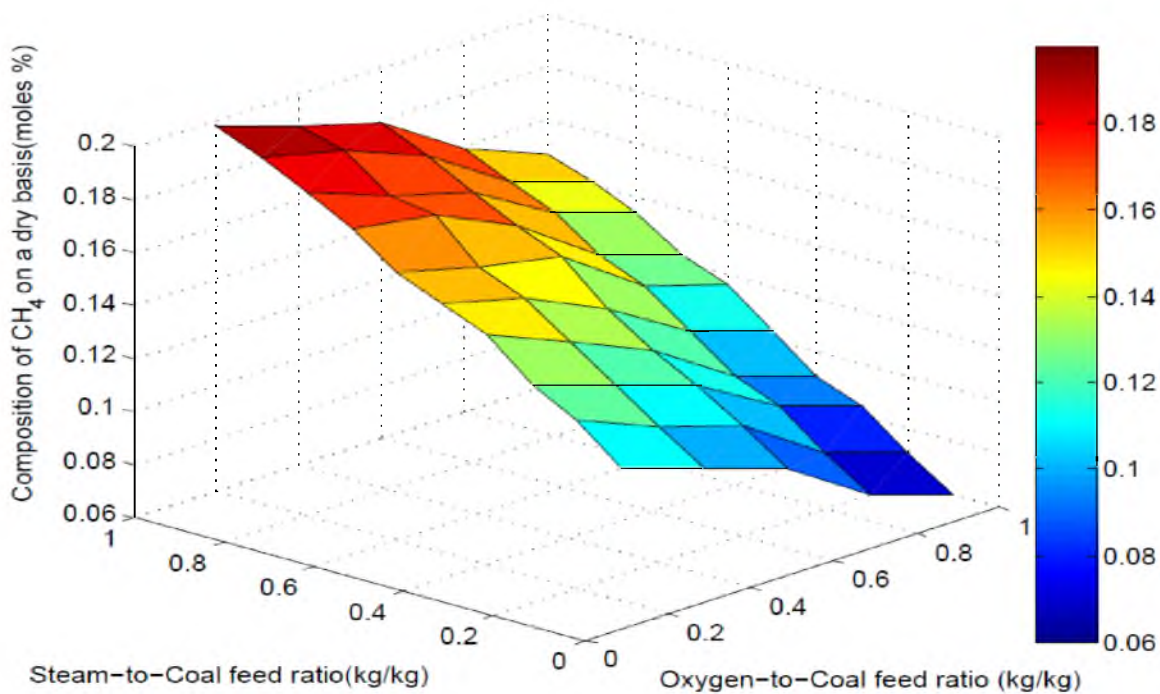


**Figure 4.35** Effect of oxygen-to-coal ratio and steam-to-coal ratio on CH<sub>4</sub> production for Australian bituminous coal (coal feed rate: 1000 kg/h, temperature of water and coal: 313 K, temperature of oxygen: 333 K)

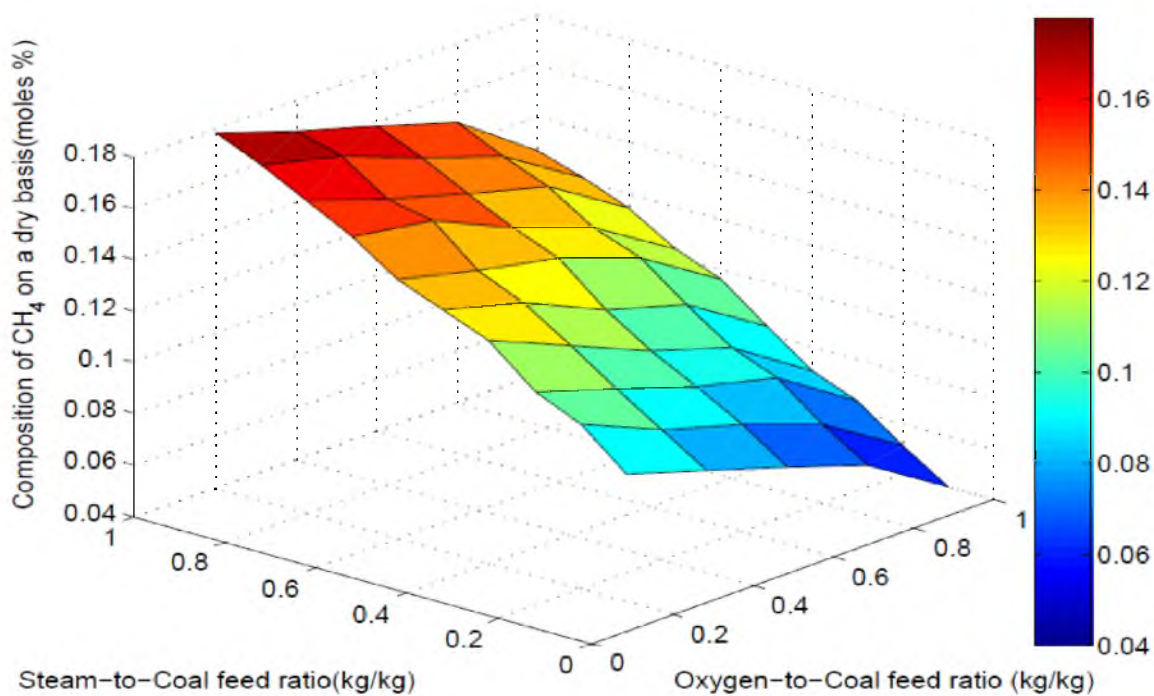


**Figure 4.36** Effect of oxygen-to-coal ratio and steam-to-coal ratio on CH<sub>4</sub> production for Indonesian roto coal (coal feed rate: 1000 kg/h, temperature of water and coal: 313 K, temperature of oxygen: 333 K)

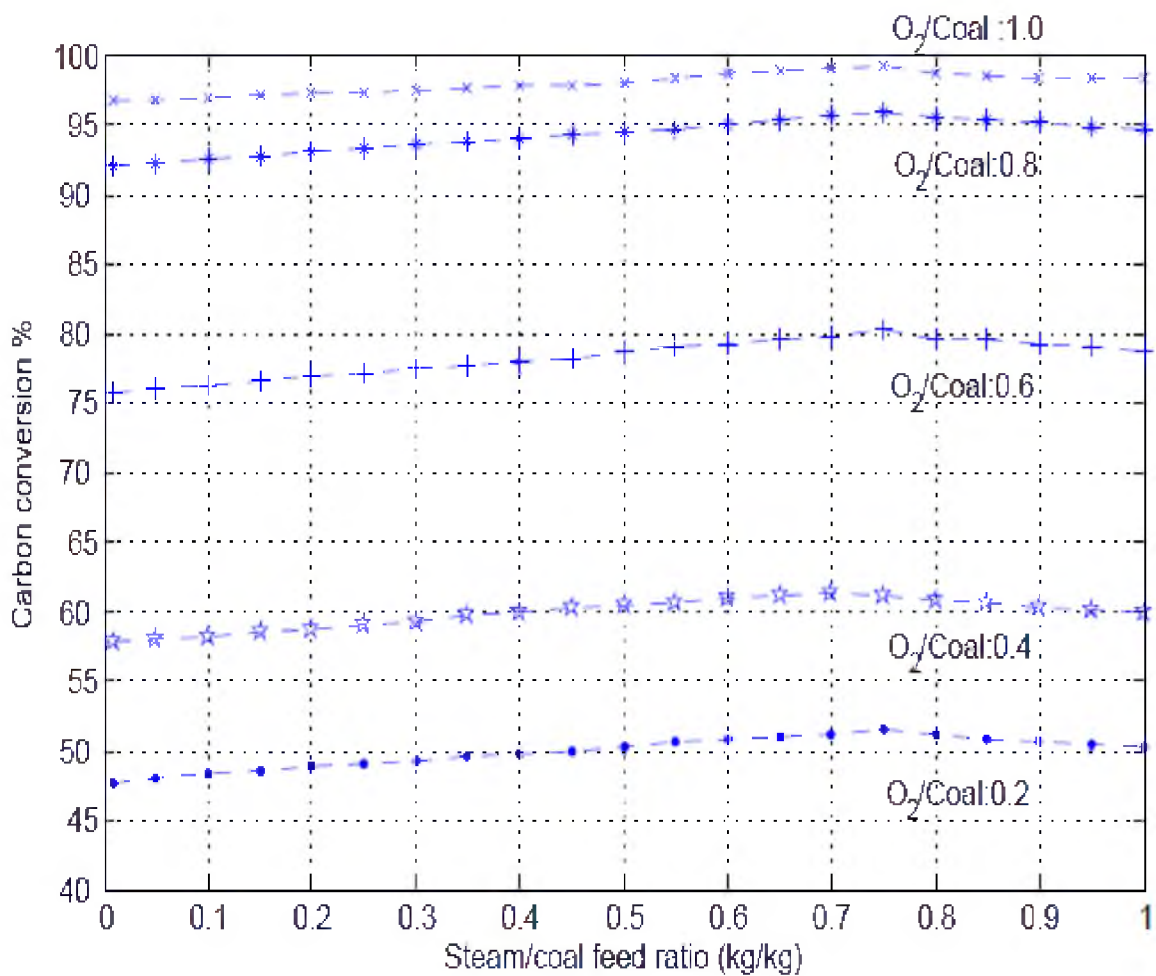


**Figure 4.37** Effect of steam-to-coal feed ratio on coal conversion at various oxygen-to-coal feed ratios at 40 bar.



## **CHAPTER 5**

### **MODELING OF ADIABATIC FLAME TEMPERATURE**

#### **5.1 Modeling of Adiabatic Flame Temperature Corresponding to Different System Parameters in Entrained Flow Gasifier**

In this study, the adiabatic flame temperature was modelled by using operating input parameters. The aim of this work was to develop the basic correlations between the flame temperature as a response and input parameters, and to predict the flame temperature roughly in the entrained flow gasifier without any gasification calculations. Then, the results have been compared with the simulation to make the consistency between variables.

Recently, the concentration of methane produced during coal gasification has been used to predict the adiabatic flame temperature. Optical monitoring systems have been following the methane absorbance peaks and based on these peaks, the temperature can be determined in the gasifier. However, there are not enough studies for this new field and too few researchers who are interested in optical measurements for measuring temperature. The relationship between flame temperature and methane product was evaluated according to ChemCAD simulation results in this study. The important note is that the reliability of the results should be supported by experiments to make a good decision.

The gasification results of Australian bituminous coal have been used to calculate the flame temperature in entrained flow gasifier. There are two main input parameters to adjust the temperature of Australian coal: oxygen-to-coal feed ratio (kg/kg) and steam-to-coal feed ratio (kg/kg). The other operating conditions such as initial temperature of coal and oxygen, gasifier pressure and steam temperature have been kept constant. The temperature of coal and water were considered as 313 K, the temperature of air was 333 K and total pressure was assumed to be 40 bar. The methodology of the study to find model equations is given below.

## **5.2 The Correlation between Methane Concentration and Gasification Temperature**

The adiabatic temperature of Australian bituminous coal and the concentration of methane were determined based on different oxygen-to-coal and steam-to-coal feed ratios at constant operating conditions. The flame temperature and methane production were considered as output response with increasing oxygen-to-coal feed ratio at the steam-to-coal ratios of 0.6, 0.8, 1.0 and 1.2 kg/kg, respectively. Here, the pressure was selected at 40 bar. Secondly, the adiabatic flame temperature and methane product gas distributions were indicated with increasing steam-to-coal ratio at different oxygen-to-coal ratios of 1.0, 1.2 and 1.4 kg/kg, respectively.

Then, the relationship between flame temperature and composition of methane was illustrated with steam-to-coal ratio of 0.8 kg/kg and oxygen-to-coal ratio of 1.0 kg/kg at constant pressure and temperature. The aim of this step was to understand the trend of adiabatic flame temperature corresponding to methane production. This approach also provides the overview about the estimation of flame temperature and the required

methane production to get high temperature value as well. If the methane concentration is known in the gasifier, the adiabatic flame temperature can be estimated roughly.

The correlations have been developed and shown in the chart. According to the relationship between adiabatic flame temperature and fraction of methane product gas, the models have been developed.

### **5.3 Effect of Oxygen-to-Coal Ratio on Adiabatic Flame**

#### **Temperature and Composition of Methane**

##### **at Different Steam-to-Coal Feed Ratios**

The tendency between adiabatic flame temperature and methane product with increasing oxygen-to-coal feed ratio at different steam-to-coal ratio is illustrated in Figure 5.1. The blue line indicates the flame temperature distribution and the green line presents the CH<sub>4</sub> production of Australian bituminous coal. The ratio of oxygen-to-coal varied from 0.019 to 2.6 kg/kg. In addition to this, the steam-to-coal ratio was changed from ratio of 0.6 kg/kg to ratio of 1.2 kg/kg. As can be seen from the graph, the adiabatic flame temperature increases when the amount of oxygen-to-coal ratio increases until 2.0 kg/kg. At that point, the gasification of coal just finished roughly. It is clear that the decreasing line occurs after the ratio of 2.0. The reason for this tendency is due to the fact that gasification products absorb the heat from the gasifier. Thus, this situation causes a decrease in the flame temperature, eventually. Therefore, the gasification regime can occur until the ratio of 2.0 kg/kg and after that, complete combustion occurs.

The second parametric observation is about methane production. The ppm unit is usually used for low concentration of products in industry. As expected, the composition of methane is very low compared to other gasification products. In this part, the ppm

level for methane was chosen to develop the empirical model. The amount of  $\text{CH}_4$  slightly decreases with increasing oxygen-to-coal ratio. The reduction in the fraction of methane with increasing oxygen-to-coal ratio follows from the smaller quantity of hydrogen produced. In reality, a reasonable range for entrained-flow gasifiers (the only type that is really relevant here, since others do not approach chemical equilibrium) is 0-2000 ppm, with the most interest being in the 100-500 ppm range. The 400-500 ppm range could be reached before an oxygen-to-coal ratio of 2.0 kg/kg at low ratios of steam-to-coal. With increasing steam-to-coal ratio (see Figure 5.1), this optimum range switched to right side of oxygen-to-coal ratio of 2.0 or around the ratio of 2.2-2.3. However, at these ratios, the gasification process almost finished and it is much better to catch this optimum range in the gasification regime.

#### **5.4 Effect of Steam-to-Coal Ratio on Adiabatic Flame**

##### **Temperature and Composition of Methane at Different Oxygen-to-Coal Feed Ratios**

This section contains the temperature and methane distribution related to steam-to-coal feed ratio at constant temperature of coal, water and system pressure. The aim of this section is to comprehend the importance of steam-to-coal ratio on adiabatic flame temperature and  $\text{CH}_4$  production. As similar to section 1, the ChemCAD software program was used to determine the adiabatic flame temperature and  $\text{CH}_4$  product gas with increasing steam-to-coal feed ratio at different oxygen-to-coal feed ratios such as 1.0, 1.2 and 1.4 kg/kg in the entrained flow gasifier.

Figure 5.2 displays the adiabatic flame temperature and methane distribution based on steam-to-coal feed ratio (kg/kg) at pressure (40 bar). According to graph, the

flame temperature, the blue line, decreases with increasing steam-to-coal ratio. After the ratio of 0.91, there is not much change on temperature profile. Although an increase in steam-to-coal feed ratio promotes the char-steam reaction, the temperature decreases because the char-steam reaction is highly endothermic and lowers the reaction temperature.

On the other hand, the methane concentration, the green line, increases slightly while increasing steam-to-coal ratio for each oxygen-to-coal feed ratio. However, the steam-to-coal ratio does not have an important influence on methane production. It can be concluded that there is a reverse proportion between methane production and flame temperature. The lowest concentration of methane has been occurred at the highest flame temperature and minimum steam-to-coal ratio.

### **5.5 Modeling of ChemCAD Results**

In the previous sections, the ChemCAD simulation results for coal gasification of Australian bituminous coal and Indonesian roto coal were shown with figures. Then the relationship between adiabatic flame temperature and the concentration of methane with respect to different input parameters was evaluated (see Chapter 4 and Chapter 5). The last step is to use ChemCAD results to develop the correlation between the flame temperature and the methane concentration. The flame temperature and methane production distribution were illustrated in Figure 5.3 and case 1 denotes the parameters as oxygen-to-coal feed ratio and pressure at constant steam-to-coal ratio and coal flow rate (1000 kg/h).

The second graphic display called case 2, represents steam-to-coal ratio and pressure at constant oxygen-to-coal ratio, coal flow rate and temperature of input

parameters. In case 1, the oxygen-to-coal ratio and pressure increase from right side to left side while steam-to-coal ratio keeps constant at 0.8 kg/kg. As can be seen in the figure below, the temperature increases while the composition of methane decreases dramatically. However, the temperature of gasifier begins to decrease after oxygen-to-coal the ratio of 2.0 kg/kg. The reason for this trend can be explained because all species are completely burned at oxygen-to-coal ratio of 2.0, so additional oxygen inputs delutes the gas and absorbs heat. After this observation, the modeling of case 1 has been divided into two subparts: until gasification and after gasification.

Case 2 follows a different path. It includes the effect of steam and pressure on concentration of methane and flame temperature. The ratio of steam-to-coal again increases from left to right and there is clearly a reverse proportion between flame temperature and  $\text{CH}_4$  production at constant oxygen-to-coal ratio of 1.0 kg/kg. The adiabatic flame temperature reaches the minimum level at the highest steam-to-coal ratio, although an increase in steam-to-coal ratio promotes the char-steam reaction, the temperature decreases because the char-steam reaction is highly endothermic and lowers the reaction temperature.

Figure 5.3 demonstrates that the composition of methane for both cases is very low because it is an unexpected product in the entrained flow gasifier. It is basically a reasonable observation as the fraction of tar,  $\text{NO}_x$  compounds and methane are negligible in the entrained flow gasifier as mentioned in the Chapter 1. The reasonable range of composition of methane is generally assumed to be 0-2000 ppm and this study shows that the concentration of methane is an acceptable level for both cases. The problem is that it is very difficult to compare that results with actual ones due to the lack of studies.

However, for case 1, the methane production, 450 ppm, was reached at the oxygen-to-coal ratio of 2.0 kg/kg. In addition to this, the steam-to-coal ratio does not have a great influence on methane production. The fraction of CH<sub>4</sub> did not change significantly as the steam-to-coal feed ratio changed. Therefore, the effect of oxygen-to-coal ratio is more important than the steam-to-coal ratio for methane production in the gasifier.

In the model, firstly, the concentration of methane was basically considered as a input parameter to predict the adiabatic flame temperature and then, the other input parameters such as oxygen-to-coal ratio, steam-to-coal ratio and pressure were taken into consideration to estimate the flame temperature relatively.

### 5.5.1 Linear Model

The adiabatic flame temperature can be determined by using methane parameter in linear model as shown:

$$y = a_1 * t + a_0 \quad (5.1)$$

where y denotes adiabatic flame temperature, T, and t express the methane gas in terms of ppm unit as well. To find the a<sub>1</sub> and a<sub>0</sub> coefficients, Matlab<sup>TM</sup> software program gives the code polyfit (t,y,1).

For case 1, during gasification, the equation can be expressed as

$$T_{\text{flame}} = -0.4 * [\text{CH}_4]_{\text{ppm}} + 2709.7 \quad (5.2)$$

For case 1, after the gasification process, the model equation is equal to

$$T_{\text{flame}} = 0.6 * [\text{CH}_4]_{\text{ppm}} + 2224.2 \quad (5.3)$$

For case 2, the first order equation is

$$T_{\text{flame}} = -0.2 * [\text{CH}_4]_{\text{ppm}} + 2341.0 \quad (5.4)$$

### 5.5.2 Second Order Polynomial Model

Based on the plot, it is possible that the data can be correlated by a second order polynomial function as shown below:

$$y = a_2 * t^2 + a_1 * t + a_0 \quad (5.5)$$

The unknown coefficients  $a_0$ ,  $a_1$ , and  $a_2$  are computed by minimizing the sum of the squares of the deviations of the data from the model (least-squares fit). To find the polynomial coefficients, in the Matlab, type `p=polyfit(t,y,2)` at the command line. Matlab calculates the polynomial coefficients in descending powers. For second order polynomial model, the model equation is:

For Case 1, during gasification process:

$$T_{\text{flame}} = 0.000002 * [\text{CH}_4]_{\text{ppm}}^2 - 0.5 * [\text{CH}_4]_{\text{ppm}} + 2761.4 \quad (5.6)$$



For case 1, after gasification:

$$T_{\text{flame}} = 0.0000004 * [\text{CH}_4]_{\text{ppm}}^2 + 0.6 * [\text{CH}_4]_{\text{ppm}} + 2230.9 \quad (5.7)$$

For case 2, the second order model can be exhibited as

$$T_{\text{flame}} = 0.0000012 * [\text{CH}_4]_{\text{ppm}}^2 - 0.2 * [\text{CH}_4]_{\text{ppm}} + 2345.4 \quad (5.8)$$

### 5.5.3 Power Law

Another type of model is the power law. This model can be shown as

$$y = a * t^b \quad (5.9)$$

However, it is difficult to estimate a and b coefficients with this form. By taking logarithm form, these coefficients can be found easily.

$$\text{Log } y = \text{log } a + b * \text{log } t \quad (5.10)$$

Now, using polyfit(t,y,1) Matlab code, the a and b coefficients can be determined.

The power law model result in this study is:

For case 1, during gasification process it can be expressed as

$$T_{\text{flame}} = 12603.75 * [\text{CH}_4]_{\text{ppm}}^{-0.2487} \quad (5.11)$$

For case 1, after gasification it is written as

$$T_{\text{flame}} = 1776.642 * [\text{CH}_4]_{\text{ppm}}^{0.0547} \quad (5.12)$$

For case 2, the power law is shown as

$$T_{\text{flame}} = 3539.97 * [\text{CH}_4]_{\text{ppm}}^{-0.0701} \quad (5.13)$$

Figure 5.4 and Figure 5.5 show the summary of empirical models, respectively. As can be seen from the figures, second order polynomial model does not provide a good approach for both cases. The results of second order expression are clearly irrelevant and this model can not identify the estimation of adiabatic flame temperature. On the other hand, first order approximation gave a reasonable approach for both cases with minimum error percentage. Even though power law model provides an opportunity for case 2, it does not show a satisfying result for case 1 especially during the coal gasification.

#### 5.5.4 Response Surface Methodology (RSM)

Response Surface Methodology (RSM) is a tool for understanding the quantitative relationship between multiple input variables and one output variable. Briefly,  $z$  can be considered as a polynomial function of two inputs,  $x$  and  $y$ . The function of  $z = f(x,y)$  describes a two dimensional surface in the space  $(x,y,z)$ . In general, this model can have as many input variables as the operator wants and the result becomes a hypersurface. Also, the model can have multiple output variables with a separate hypersurface for each one.

Any order of polynomial could be used to model local surface patches, but a quadratic function can be regarded as a successful compromise between the number of data points required to uniquely model the surface and the fidelity with which the model fits the true surface. For three inputs ( $x_1, x_2, x_3$ ), the equation of a quadratic response surface is

$$y = a_{11} * x_1^2 + a_{22} * x_2^2 + a_{33} * x_3^2 \dots \dots \dots \text{quadratic terms}$$

$$b_{12} * x_1 * x_2 + b_{13} * x_1 * x_3 + b_{23} * x_2 * x_3 \dots \dots \dots \text{interaction terms}$$

$$c_0 + c_1 * x_1 + c_2 * x_2 + c_3 * x_3 \dots \dots \dots \text{linear terms}$$

Here,  $a_{11}, a_{22}, a_{33}, b_{12}, b_{13}, b_{23}, c_1, c_2, c_3$  and  $c_0$  are coefficients of variables to find the output parameter after calculation.

To summarize the theoretical explanation of quadratic surface model, the goal is to obtain a surface model for each response where the response is adiabatic flame temperature. The factors used in modeling in order to determine the output temperature are oxygen-to-coal feed ratio ( $x_1$ ), steam-to-coal feed ratio ( $x_2$ ) and pressure ( $x_3$ ).

After specifying input variables, the matrix form was formed and the 100 different random variables from database were put in the matrix form numerically. Then, the model was run and then coefficients for each term were calculated. Based on these coefficients and parameters, the adiabatic flame temperature of Australian bituminous coal was determined and shown in Appendix A. Again,  $x_1, x_2$  and  $x_3$  terms are oxygen-to-coal feed ratio, steam-to-coal and pressure, respectively. The coefficients of the equation were:

$$\begin{aligned}
 T_{\text{flame}} = & 244.5*x_1^2 + 730.6*x_2^2 - 0.1*x_3^2 \dots\dots\dots \text{quadratic terms} \\
 & 80.7*x_1*x_2 + 2.6*x_1*x_3 - 1.6*x_2*x_3 \dots\dots\dots \text{interaction terms} \\
 & 1926.1 - 231.9*x_1 - 857.8 *x_2 + 5.9*x_3 \dots\dots\dots \text{linear terms} \quad (5.14)
 \end{aligned}$$

### 5.5.5 Multivariate Power Model

Multivariate power expression comprises two types of models, namely multivariate nonlinear and multivariate linear regression, respectively. The multivariate nonlinear regression (MNR) model with two or more predictor variables ( $x_1, x_2, \dots, x_n$ ) is given as

$$y = a_0 x_1^{a_1} x_2^{a_2} x_3^{a_3} \dots\dots\dots x_{n-1}^{a_{n-1}} x_n^{a_n} \quad (5.15)$$

where  $a_i$  ( $i=0,1,2,\dots,n$ ) represent constants to be estimated. The multivariable linear regression (MLR) can be stated as

$$y = a_0 + a_1 x_1 + a_2 x_2 + \dots\dots\dots + a_{n-1} x_{n-1} + a_n x_n + e \quad (5.16)$$

where  $e$  represent the residual. The MLR problem is easier to solve than the MNR problem. It is however, possible to convert Equation (5.15) into a multivariable linear regression problem by taking logarithms of both sides

$$\log(y) = \log(a_0) + a_1 \log(x_1) + \dots\dots\dots + a_{n-1} \log(x_{n-1}) + a_n \log(x_n) \quad (5.17)$$

In the present study, multivariate power model has been developed to predict the adiabatic flame temperature of Australian bituminous coal using coal properties such as oxygen-to-coal feed ratio ( $x_1$ ), steam-to-coal feed ratio ( $x_2$ ), pressure ( $x_3$ ), and the amount of methane ( $x_4$ ).

To begin, multivariate power law was performed to develop a nonlinear model for predicting the adiabatic flame temperature of Australian bituminous coal respectively, wherein the four model inputs ( $x_1$ -  $x_4$ ) comprise the proximate analysis of a coal sample and gasification parameters. The set consisting of 100 data points were used for the development of power law based models. The power-based model for the adiabatic flame temperature ( $y$ ) is given as

$$T_{\text{flame}} = 4023.46 * (x_1)^{0.0557} * (x_2)^{0.0281} * (x_3)^{-0.0028} * (x_4)^{-0.0871} \quad (5.18)$$

The summary of two empirical models have been done and shown in Appendix A. Quadratic surface model or response surface methodology gives appropriate results at the high ratio of oxygen-to-coal and high ratio of steam-to-coal. The model results are very close to results of ChemCAD. Similarly, if the ratio of oxygen-to-coal is low, the steam-to-coal ratio is important to figure out which model gives best approach. Response surface methodology provides good temperature results at the high steam-to-coal ratio with high oxygen-to-coal ratio relatively. On the other hand, multivariate regression exhibits a reasonable model if the steam-to-coal ratio is low and oxygen-to-coal ratio is high, but in reverse, with the low ratio of oxygen-to-coal and high amount of steam-to-coal, quadratic surface model should be preferred rather than multivariate power model.

Finally, the last input parameter called pressure was investigated on the effect of adiabatic flame temperature. Both models can be accepted if the amount of pressure is high unless the ratio of steam-to-coal and oxygen-to-coal is low or high. Otherwise, multivariate power model supports the ChemCAD temperature results at low pressure and steam-to-coal ratio and a high amount of oxygen. However, quadratic surface model is a logical approach at the low pressure and oxygen-to-coal ratio with a high ratio of steam-to-coal.

### 5.6 Sensitivity Analysis

The last part of this chapter is to investigate the importance of input parameters on adiabatic flame temperature of Australian bituminous coal. The aim of sensitivity analysis is to find the effect of input parameters on response variable or variables. It is possible to have an idea about the influence of the input variables on the output response generally. Here, the four input parameters have been investigated on the adiabatic flame temperature after coal gasification in the entrained flow gasifier. These parameters were selected as oxygen-to-coal feed ratio ( $x_1$ ), steam-to-coal feed ratio ( $x_2$ ), pressure ( $x_3$ ) and the concentration of methane ( $x_4$ ). The temperature of coal or water, coal particle size and coal flow rate were not taken into consideration due to their constant values during all the simulation.

The Monte Carlo approximation method was followed to find the sensitivity coefficients of each parameters and then, the results were illustrated in Figure 5.6. Basically, 100 different random samples were chosen from database for using calculation of sensitivity coefficients of each parameter. The Equation 2.26 mentioned in Chapter 2 was used to determine the coefficients as well.

In a sequential random sample, the difference of two vector immediate neighbor vectors is only the random number of one parameter. Thus, the difference of model outputs corresponding to a pair of immediate neighbor vectors is caused by the change of only one model input parameter. Therefore, sensitivity coefficients can be estimated based on the differences of model outputs and inputs. The expression of sensitivity analysis can be written follows:

$$\widehat{SC}_i = \frac{1}{n} \sum_{j=1}^n \frac{\Delta y_{ij}}{\Delta x_{ij}} \quad (2.26)$$

Where  $\widehat{SC}_i$  is the estimated sensitivity coefficient of model input  $x_i$ ,  $\Delta x_{ij}$  and  $\Delta y_{ij}$  are respectively the  $j$  th differences of  $x_i$  and model output  $y$  (here,  $y$  is adiabatic flame temperature) caused by the change of  $x_i$ , and  $n$  is the sample size. The estimated sensitivity coefficients are global. Essentially, Equation (2.26) is the Monte Carlo integration approximation of the integral:

$$\int_{-\infty}^{\infty} \dots \int_{-\infty}^{\infty} \frac{\partial y}{\partial x_i} f(x) dx_1 \dots dx_p \approx \frac{1}{n} \sum_{j=1}^n \frac{\Delta y_{ij}}{\Delta x_{ij}},$$

Where  $f(x)$  is assumed to be a multinormal distribution function. Figure 5.6 indicates that oxygen-to-coal ratio has the most influential effect on adiabatic flame temperature of Australian bituminous coal. The steam-to-coal ratio follows the oxygen-to-coal ratio as an important input parameter. The  $\text{CH}_4$  production called mutual independent parameter does not have a great effect on temperature. In conclusion, the importance of parameters can be ordered as  $x_1 > x_2 > x_3 > x_4$ .

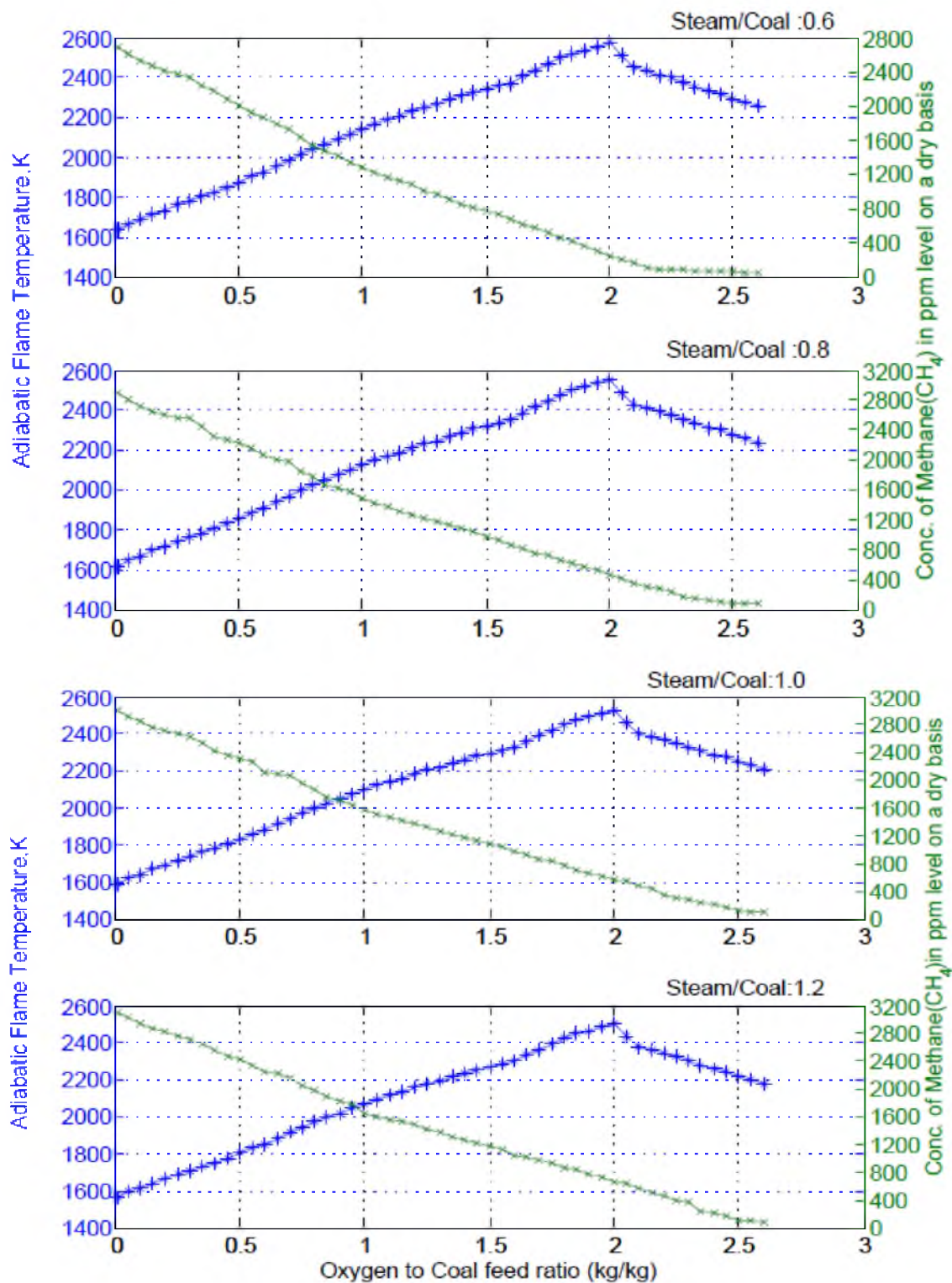


**Figure 5.1.** Adiabatic flame temperature and the concentration of methane profile of Australian bituminous coal versus oxygen-to-coal ratio at varying steam-to-coal ratios. (Blue line: Adiabatic flame temp., Green line: CH<sub>4</sub> conc.)



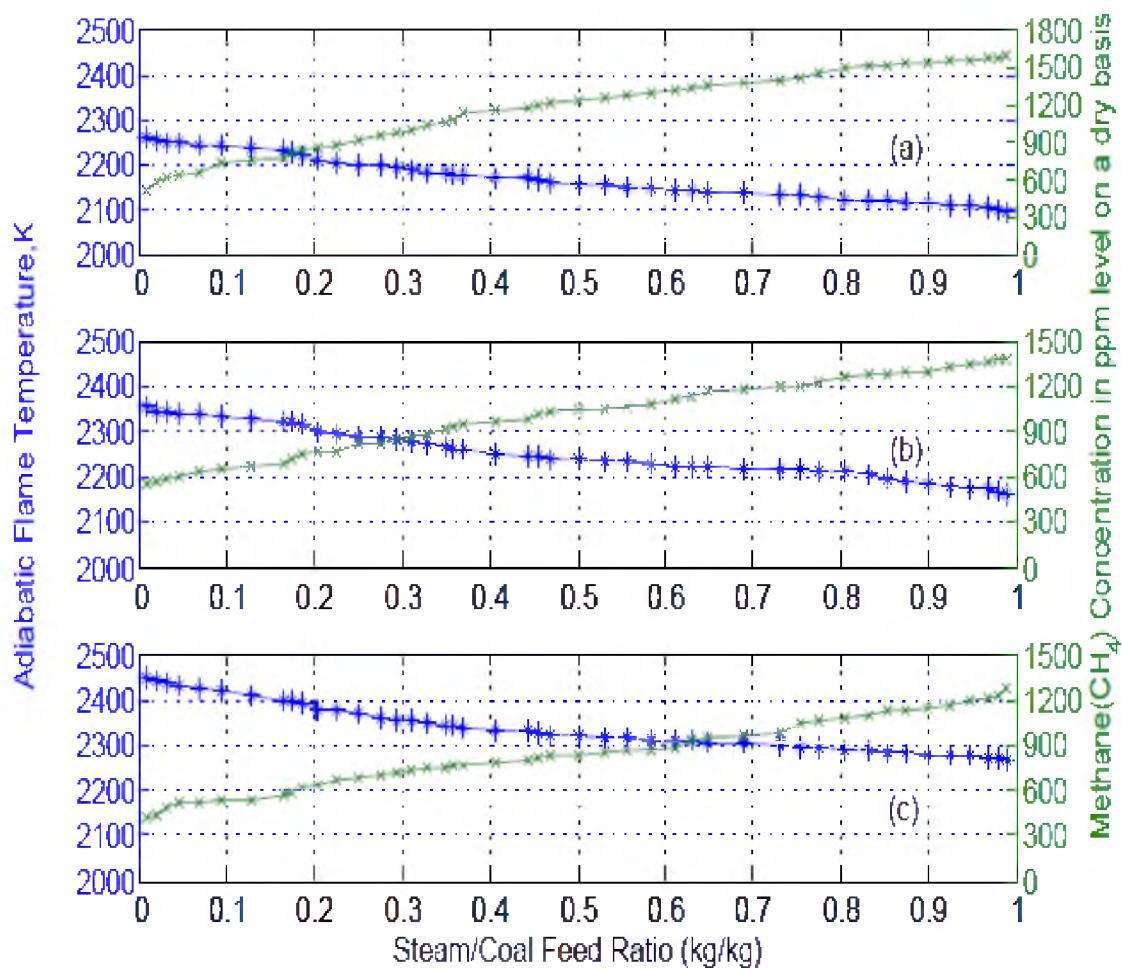


**Figure 5.2.** Adiabatic flame temperature and concentration of methane profile of Australian bituminous coal versus steam-to-coal ratio. Operating conditions: (a) oxygen-to-coal ratio of 1.0 kg/kg, (b) oxygen-to-coal ratio of 1.2 kg/kg (c) oxygen-to-coal ratio of 1.4 kg/kg

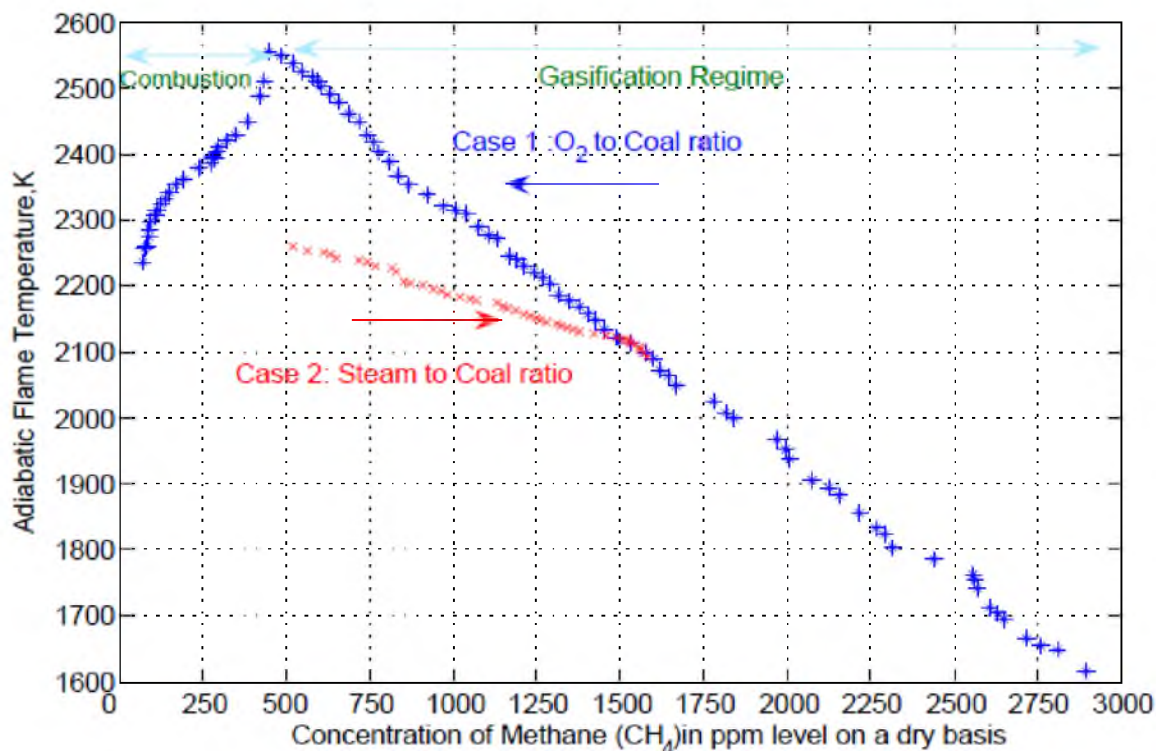


**Figure 5.3.** Adiabatic flame temperature and CH<sub>4</sub> gas profiles of Australian bituminous coal at different cases

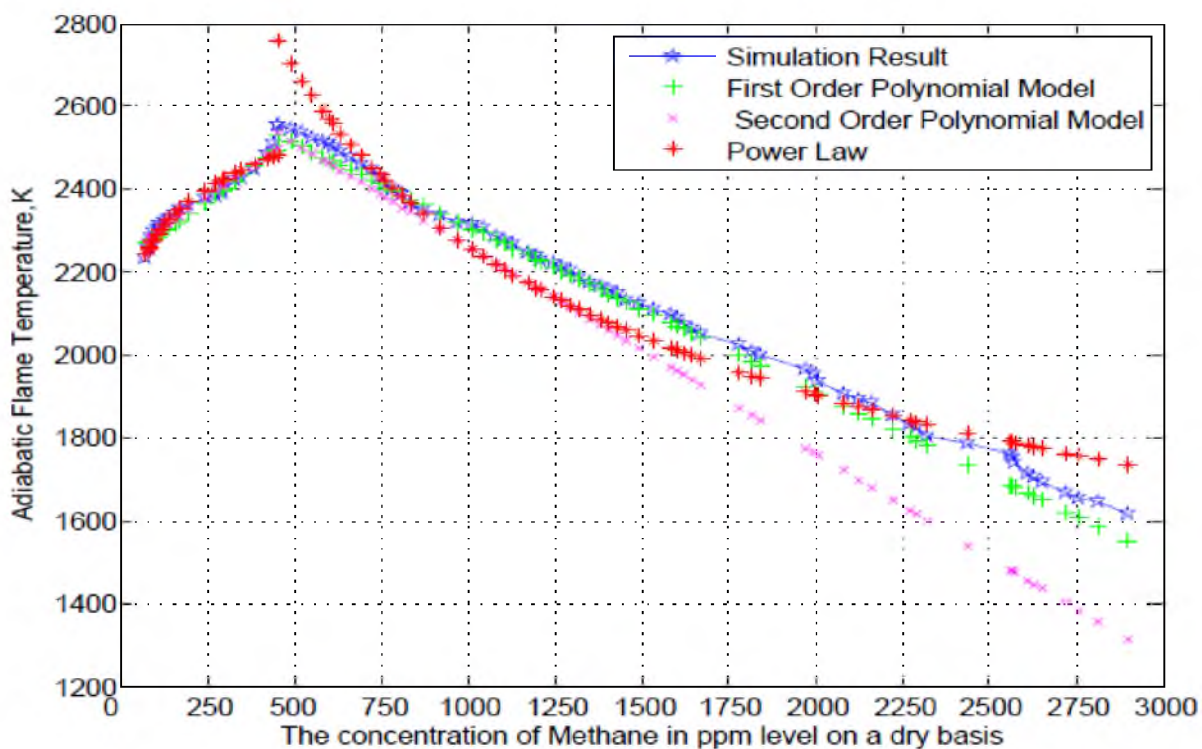


**Figure 5.4.** The simulation result and the basic polynomial models for case 1

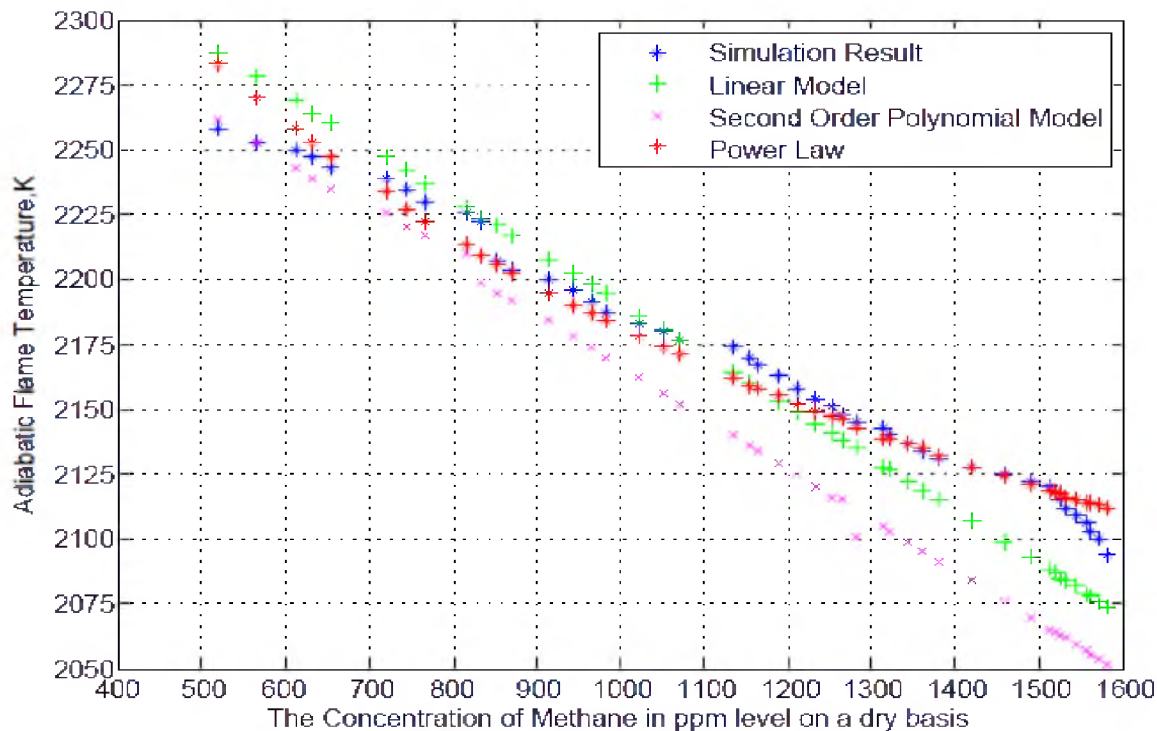


Figure 5.5. The simulation result and the basic polynomial models for case 2

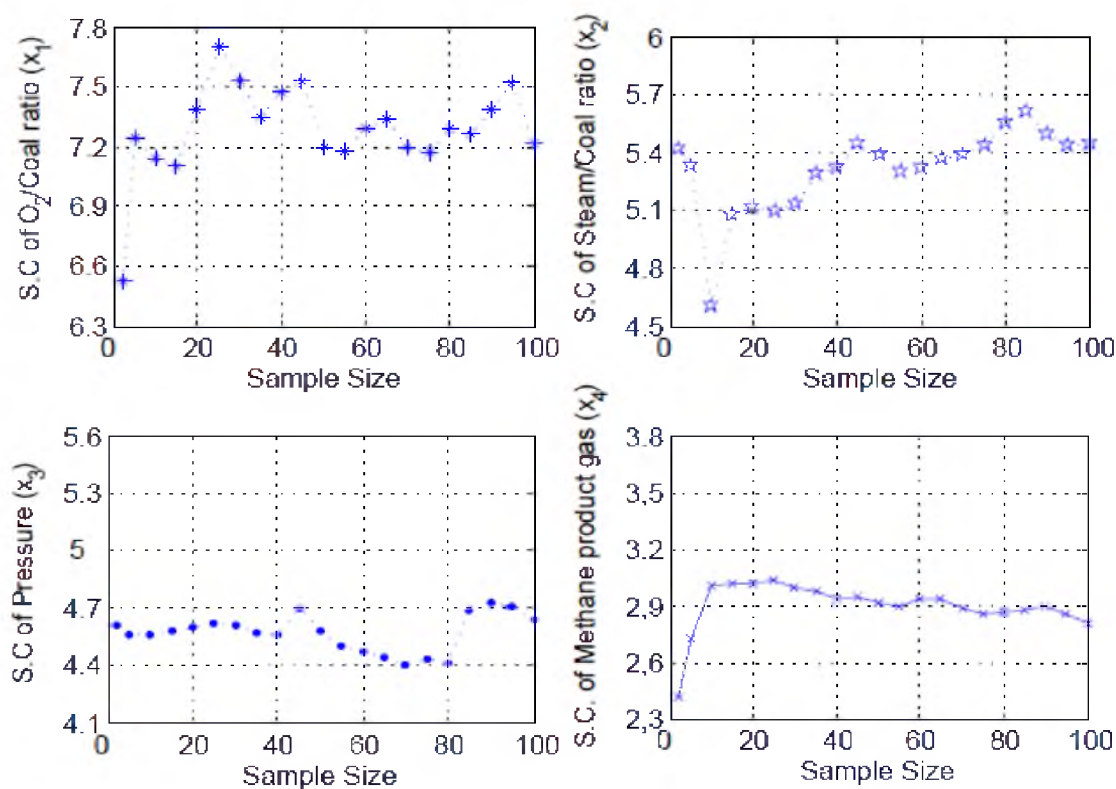


Figure 5.6. Sensitivity coefficients of input parameters

## **CHAPTER 6**

### **CONCLUSIONS AND RECOMMENDATIONS**

#### **FOR FUTURE WORK**

##### **6.1 Summary of Results**

This research reports the results of parametric studies using the ChemCAD simulation program and an empirical model. The objectives of this study were to investigate the effect of various operating conditions such as oxygen-to-coal feed ratio (kg/kg), steam-to-coal feed ratio (kg/kg), and pressure (bar) on estimation of adiabatic flame temperature of Australian bituminous coal and Indonesian roto coal in an entrained flow reactor and figure out the composition of product gases, syngas efficiency, carbon conversion and cold gas efficiency. Then, the relationship between adiabatic flame temperature of coal and methane product gas with different input parameters was investigated to find a correlation according to simulation results. During the simulation, the temperature of coal and water remained constant as 313 K and temperature of oxygen was held at 333 K.

To illustrate the effects of these parameters on the gasification process variables, simulation results were obtained over a range of steam, oxygen feed rates and pressure at constant coal feed rate, particle size and temperature of coal, water and oxygen. The maximum solids and gas temperatures in the entrained flow reactor were particularly

interesting. These temperatures were more sensitive to the concentration of oxygen in the feed than changes in steam feed rate. As explained in Chapter 3: graphs of adiabatic flame temperatures captured at various oxygen-to-coal and steam-to-coal feed ratio show peak values fall gradually with increasing steam-to-coal ratio and pressure. However, they were rapidly increasing with the rise of the oxygen and pressure.

The steam-to-coal ratio in the feed has a significant effect on the composition of product gas. As the ratio increases, the percentages of carbon dioxide increase considerably, hydrogen and methane rise up slightly. On the other hand, the percentage of carbon monoxide decreases rapidly. Both, the higher amount of steam and the lower temperature resulting from it contribute to this trend. The former tends to promote the coal-steam and water gas shift reactions, while the latter tends to retard the coal-carbon dioxide and coal-hydrogen reactions. Although an increase in the steam-to-coal feed ratio promotes the char-steam reactions, the temperature decreases because the char-steam reaction is highly endothermic and lowers the temperature.

According to the results, the amount of steam in the pyrolysis stage is almost constant. Therefore, the effect of steam-to-coal feed ratio on carbon conversion is not impressive as the effect of oxygen-to-coal on carbon conversion. However, if the steam-to-coal ratio increases, the amount of steam keeps promoting carbon-steam reactions in the direction of CO and H<sub>2</sub> formation.

Furthermore, the oxygen-to-coal in the feed has a great effect on the composition of the product gas. The slight concentration changes of methane and hydrogen are caused by the competitive interactions between the combustion and gasification reactions, the rate of which is very sensitive to the temperature variations produced. Since a higher

oxygen feed rate increases the flame temperature of the system, the oxidation reactions proceed to a greater extent. Consequently, the concentration of formed carbon dioxide increases significantly. Moreover, although an increase in the oxygen-to-coal feed ratio tends to increase the temperature, which in turn reverses the water gas shift reaction, it also tends to moderate the coal-steam, and hence, the coal-carbon dioxide reactions during the gasification period. Eventually, a point reached beyond which a remarkable change in the carbon monoxide and carbon dioxide yield. The reduction in the fraction of methane produced by increasing oxygen-to-coal ratio and pressure was followed by a small quantity of hydrogen forming. As mentioned before, due to the exothermic combustion, the adiabatic flame temperature of coals rises as the oxygen-to-coal ratio and pressure increase. The increase of oxygen-to-coal ratio also results in the increase of carbon conversion. For the given oxygen-to-coal ratio, the steam-to-coal ratio maximizes the carbon conversion. Hence, the coal conversion increases significantly as the oxygen feed increases. The steam-to-coal ratio does not affect coal conversion significantly.

Another observation is that the ratio of hydrogen-to-carbon monoxide decreases due to an increase in the amount of carbon monoxide with increase of the adiabatic flame temperature or oxygen-to-coal feed ratio. The steam-to-coal ratio has a negative effect of syngas efficiency because of the decrease of carbon monoxide. It also caused the increase in hydrogen-to-carbon monoxide ratio in the entrained flow gasifier. The coal types are important figures to predict the adiabatic flame temperature and gasification products. The reason of the different findings about the flame temperature and gasification products can be explained by the different properties of Australian bituminous coal and Indonesian roto coal.

The relationship between methane production and the adiabatic flame temperature of Australian bituminous coal was investigated in Chapter 5. The purpose of this study was to predict flame temperature based on methane concentration in ppm level without any calculation. The input parameters selected were oxygen-to-coal feed ratio, pressure and steam-to-coal ratio. Simulation results were used to estimate the temperature range. According to results, there was an inverse proportion between concentration of methane and adiabatic flame temperature with increasing oxygen-to-coal. This regime was monitored until the value of oxygen-to-coal ratio was 2.0 kg/kg. Even though the concentration of methane (ppm level) was decreasing, the flame temperature started to go down after the ratio of 2.0 kg/kg due to terminating the gasification process. After that point, it was difficult to say that gasification is going on. However, the combustion process and reactions are able to continue even though coal gasification comes to an end. The estimation of temperature is also possible by looking at the concentration of methane at various oxygen-to-coal and steam-to-coal ratio. The minimum ppm level of methane occurred at high temperature points and this can be possible with a high amount of oxygen-to-coal feed ratios. In other words, the optimum composition of methane in the gasifier could be reached at a high adiabatic flame temperature regime. From that point, if the concentration of methane is known after finishing gasification, the temperature range may be estimated successfully. Nevertheless, the simulation results must be supported by experiments to have a certain decision.

The adiabatic flame temperature based on methane production can be figured out with changing steam-to-coal and pressure parameters. As illustrated in Chapter 5, the adiabatic flame temperature decreased considerably with increasing steam-to-coal ratio

while the yield of methane showed insensitivity to it. The optimum concentration of methane can be described as 0-500 ppm, and the reasonable range of concentration might be taken until 2000 ppm. According to the ppm level of CH<sub>4</sub> in the gasification step, the amount of parameters and flame temperature can be estimated roughly. However, these findings should be in compliance with the experimental studies.

## **6.2 Recommendations for Future Work**

Under practical operating conditions, the particle size of coal must be taken in applying the hypothetical mechanism and empirical correlation because the char-steam and char-oxygen reactions are strongly affected by the behavior of coal particles. In this study, the particle size of both coal types were assumed as 100 μm during the set-up of simulation program. The gasification temperature will increase or decrease with different sizes of coal. This parameter has also a great influence on the residence time of coal reactions. Therefore, it is essential to investigate the effect of coal particle size on coal gasification temperature in the entrained flow gasifier.

In addition, the steady state conditions and one dimensional approach were followed for operating conditions during the ChemCAD simulation. The multidistribution of temperature in the gasifier could occur if the flow was more than one dimension. It is essential to take into consideration governing equations of coal gasification to find the temperature dispersion in the gasifier. Therefore, it is highly recommended to study the effect of unsteady state conditions and dimensional factors on the temperature of gasifier. Finally, temperatures measured at the top and bottom of the gasifier differ in values. During this study, the outside temperature was determined by ChemCAD simulation program. However, in reality, the temperatures depend on the reactions that occurred in



various parts inside the gasifier. For example, the temperature in the burner zone is higher than that of the reduction zone due to the combustion reactions and heat. Furthermore, temperature significantly differs near the wall from that of the farthest. The advanced model or design program including these important factors is utilized to attain accurate temperature distribution in the gasifier. In conclusion, the reasonable temperature results for each section inside the gasifier are obtained from model equations and operating conditions. Therefore, in future research, it is recommended to factor that certain temperatures can be measured at any point inside the gasifier.

## APPENDIX A

### ADIABATIC FLAME TEMPERATURE RESULTS

**Table A1.** Parameters and Temperature Results

Sample No.	Oxygen-to-Coal $X_1$ , kg/kg	Steam-to-Coal $X_2$ , kg/kg	Pressure $X_3$ , bar	Adiabatic FlameTemp., K	Quadratic surface response, Temp., K	Multi-power model, Temp., K
1	1.0	0.045	20	2144	2033	2085
2	0.25	1.20	40	1976	1956	1858
3	0.20	0.80	30	1708	1748	2203
4	0.70	1.20	50	2208	2014	2006
5	1.60	1.00	50	2468	2356	2238
6	1.00	0.185	40	2054	1988	2114
7	1.25	1.20	80	2490	2100	2134
8	0.55	0.80	50	1891	1742	1958
9	1.05	1.20	70	2404	2056	2092
10	1.00	0.204	50	2037	1969	2114
11	1.60	1.20	60	2599	2487	2238
12	1.10	0.80	40	2168	1958	2119
13	1.00	0.310	30	1940	1918	2117
14	1.20	0.093	40	2228	2130	2141
15	1.50	0.80	70	2332	2113	2203
16	1.00	0.444	60	1889	1845	2101
17	1.85	1.00	20	2600	2496	2349
18	0.40	0.60	50	1690	1689	1906
19	1.90	1.20	40	2753	2772	2323
20	1.00	0.50	80	1866	1709	2095
21	1.20	0.407	50	2006	1980	2155
22	0.50	0.232	40	1966	1834	1872
23	1.70	1.20	40	2651	2602	2265
24	1.00	0.329	70	1955	1830	2106
25	1.20	0.532	30	1948	1957	2158
26	0.90	0.60	30	1946	1836	2081
27	1.10	0.60	40	2048	1921	2134

Table A.1 Continued

Sample No.	Oxygen-to-Coal $X_1$ , kg/kg	Steam-to-Coal $X_2$ , kg/kg	Pressure $X_3$ , bar	Adiabatic FlameTemp., K	Quadratic surface response, Temp., K	Multi-power model, Temp., K
28	0.10	1.00	50	1734	1764	1728
29	1.20	0.732	80	1917	1822	2146
30	1.00	0.612	50	1820	1863	2099
31	1.40	0.009	40	2425	2295	2101
32	1.90	0.60	30	2392	2415	2451
33	1.40	0.045	50	2352	2272	2157
34	0.85	1.00	40	2160	1947	2058
35	1.00	0.556	80	1848	1701	2097
36	1.20	0.970	70	1844	1982	2140
37	1.55	0.60	60	2233	2156	2247
38	0.65	1.20	30	2166	2044	2001
39	1.30	0.80	40	2246	2063	2170
40	1.15	1.20	50	2428	2215	2125
41	1.00	0.90	20	1714	1932	2101
42	1.40	0.348	70	2132	2049	2206
43	0.15	1.00	30	1798	1832	1800
44	1.45	0.80	40	2308	2155	2206
45	0.50	1.20	50	2098	1956	1950
46	1.00	0.980	30	1711	1997	2098
47	1.40	0.359	20	2090	2047	2218
48	1.25	0.60	70	2131	1910	2155
49	0.40	1.00	40	1914	1831	1919
50	1.00	0.776	60	1772	1851	2093
51	1.40	0.833	40	1929	2136	2194
52	1.20	0.80	80	2236	1838	2124
53	0.75	1.00	30	2116	1921	2030
54	1.00	0.732	70	1792	1784	2098
55	1.00	0.032	50	2185	2087	2065
56	1.00	0.045	60	2169	2051	2077
57	1.00	0.069	70	2157	1986	2094
58	0.30	0.60	40	1642	1710	1968
59	1.75	1.00	80	2582	2351	2257
60	1.20	0.093	40	2228	2130	2141
61	1.65	1.20	60	2600	2528	2239
62	1.40	0.165	30	2259	2166	2225
63	0.20	1.20	40	1949	1952	1832
64	1.00	0.532	30	1842	1872	2104

Table A.1 Continued

Sample No.	Oxygen-to-Coal $X_1$ , kg/kg	Steam-to-Coal $X_2$ , kg/kg	Pressure $X_3$ , bar	Adiabatic FlameTemp., K	Quadratic surface response, Temp., K	Multi-power model, Temp., K
65	1.85	1.20	50	2744	2725	2296
66	0.50	0.80	40	1856	1762	1946
67	1.20	0.204	40	2141	2063	2159
68	1.10	1.20	60	2415	2147	2111
69	1.00	0.732	20	1777	1868	2108
70	0.30	1.20	50	2004	1918	1877
71	1.65	0.60	40	2268	2247	2306
72	0.10	1.20	20	1889	1983	1763
73	1.90	0.60	30	2392	2415	2451
74	1.00	0.370	80	1917	1744	2093
75	0.01	1.20	30	1840	1978	1553
78	1.00	0.690	70	1800	1778	2098
79	1.70	1.20	40	2651	2601	2265
80	1.20	0.456	80	2006	1828	2147
81	1.85	1.00	50	2618	2562	2316
82	1.35	1.00	30	2374	2185	2185
83	1.00	0.854	60	1738	1876	2091
84	1.95	1.00	50	2654	2652	2350
85	1.40	0.690	40	1981	2092	2208
86	1.60	1.00	40	2462	2361	2243
87	1.35	0.80	30	2264	2081	2187
88	1.00	0.980	50	1718	1975	2095
89	0.85	0.80	40	2050	1855	2055
90	1.65	0.80	40	2388	2293	2271
91	1.20	0.754	40	1884	1994	2153
92	1.70	0.80	80	2440	2213	2256
93	1.00	0.129	30	2096	2009	2117
94	1.95	1.20	40	2773	2817	2342
95	1.40	0.732	50	1979	2095	2207
96	0.95	0.80	40	2100	1893	2078
97	1.00	0.019	50	2213	2098	2049
98	0.65	0.8	60	1950	1721	1985
99	1.40	0.925	70	1928	2091	2185
100	1.00	0.069	60	2151	2032	2096

## APPENDIX B

### DESIGN PARAMETERS

**Table B1.** Design and Input Parameters of the ChemCAD Simulation

Input parameters	Design variables
Space	1D
Time	Steady State
Solver equation	Energy, Mass, Flow
Wall function	Standart
Carrier Gas	Nitrogen
Particle type	Pulverized coal
Temperature of oxygen, K	333
Temperature of coal and water, K	313
Particle size of coal, $\mu\text{m}$	100

## REFERENCES

- (1) Crnomarkovic N, Repic B, Mladenovic R, Neskovic O. Experimental investigation of steam in entrained flow coal gasification. *Fuel* 2007; 86: 194-202.
- (2) Hold N. Coal gasification research, development and demonstration needs and opportunities. Paper presented at the gasification technologies conference. San Francisco, CA; 2001.
- (3) Seo M, Guo J. Gasification characteristics of coal and biomass blend in a dual circulating fluidized bed reactor. *Energy & Fuel* 2010; 24: 3108-18.
- (4) Molina A, Mondragon F. Reactivity of coal gasification with steam and CO<sub>2</sub>. *Fuel* 1988; 77: 1831-9.
- (5) Watanabe H, Otaka M. Numerical simulation of coal gasification in entrained flow coal gasifier. *Fuel* 2006; 85: 1935-43.
- (6) Probst F, Hicks E. *Synthetic Fuels*. Second edition. New York; NY: Mc Graw Hill; 1982.
- (7) Collot AG. Matching gasification technologies to coal properties. *International Journal of Coal Geology* 2006; 65: 191-212.
- (8) Matyas J, Sundaram K, Rodriguez P, Edmunson A. Slag penetration into refractory lining of slagging coal gasifier. 25th annual international Pittsburgh coal conference. Pittsburgh, PA; 2008.
- (9) Bell D, Towler B. *Coal gasification and its applications*. First edition. Burlington; MA: William Andrew; 2011.
- (10) Heppner J. Gasification facilities for testing tunable diode lasers at high pressure conditions. University turbine systems research fellow electric power systems research institute. Charlotte, NC; 2008.
- (11) Abdelaziz A, Megahed M, Halawa M. Stability and calibration of platinum/palladium thermocouples following heat treatment. *Measurement* 2004; 35: 413-20.

- (12) Hanson R. Applications of quantitative laser sensors to kinetics, propulsion and practical energy systems. *Proceedings of the combustion institute* 2011; 33: 1-40.
- (13) Higan C, Burgt M. *Gasification*. Second edition. Boston; MA: Gulf Professional Publishing; 2008.
- (14) Lee J, Kim Y, Lee WJ. Coal gasification kinetics derived from pyrolysis in a fluidized bed reactor. *Energy* 1998; 23: 475-88.
- (15) Taba L, Irfan M. The effect of temperature on various parameters in coal, biomass and CO-gasification: A review. *Renewable and Sustainable Energy Reviews* 2012; 16: 5584-96.
- (16) Nguyen T, Lim Y, Song B. Two-stage equilibrium model applicable to the wide wide range of operating conditions in the entrained flow gasifiers. *Fuel* 2010; 89: 3901-10.
- (17) Yoshida H, Kiyona F, Tajima H, Ogasawara K. Two stage equilibrium model for a coal gasifier to predict the accurate carbon in hydrogen production. *Fuel* 2008; 87: 2186-93.
- (18) Higan C. New developments in soot management. Paper presented at IChemE Conference. *Gasification: The clean choice for carbon management*. Noordwick, UK; 2002.
- (19) Yun Y, Ju J. Operation performance of a pilot scale gasification/ melting process for liquid and slurry types wastes. *Korean Journal Chemical Engineering* 2003; 20: 1037-44.
- (20) Lee WJ, Kim SD, Song H. Steam gasification of an Australian bituminous coal in a fluidized bed. *Korean Journal of Chemical Engineering* 2002; 19: 1091-96.
- (21) Lee J, Kim SD, Song H. Steam gasification of coal with salt mixture of potassium and nickel in a fluidized bed reactor. *Korean Journal of Chemical Engineering* 2001; 18: 640-45.
- (22) Feroso, J., *Pressure CO-gasification of coal and biomass for the production of hydrogen*. PhD dissertation. University of Oviedo, Spain; 2009.
- (23) Pohorely M, Vosecky M, Hejdova P, Puncocha M, Skoblja S. Gasification of coal and PET in fluidized bed reactor. *Fuel* 2006; 85: 2458-68.
- (24) Kim J, Lee H, Kim D. Coal gasification characteristics in a downer reactor. *Fuel* 2001; 80: 1915-22.

- (25) Lapuerta M, Hernandez J, Pazo A. Gasification and CO-gasification of biomass wastes: effect of the biomass origin and the gasifier operating conditions. *Fuel Processing Technology* 2008; 89: 828–37.
- (26) Lahijani P, Zainal A. Gasification of palm empty fruit bunch in a bubbling fluidized bed: performance and agglomeration study. *Bioresource Technology* 2011; 102: 2068–76.
- (27) Anjum MF, Tasadduq I, Al-Sultan K. Response surface methodology: a neutral network approach. *European Journal of Operational Research* 1997; 101: 65-73.
- (28) Penny DJ, Lindfield G. *Numerical methods using matlab*. First edition. Upper Saddle River, NJ: Prentice-Hall Inc; 1999.
- (29) Chavan P, Mall B, Rajurkar D. Development of data-driven models for fluidized-bed coal gasification process. *Fuel* 2012; 93: 44-51.
- (30) Fang S, Gentner G. Estimation of sensitivity coefficients of nonlinear model input parameters which have a multinormal distribution. *Computer Physics Communications* 2003; 157: 9-16.
- (31) Frey H, Patil S. Identification and review of sensitivity analysis methods. *Risk Analysis* 2002; 22: 553-78.
- (32) Helton C, Davis F. Illustration of sampling-based methods for uncertainty and sensitivity analysis. *Risk Analysis* 2002; 22: 591-622.
- (33) Sobol IM. Sensitivity analysis for non-linear mathematical model. *Mathematical Modelling Computational Expression* 1993; 1: 407–14.
- (34) Williams A, Pourkashanian M, Jones JM, Skorupska N. Modeling coal combustion: the current position. *Fuel* 2002; 81: 605-18.
- (35) Harris D, Roberts D. Gasification behaviour of Australian bituminous coals at high pressure and temperature. *Fuel* 2006; 85: 134-42.
- (36) ChemCAD Group, <http://www.chemstations.com>.
- (37) Ahn D, Gibbs B. Gasification kinetics of Indonesian sub-bituminous coal-char with CO<sub>2</sub> at elevated pressure. *Fuel* 2001; 80: 1651-58.
- (38) Feroso J, Arias B, Pevida C. High-pressure co-gasification of coal with biomass and petroleum coke. *Fuel Processing Technology* 2009; 90: 926-32.
- (39) Fournier G, Hartevelde W, Prins M. A water quench for the Shell coal gasification Process. 25th annual international Pittsburgh conference. Pittsburgh, PA; 2008.



- (40) Liosson R, Chauvin R. Pyrolysis rapide du charbon. *Chemie et Industrie* 1964; 91: 269-74.
- (41) Li X, Grace R, Watkinson P. Equilibrium modeling of gasification: a free energy minimization approach and its application to a circulating fluidized bed coal gasifier. *Fuel* 2001; 80: 1995-2000.
- (42) Ma R, Felder RM, Ferrel JK. Modeling a pilot scale fluidized bed coal gasification reactor. *Fuel Processing Technology* 1988; 19: 265-290.
- (43) Pinto F, Franco C, Tavares C. Effect of experimental conditions on CO gasification of coal, biomass and plastics wastes with air-to-steam mixtures in a fluidized bed. *Fuel* 2003; 82: 1967-76.
- (44) Zuideveld P. Shell coal gasification process for power and hydrogen/chemicals, gasification technologies council annual conference. Houston, TX; 2004.